Large-scale Wireless Networks: Stochastic Geometry and Ordering

by

Junghoon Lee

A Dissertation Presented in Partial Fulfillment
of the Requirement for the Degree
Doctor of Philosophy

Approved March 2014 by the
Graduate Supervisory Committee:

Cihan Tepedelenlioğlu, Chair
Andreas Spanias
Martin Reisslein
Oliver Kosut

ARIZONA STATE UNIVERSITY

May 2014

ABSTRACT

Recently, the location of the nodes in wireless networks has been modeled as point processes. In this dissertation, various scenarios of wireless communications in large-scale networks modeled as point processes are considered.

The first part of the dissertation considers signal reception and detection problems with symmetric alpha stable noise which is from an interfering network modeled as a Poisson point process. For the signal reception problem, the performance of space-time coding (STC) over fading channels with alpha stable noise is studied. We derive pairwise error probability (PEP) of orthogonal STCs. For general STCs, we propose a maximum-likelihood (ML) receiver, and its approximation. The resulting asymptotically optimal receiver (AOR) does not depend on noise parameters and is computationally simple, and close to the ML performance. Then, signal detection in coexisting wireless sensor networks (WSNs) is considered. We define a binary hypothesis testing problem for the signal detection in coexisting WSNs. For the problem, we introduce the ML detector and simpler alternatives. The proposed mixed-fractional lower order moment (FLOM) detector is computationally simple and close to the ML performance.

Stochastic orders are binary relations defined on probability. The second part of the dissertation introduces stochastic ordering of interferences in large-scale networks modeled as point processes. Since closed-form results for the interference distributions for such networks are only available in limited cases, it is of interest to compare network interferences using stochastic. In this dissertation, conditions on the fading distribution and path-loss model are given to establish stochastic ordering between interferences. Moreover, Laplace functional (LF) ordering is defined between point processes and applied for comparing interference. Then, the LF orderings of general classes of point processes are introduced. It is also shown that the LF ordering is pre-

served when independent operations such as marking, thinning, random translation, and superposition are applied. The LF ordering of point processes is a useful tool for comparing spatial deployments of wireless networks and can be used to establish comparisons of several performance metrics such as coverage probability, achievable rate, and resource allocation even when closed form expressions for such metrics are unavailable.

Dedicated to my dear family for their love and support.

ACKNOWLEDGEMENTS

First of all, I would like to thank God for taking care of my own way and my future. I always believe in and pray to you.

I would like to express my gratitude to my advisor Prof. Cihan Tepedelenlioğlu, whose valuable guidance and support were essential for me to accomplish this work. In addition to academics, interaction with him has helped me develop several other skills which will be useful throughout my life.

I would like to extend my thanks to all members of my committee, Prof. Andreas Spanias, Prof. Martin Reisslein and Prof. Oliver Kosut for their comments and patience. I would also take this opportunity to thank all the faculty members from whom I have learned, including, but not limited to Prof. Tolga Duman and Prof. Junshan Zhang. This work would not have been possible without those course-works as the building blocks for my research.

I am grateful to all my friends and colleagues in the Signal Processing and Communication group. Thanks to Dr. Adithya Rajan, Dr. Sivaraman Dasarathan, Dr. Yuan Zhang and Ruochen Zeng for their help and several useful discussions. I also want to thank Dr. Anita Todd for her help and prayer.

I sincerely appreciate the support and the prayer from my father and mother, who always encourage me to pursue my goal. I will never be able to thank them enough for that. I also thank my parents in law for their constant encouragement. My sincere thanks to my wife Suyeon for standing by me through thick and thin of graduate school. My graduation would not have been possible without her understanding, encouragement and devotion. Last but not least, my lovely kids, Kyuri and Kyuseo always make me happy and provide me with full energy for doing my study and research. I truly thank Kyuri and Kyuseo for being my lovely kids.

TABLE OF CONTENTS

CHAPTER Page

CHAPTER Page

CHAPTER Page

LIST OF TABLES

Table Page

LIST OF FIGURES

Figure Page

Figure Page

Chapter 1

INTRODUCTION

1.1 Stochastic Wireless Networks

With the proliferation of wireless devices at home and outdoors, modeling their spatial location is of utmost importance in applications such as cellular, cognitive, sensor networks, just to name a few. For the last several decades, deterministic models include square, triangular, and hexagonal lattices [1, 2] have been considered as network models since it provides highly simplified system models for analysis and system level simulations for design. As an example, the hexagonal deterministic cellular system is shown in Fig. 1.1 (A). However, the deterministic models can not reflect the irregularity of real networks due to geographical factors such as buildings and hills and irregular deployment of various types of transmitters such as microcells,

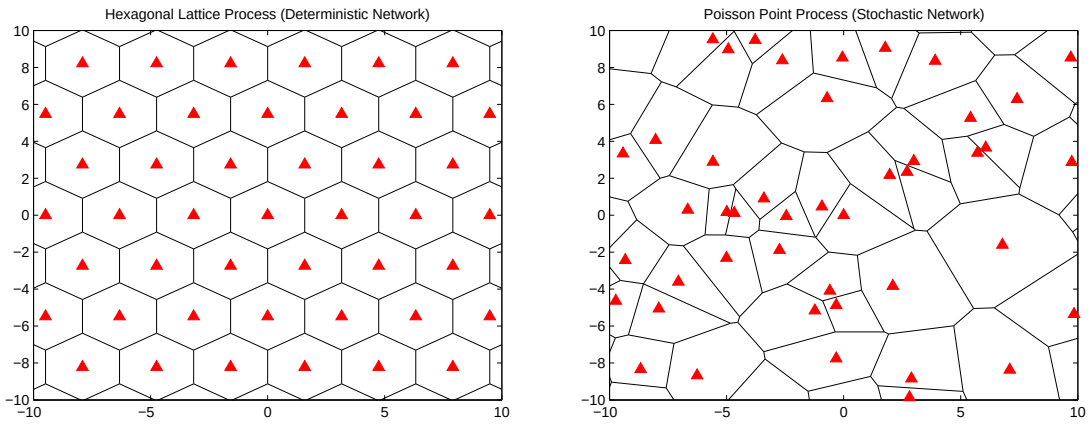

(A) Deterministic network (B) Stochastic network

Figure 1.1: Illustration of deterministic and stochastic networks

picocells, and femtocells in cellular networks. In real systems, it is also impossible for each node to know or predict the locations and channels of all but perhaps a few other nodes. This has led to an increasing interest in stochastic geometry recently [3, 4, 5] as shown in Fig. 1.1 (B). The stochastic geometry is the main mathematical tool that has recently proved most helpful in circumventing the above unrealistic assumptions. Stochastic geometry allows to study the average behavior over many spatial realizations of a network whose nodes are placed according to some probability distribution. Stochastic geometry is a rich branch of applied probability which allows the study of random phenomena on the plane or in higher dimensions. Random point pattern or *point processes* are the most basic and important such objects, hence *point process theory* is often considered to be the main sub-field of stochastic geometry [6]. Point processes provide an appropriate framework for modeling spatial distributions of random networks, and enable the study of performance of these systems measured in terms of throughput, error rate, coverage, and amount of interference. Unfortunately, for most realistic wireless node distributions, these performance metrics which are often averaged across the point process, are intractable. Stationary Poisson processes provide a tractable framework, but suffer from notorious modeling issues in matching real network distributions. In this dissertation, we propose to use stochastic orders to address this issue.

Stochastic orders are binary relations defined on probability distributions which capture intuitive notions like being larger or being more variable. The theory of stochastic orders (or dominance) provides a comprehensive framework to compare two random variables (RVs) or vectors [7]. The simplest and most widely used stochastic order compares the cumulative distribution functions (CDF) of two RVs, which defines a partial order between pairs of RVs. There are many other stochastic orders that capture comparisons of RVs in terms of size, and variability. In this dissertation,

we extend the stochastic ordering concept to compare point processes. Stochastic ordering of point processes provide an ideal framework for comparing two deployment / usage scenarios even in cases where the performance metrics cannot be computed in closed form. These partial orders capture intuitive notions like one point process being "greater", or "more variable". More generally, different definitions of ordering can capture effects of clustering, variability of interference, and density or mobility of nodes. Existing works on point process modeling for wireless networks have paid little attention to how two intractable scenarios can be nevertheless compared to aid in system optimization.

In this dissertation, the main quantity of interest is the network interference. We study on the statistics of the (aggregate) interference amplitude and power in large wireless networks as shown in Fig. 1.2. The receiver is being interfered by interference sources distributed as a point process. The point process describes all interfering nodes [8]. The accumulated interference to the receiver at the origin is of interest to quantify and it is given by

$$I = \sum_{x \in \Phi} h_{\mathrm{I}}^{(x)} g(\|x\|) \tag{1.1}$$

where Φ denotes the set of all interfering nodes which is modeled as a point process on $\mathbb{R}^d$ and $h_{\mathrm{I}}^{(x)}$ is a random variable capturing the fading coefficient between the receiver and the x^{th} interfering node. Here, typically $d = 2$ or $d = 3$, though this assumption is not necessary. Moreover, $\{h_{\mathrm{I}}^{(x)}\}_x$ are i.i.d. random variables and independent of the point process. The path-loss is captured by a function $g(\cdot) : \mathbb{R}^+ \to \mathbb{R}^+$ which is a continuous, positive, non-increasing function of $\|x\|$ and assumed to depend only on the Euclidean distance $\|x\|$ from the node x to the receiver at the origin. The locations of the interfering nodes Φ, together with the path loss law $g(\|x\|)$, and the fading statistics $h_{\mathrm{I}}^{(x)}$ determine the interference. In this dissertation, we study the statistics

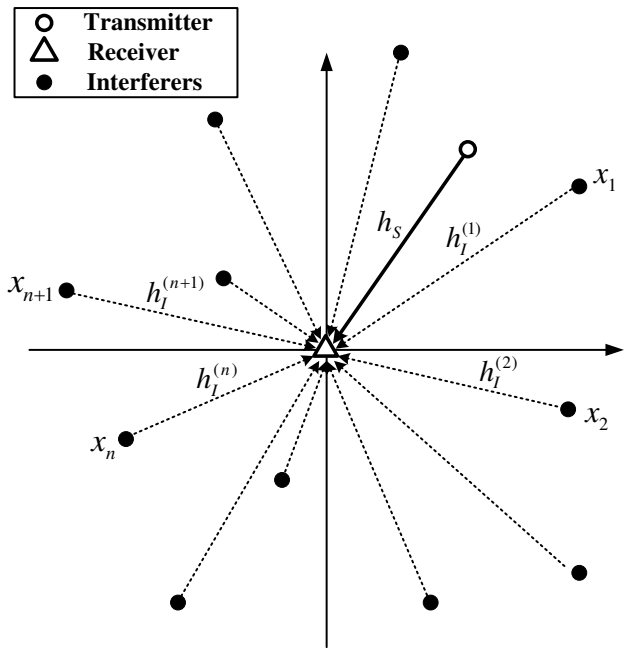

Figure 1.2: Illustration of a wireless network. The black dots represent interfering nodes which form a point process Φ and the dotted lines represent their interfering signals. The white dot and the triangle at the origin are the desired transmit/receiver pair which are not part of the point process.

of the (aggregate) interference amplitude and power in large-scale wireless networks that are subject to several sources of randomness, including the fading statistics, the signal attenuations and the node distribution. We also propose receivers for several systems such as multiple antennas systems and sensor network systems in the presence of the network interference.

One of the primary focus area of this dissertation is a cellular network, where base stations (BSs) are usually modeled by fixed pattern on the plane. Lattice points can be used to model such a regularly fixed pattern as shown in Fig. 1.1 (A). However, this approach fails to capture the irregularity and randomness of a real network. In order to introduce an additional source of randomness: the positions of the base stations,

instead of assuming they are placed deterministically on a regular grid, their location can be modeled as a homogeneous Poisson point process (please see Fig. 1.1 (B)). Such an approach for modeling base station (BS) locations has been considered as early as 1997 [9, 10]. This approach has been recently applied to the analysis of cellular networks due to the ability to derive tractable expressions for coverage and rate for one-tier [11] and heterogeneous networks [12, 13, 14, 15, 16, 17]. In addition to these papers, heterogeneous network with load-aware modeling has been studied in [18]. In the case of uplink scenario, [19] has proposed the framework. The effect of fractional frequency reuse in cellular networks has been analyzed in [20, 21]. In order to improve a cell-edge performance, cooperative transmission schemes have been analyzed in [22, 23, 24]. Non-uniform user distribution [25], load balancing between users [26], mobility [27] and data offloading [28] in cellular networks with point processes have been studied. Energy efficiency and power consumption have been also analyzed in [29, 30]. The handover rate and sojourn time in mobile networks have been analyzed in [31]. The device to device (D2D) communication in cellular network has been studied in [32, 33]. In [34], the point processes which are different from stationary Poisson point process have been assumed and approximation of performance using deployment gap has been proposed. However, most of works have focused averaged single user performance and assumed a stationary Poisson point process. In the network performance point of view, it is important to consider all of served users or a group of users in especially multicast/broadcast scenario. Other point processes than a stationary Poisson should be also considered to capture various real effects such as geographical factors and randomness even though a closed form expressions for the performance metrics such as coverage probability and achievable rate is not analytically tractable with this assumption. In the literature on modeling cellular device location, there is a need to relate the performance metrics, which often have

convexity or monotonicity properties, to the stochastic orders that capture intuitive notions such as clustering (variability) and node density (monotonicity). Therefore, this dissertation sheds light on the connections between spatial modeling of cellular systems and their performances.

For another important application, consider a cognitive network. In a cognitive network, there is an increasing interest in developing efficient methods for spectrum management and sharing. This motivates to exploit spectrum opportunities in space, time, frequency while protecting users of the primary network from excessive interference due to spectrum access from secondary networks. The interference from secondary networks is the performance limiting factor of primary network. Therefore, interference analysis has been studied in [35, 36, 37], where secondary users are modeled as a stationary Poisson point process. In [38], the outage probability has been analyzed in the presence of interference from secondary users and the interference has been approximated using a Poisson cluster process. Most of works with point processes have focused interference analysis and assumed a stationary Poisson point process. The works of this dissertation provide the chance to overcome such a limited scenario and also devote some attention to find another useful applications to cognitive networks.

1.2 Contributions of the Dissertation

In what follows, we clearly identify and summarize the contributions of this dissertation.

To the best of our knowledge, there is no analysis of MIMO systems over fading channels with symmetric α-stable noise which is from Poisson distributed interferers. In this dissertation, we design receivers for, and analyze the effect of, symmetric α-stable noise on space-time coded systems. We derive the pairwise error probability

(PEP) of orthogonal space-time block codes (STBCs) with a benchmark genie-aided receiver (GAR) and the minimum distance receiver (MDR), which is optimal in the Gaussian case. Based on the analytical result, it is revealed that the conventional MDR receiver is not suitable for symmetric α-stable noise environments. As For general space-time codes, we propose a maximum-likelihood (ML) receiver and its approximation at high signal-to-noise ratio (SNR) which does not depend on noise parameters and is computationally simple. Based on the simulation results, we propose to use the resulting asymptotically optimal receiver (AOR) for the impulsive noise which provides close performance to the ML receiver with relatively low complexity.

We consider the detection of the aggregated sensing signal from the desired wireless sensor network in the presence of aggregated interference from the interfering network. To the best of our knowledge, in the literature, there is no study on the signal detection with interference in coexisting wireless sensor networks. In this dissertation, we show that the problem becomes a binary hypothesis testing problem of detecting α-stable random signals in α-stable random noise, which has not been considered in the literature. We design simple and robust detectors for the detection problem which show the reasonable detection performance and robustness to uncertainties in the knowledge of parameters of α-stable random variables compared to the ML detector which has high computational complexity due to the lack of closed-form expression.

In general, the closed-form expression and exact analysis for aggregate interference are not tractable except for some limited cases. Using stochastic ordering, however, we can compare the scenarios and decide which one is the better situation than other. We derive the conditions on the fading distribution and path-loss model to establish stochastic ordering between interferences. By definition of new stochastic ordering for

point processes, the Laplace functional (LF) order, the condition on spatial distribution for interferes is given in this dissertation. From the results in this dissertation, we gain insights about qualitative behaviors for system design. These insights can help guide the placement of additional nodes and judge the goodness of a concrete deployment of nodes, which includes how to deploy the additional nodes for less interference to other system. Moreover, by obtaining the statistical property of fading channels or estimating the path-loss exponent, we can compare the performance metrics such as coverage probability and ergodic capacity without actual system evaluation. The stochastic ordering also provides important keys as a upper or lower bound of actual performances.

The stochastic ordering can be applied to general classes of point processes. Through the preservation properties of LF ordering with respect to independent operations on a point process such as marking, thinning, random translation, and superposition, we consider several effects of real systems such as propagation effects over wireless channels, multiple access schemes, heterogeneous network scenarios, and mobile networks and compare performances without having to obtain closed-form results for a wide range of performance metrics such as a coverage probability, an achievable rate, and a resource allocation under these real system effects. In addition to the performance comparison, the stochastic ordering of point processes provides guidelines for system design such as network deployments and user selection schemes.

1.3 Outline of the Dissertation

The rest of the dissertation is organized as follows. Chapter 3 analyzes the performance of space-time coding over fading channels with impulsive noise which is from the interfering network modeled by the homogeneous Point point process and proposes the asymptotically optimal receiver for the impulsive noise. Chapter 4 con-

siders signal detection in coexisting Poisson distributed networks and proposes the mixed-FLOM detector which is simple and robust to errors in system parameters. Chapter 5 compares the interferences in various scenarios using stochastic ordering tools and derives several analytical conditions for stochastic ordering of interferences. The stochastic ordering of point processes is extended to general classes of point processes and the preservation properties of the stochastic ordering is studied in Chapter 6. Chapter 6 also introduces useful applications of the stochastic ordering of point processes to various wireless network setups. Finally the conclusions are presented in Chapter 7.

Chapter 2

MATHEMATICAL PRELIMINARIES

In this chapter, we give a brief overview of some terminology and mathematical tools used in the forthcoming chapters.

2.1 Some Special Classes of Functions

In what follows, some classes of functions such as completely monotone functions and completely monotone derivative functions are described.

2.1.1 Completely Monotonic Functions

A function $g : (0, \infty) \to \mathbb{R}$ is completely monotonic (c.m.), if and only if it has derivatives of all orders which satisfy

$$(-1)^n \frac{\mathrm{d}^n}{\mathrm{d}x^n} g(x) \geq 0, \tag{2.1}$$

for all $n \in \mathbb{N} \cup \{0\}$, where the derivative of order $n = 0$ is defined as $g(x)$ itself. The celebrated Bernstein's theorem [39] asserts that, $g : (0, \infty) \to \mathbb{R}$ is c.m. if and only if it can be written as a mixture of decaying exponentials:

$$g(x) = \int_0^\infty \exp(-ux)\mu(\mathrm{d}u), \tag{2.2}$$

which is a Lebesgue integral with respect to a positive measure μ on $[0, \infty)$. As an example, $g(x) = 0.5 \exp(-x)$ is a c.m. function in a wireless communications context, as it corresponds to the SER of differential phase shift keying in AWGN.

If the first derivative of a function $g : (0, \infty) \to \mathbb{R}$ satisfy the c.m. property in (2.1), the function is called a completely monotonic derivative (c.m.d.) function. As

an example, $\log(1+x)$ is a c.m.d. function with x in a wireless communications context, as it corresponds to the achievable rate.

2.2 Stochastic Ordering of Random Variables

Stochastic orders are binary relations between random variables, which can be used to compare them based on a variety of criteria. We briefly review some common stochastic orders between random variables, which can be found in [7, 40].

2.2.1 Usual Stochastic Ordering

Let X and Y be two random variables (RVs) such that

$$P\left(X > x\right) \leq P\left(Y > x\right), -\infty < x < \infty. \tag{2.3}$$

Then X is said to be smaller than Y in the *usual stochastic order* (denoted by $X \leq_{\text{st}} Y$). Roughly speaking, (2.3) says that X is less likely than Y to take on large values. To see the interpretation of this in the context of wireless communications, when X and Y are distributions of instantaneous SNRs due to fading, (2.3) is a comparison of outage probabilities. Since X, Y are positive in this case, $x \in \mathbb{R}^+$ is sufficient in (2.3).

2.2.2 Laplace Transform Ordering

Let X and Y be two non-negative random variables such that

$$\mathcal{L}_X(s) = \mathbb{E}[\exp\left(-sX\right)] \geq \mathbb{E}[\exp\left(-sY\right)] = \mathcal{L}_Y(s) \text{ for } s > 0. \tag{2.4}$$

Then X is said to be smaller than Y in the *Laplace transform* (LT) *order* (denoted by $X \leq_{\text{Lt}} Y$). For example, when X and Y are the instantaneous SNR distributions of a fading channel, (2.4) can be interpreted as a comparison of average bit error rates for

exponentially decaying instantaneous error rates (as in the case for differential-PSK (DPSK) modulation and Chernoff bounds for other modulations) [41]. The LT order $X \leq_{\text{Lt}} Y$ is equivalent to

$$\mathbb{E}[l(X)] \geq \mathbb{E}[l(Y)], \tag{2.5}$$

for all *completely monotonic* (c.m.) functions $l(\cdot)$ [40, pp. 96]. By definition, the derivatives of a c.m. function $l(x)$ alternate in sign: $(-1)^n \mathrm{d}^n l(x)/\mathrm{d}x^n \geq 0$, for $n = 0, 1, 2, \ldots$, and $x \geq 0$. An equivalent definition is that c.m. functions are positive mixtures of decaying exponentials [40]. A similar result to (2.5) with a reversal in the inequality states that

$$X \leq_{\text{Lt}} Y \Longleftrightarrow \mathbb{E}[l(X)] \leq \mathbb{E}[l(Y)], \tag{2.6}$$

for all $l(\cdot)$ that have a completely monotonic derivative (c.m.d.). Finally, note that $X \leq_{\text{st}} Y \Rightarrow X \leq_{\text{Lt}} Y$. This can be shown by invoking the fact that $X \leq_{\text{st}} Y$ is equivalent to $\mathbb{E}[l(X)] \leq \mathbb{E}[l(Y)]$ whenever $l(\cdot)$ is an increasing function [40], and that c.m.d. functions in (2.6) are increasing.

2.3 Point Processes

Point processes have been used to model large-scale networks [42, 3, 5, 43, 44, 45, 8, 38, 46, 47]. Since wireless nodes are usually not co-located, our focus is on *simple* point processes, where only one point can exist at a given location. In addition, we assume the point processes are locally finite, i.e., there are finitely many points in any bounded set. In what follows, we introduce some fundamental notions that will be useful.

2.3.1 Properties of Point Processes

In this section, we introduce and define several important properties of point processes.

Stationary: A point process Φ in $\mathbb{R}^d$ is *stationary* if its characteristics are invariant under translation: the point processes Φ and $\Phi_x = \Phi + x$ have the same distribution for all x in $\mathbb{R}^d$.

Isotropy: A point process Φ in $\mathbb{R}^d$ is *isotropic* if its characteristics are invariant under rotation: which is to say that Φ and $\mathbf{r}\Phi$ have the same distribution for every rotation $\mathbf{r}$ around the origin.

Motion-invariance: A stationary and isotropic point process is called *motion-invariant*.

2.3.2 Campbell's Theorem

It is often necessary to evaluate the expected sum of a function evaluated at the point process Φ. Campbell's theorem helps in evaluating such expectations. For any non-negative measurable function u,

$$\mathbb{E}\left[\sum_{x\in\Phi} u(x)\right] = \int_{\mathbb{R}^d} u(x)\Lambda(\mathrm{d}x). \tag{2.7}$$

The intensity measure Λ of Φ in (2.7) is a characteristic analogous to the mean of a real-valued random variable and defined as $\Lambda(B) = \mathbb{E}[\Phi(B)]$ for bounded subsets $B \subset \mathbb{R}^d$. So $\Lambda(B)$ is the mean number of points in B. If Φ is stationary then the intensity measure simplifies as $\Lambda(B) = \lambda|B|$ for some non-negative constant λ, which is called the intensity of Φ, where $|B|$ denotes the d dimensional volume of B. For stationary point processes, the right side in (2.7) is equal to $\lambda \int_{\mathbb{R}^d} u(x)\mathrm{d}x$. Therefore,

any two stationary point processes with same intensity lead to equal average sum of a function (when the mean value exists).

2.3.3 Laplace Functional

The *Laplace functional* L of random measure Ψ is defined by the following formula

$$L_{\Phi}(u) := \mathbb{E}\left[e^{-\int_{\mathbb{R}^d} u(x)\Psi(\mathrm{d}x)}\right] \tag{2.8}$$

where $u(\cdot)$ runs over the set $\mathcal{U}$ of all non-negative functions on $\mathbb{R}^d$. The Laplace functional completely characterizes the distribution of the random measure [3]. A point process Φ is a special case of a random measure Ψ. In the case of the Laplace functional of a point process, $\int_{\mathbb{R}^d} u(x)\Phi(\mathrm{d}x)$ can be also expressed as $\sum_{x\in\Phi} u(x)$ in (2.8). As an important example, the Laplace functional L of Poisson point process of intensity measure Λ is

$$L_{\Phi}(u) = \exp\left\{-\int_{\mathbb{R}^d} \left[1-\exp(-u(x))\right]\Lambda(\mathrm{d}x)\right\} \tag{2.9}$$

If the Poisson point process is stationary, the Laplace functional L of stationary Poisson point process Φ_{PPP} is

$$L_{\Phi_{\text{PPP}}}(u) = \exp\left\{-\lambda\int_{\mathbb{R}^d} \left[1-\exp(-u(x))\right]\mathrm{d}x\right\} \tag{2.10}$$

where λ is the intensity.

2.3.4 Voronoi Cell and Tessellation

In this section, we will introduce the concept of Voronoi cells and Voronoi tessellations. The Voronoi cell $V(x)$ of a point x of a general point process $\Phi \subset \mathbb{R}^d$ consists of those locations of $\mathbb{R}^d$ whose distance to x is not greater than their distance to any other point in Φ, i.e.,

$$V(x) := \{y \in \mathbb{R}^d : \|x-y\| \leq \|z-y\| \ \forall z \in \Phi \setminus x\}. \tag{2.11}$$

The Voronoi tessellation (or Voronoi diagram) is a decomposition of the space into the Voronoi cells of a general point process.

2.4 Alpha Stable Distribution

The interference in a wireless network follows a heavy-tailed distribution when the path loss model is given by $g(x) = \|x\|^{-\delta}, \delta > d$ and $x \in \mathbb{R}^d$, and it follows a stable distribution when the transmitting nodes form a Poisson point process.

2.4.1 The Characteristic Function

We first introduce real valued symmetric α-stable (SαS) random variables, which will later be used to define its complex counterpart used in this dissertation. A real valued (not necessarily symmetric) α-stable random variable, $w \sim S_\alpha(\sigma, \beta, \mu)$ has a characteristic function given by [48, 49]

$$\varphi(t) = \exp\left\{j\mu t - |\sigma t|^\alpha (1 - j\beta \operatorname{sign}(t)\, \omega(t, \alpha))\right\}, \tag{2.12}$$

where

$$\omega(t, \alpha) = \begin{cases} \tan\left(\frac{\pi\alpha}{2}\right) & \alpha \neq 1 \\ -\frac{2}{\pi}\log|t| & \alpha = 1 \end{cases}, \tag{2.13}$$

and

$$\operatorname{sign}(t) = \begin{cases} t = 1 & \text{if } t > 0 \\ t = 0 & \text{if } t = 0 \\ t = -1 & \text{if } t < 0 \end{cases}, \tag{2.14}$$

$\alpha \in (0, 2]$ is the characteristic exponent, $\beta \in [-1, 1]$ is the skew, $\sigma \in (0, \infty)$ is the scale and $\mu \in (-\infty, \infty)$ is the shift parameter. When $\beta = 0$, w has a symmetric distribution about μ. When $\beta = 0$ and $\mu = 0$, w is a SαS random variable. When

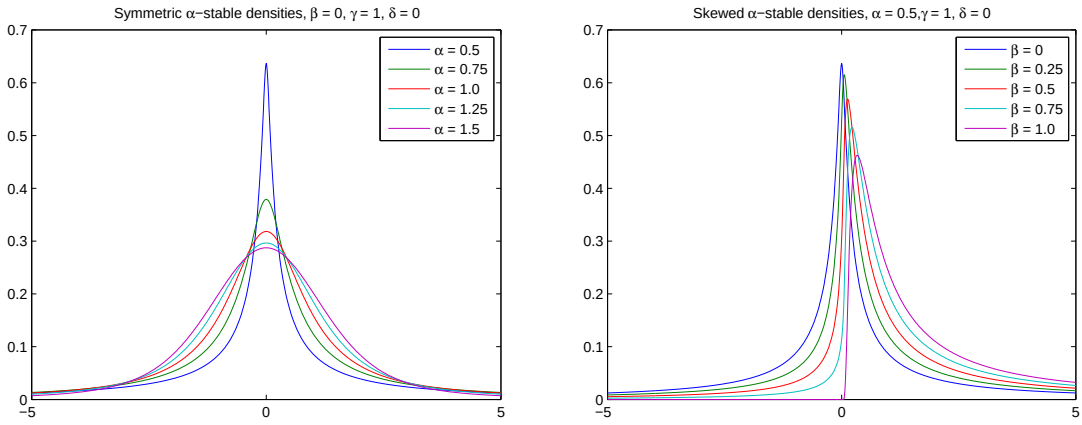

(A) Symmetric α-stable (B) Skewed α-stable

Figure 2.1: α-stable distributions

$\alpha = 2$ and $\beta = 0$, w is Gaussian, which is the only SαS random variable with finite variance. Since the Gaussian case is widely studied, we focus on $\alpha \in (0, 2)$ throughout. When $\sigma = 1$ and $\mu = 0$, w is said to be standardized [50, pp. 20]. Any SαS random variable $w \sim S_\alpha(\sigma, 0, 0)$ can be written as compound Gaussian, i.e., of the form $w = \sqrt{A}G$, where A and G are independent, with $A \sim S_{\alpha/2}\left([\cos(\pi\alpha/4)]^{2/\alpha}, 1, 0\right)$ is positive skewed α-stable random variable and $G \sim S_2(\sigma, 0, 0)$ is Gaussian random variable with mean zero and variance $2\sigma^2$ [48, pp. 38], [50, pp. 20]. The α-stable distributions for a few values of the characteristic exponent α are shown in Fig. 2.1.

2.4.2 Property and Asymptotic Expansions of Alpha Stable Distribution

In this section, we introduce an useful property of α-stable distribution. The α-stable random variables have many useful properties, a complete list of which can be found in [50, 48]. A property which is useful in this dissertation is reproduced below.

Proposition 2.4.1. *If* $x_i \sim S_\alpha(\sigma_i, \beta_i, \mu_i)$, $i = 1, ..., N$ *are independent, then* $\sum_{i=1}^N x_i \sim S_\alpha(\sigma, \beta, \mu)$, *where* $\sigma = \left(\sum_{i=1}^N \sigma_i^\alpha\right)^{1/\alpha}$, $\beta = \left(\sum_{i=1}^N \beta_i \sigma_i^\alpha\right)\left(\sum_{i=1}^N \sigma_i^\alpha\right)^{-1}$ *and* $\mu = \sum_{i=1}^N \mu_i$.

Although a closed-form expression for the PDF of SαS random variables exists only for a few special cases (e.g. Gaussian ($\alpha = 2$) and Cauchy ($\alpha = 1$)), asymptotic expansions for $\alpha \in (0, 2)$ are well known as $w \to \infty$:

$$f_\alpha(w) = \alpha C_\alpha \sigma^\alpha (1 + \beta) w^{-\alpha - 1} + O(w^{-2\alpha - 1}) \tag{2.15}$$

where the constant $C_\alpha := \Gamma(\alpha) \sin(\pi\alpha/2)/\pi$ [49]. Additionally, if $w \sim S_\alpha(\sigma, \beta, 0)$, the complementary cumulative distribution function (CCDF) of w satisfies the asymptotic relation as $\lambda \to \infty$:

$$P(w > \lambda) = C_\alpha \sigma^\alpha (1 + \beta) \lambda^{-\alpha} + O\left(\lambda^{-2\alpha}\right). \tag{2.16}$$

Chapter 3

SPACE-TIME CODING OVER FADING CHANNELS WITH STABLE NOISE

3.1 Literature Survey and Motivation

The additive Gaussian noise model has long been used because it produces simple and tractable mathematical models which are useful for gaining insight into the underlying behavior of communication systems. As the physical reality of most practical channels demonstrate much more sophisticated effects such as bursts and impulses, which arise as a consequence of man-made activity such as automobile spark plugs [51], microwave ovens [52], and network interference [53, 54, 55, 56, 57, 43], the Gaussian noise model may not be accurate. Such environments are also observed in urban and indoor channels as well as underwater acoustic channels [58, 59]. Therefore, impulsive noise which captures these physical effects should be considered. In such wireless environments, the performance is degraded both by fading and impulsive noise. To combat fading, antenna arrays are often used, giving rise to multi-input multi-output (MIMO) systems. Space-time coding has been used as one of the powerful diversity techniques in MIMO systems.

A number of performance analyses of STBC have been reported in the literature where the noise is Gaussian (see e.g., [60, 61, 62]). Recently, some works in the area of STBC in the presence of impulsive noise have also been reported. Performance of space-time diversity/coding for power line channels with Middleton Class-A noise model was studied by simulations in [63]. In [64] the code design criteria and the PEP upper bound were derived over a fading channel with Middleton Class-A noise. Subsequent work in [65] provided a closed-form expression for symbol error rate (SER)

of orthogonal STBC (OSTBC) when the noise follows a Gaussian mixture model.

Symmetric α-Stable (SαS) distributions are an important class of noise distributions which can successfully model a number of impulsive noise processes. Studies [53, 54, 55, 56, 57, 43] show that, in a multi-user network with power-law path loss, the multiple access interference results in a SαS distribution, when the interfering nodes are scattered according to a spatial Poisson point process (PPP). In [66], the performance evaluation of a MIMO system in SαS noise was performed by simulation with no closed-form expression for the error probability. Subsequent works in [43] and [67] provided closed form expressions for the bit error rate (BER) of linear diversity combining schemes for SαS noise environments in single-input multi-output (SIMO) environments. In [68, 69], the optimal linear receivers for SαS noise were studied in SIMO systems. To the best of our knowledge there is no analysis of MIMO systems over fading channels with SαS noise. To close this gap in the literature, our goal is to design receivers for, and analyze the effect of SαS noise on space-time coded systems. While the receivers derived herein apply to all space-time codes, the (PEP-based) performance analysis holds for OSTBCs.

Throughout this chapter, we use $(\cdot)^H$ for Hermitian, $(\cdot)^T$ for transpose, $\text{diag}(\mathbf{x})$ for a diagonal matrix with elements of $\mathbf{x}$ along the diagonal, $\|\cdot\|$ for the Frobenius norm for matrices and Euclidean norm for vectors, $\lambda_i(\cdot)$ for the i^{th} largest eigenvalue of a matrix, $\Re\{\cdot\}$ to denote the real part, $\Im\{\cdot\}$ to denote the imaginary part. Also, we use $E_{A,B}(C)$ to denote the expected value of the random variable C with respect to the distributions of the random variables A, B. Finally, we write $f(x) = O(g(x))$ as $x \to a$ to indicate that $\limsup_{x\to a} |f(x)/g(x)| < \infty$.

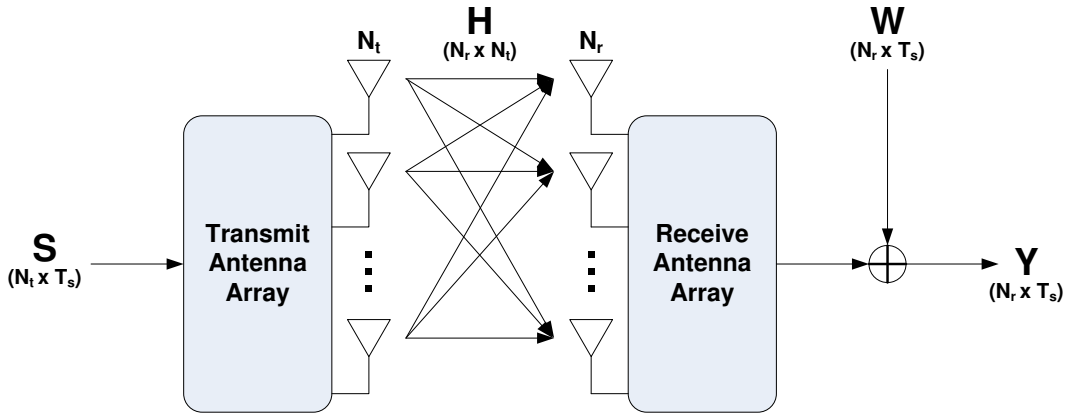

Figure 3.1: Space-Time Coding

3.2 System Model

A space-time code (STC) is a method employed to improve the reliability of data transmission in wireless communication systems using multiple transmit antennas. STCs rely on transmitting multiple, redundant copies of a data stream to the receiver to obtain coding gain and diversity gain as shown in Fig. 3.1. We consider a wireless communication system where the transmitter is equipped with N_{t} antennas and the receiver with N_{r} antennas. We consider the following standard MIMO flat-fading channel model:

$$\mathbf{Y} = \sqrt{\rho}\mathbf{H}\mathbf{S} + \mathbf{W} \tag{3.1}$$

where $\mathbf{Y}$ is the $N_{\mathrm{r}} \times T_{\mathrm{s}}$ received signal matrix, and T_{s} is the length of the transmitted data block; $\mathbf{H}$ is an $N_{\mathrm{r}} \times N_{\mathrm{t}}$ matrix, with independent and identical distributed (i.i.d.) circularly symmetric complex Gaussian entries with mean zero and variance 1; the average transmitted power at each transmitting antenna is denoted by the scalar ρ; $\mathbf{S}$ is the $N_{\mathrm{t}} \times T_{\mathrm{s}}$ transmitted data block, which is transmitted from a codeword set $\mathcal{S}$ with equal probability; $\mathbf{W}$ is the $N_{\mathrm{r}} \times T_{\mathrm{s}}$ network interference matrix. In this dissertation, $\mathbf{W}$ is the $N_{\mathrm{r}} \times T_{\mathrm{s}}$ additive impulsive noise matrix, with elements that

have a SαS distribution. In the following, we will briefly introduce two noise models (Model I and II) which assume dependent and independent noise components across antennas. In both Model I and II, the T_s columns of $\mathbf{W}$, $\mathbf{w}_1, ..., \mathbf{w}_{T_s}$, in (3.1) are independent.

- Under Model I, we assume $\mathbf{w}_k := [w_{1,k}, w_{2,k}, ..., w_{N_r,k}]^T$ is a complex isotropic SαS random vector, defined as

$$\mathbf{w}_k = \sqrt{A_k}(\mathbf{G}_k^R + j\mathbf{G}_k^I) \tag{3.2}$$

  where the scalar random variable $A_k \sim S_{\alpha/2}\left([\cos(\pi\alpha/4)]^{2/\alpha}, 1, 0\right)$ is independent of $\mathbf{G}_k^R$ and $\mathbf{G}_k^I$ which are Gaussian random vectors with i.i.d. elements which have mean zero and variance σ^2. This is a good assumption when the receiving antennas are influenced by the same physical process creating the impulse, thereby making the A_k of each branch the same. This might, for example, be an accurate model for a multi-antenna system where the antenna elements spaced closely. Mathematically, it is not difficult to see that in this case $w_{1,k}, w_{2,k}, ..., w_{N_r,k}$ will be statistically dependent [50, pp. 83].

- Under Model II, the j, k element of $\mathbf{W}$ is given by

$$[\mathbf{W}]_{j,k} = \sqrt{A_{j,k}}(G_{j,k}^R + jG_{j,k}^I) \tag{3.3}$$

  where $A_{j,k}, G_{j,k}^R$ and $G_{j,k}^I$ are distributed as in Model I, but are i.i.d., and $[\mathbf{W}]_{j,k}$ is the (j, k) element of matrix $\mathbf{W}$.

In both Model I and II, $w_{j,k}$ has a unity scale parameter ($\sigma = 1$), since any scale is subsumed in ρ in (3.1). It can be shown that only the moments of order α or less exist for any SαS random variable [48, pp. 22], as a result of which the conventional definition of SNR holds only for the Gaussian case ($\alpha = 2$). However, with a slight

abuse of terminology, we will refer to ρ as the SNR, even when $\alpha < 2$, since ρ quantifies the relative scale of the signal versus the noise.

3.3 Receiver Design and Performance

We assume throughout that the channel $\mathbf{H}$ is known at the receiver. Under Model I, we start with the GAR for which A_k are assumed known at the receiver at each time $k = 1, ..., T_{\mathrm{s}}$. The GAR is optimal when A_k are known, so that its performance can serve as a benchmark for any practical receiver that does not have this knowledge.

3.3.1 Genie-aided Receiver

The GAR maximizes the posterior probability and hence minimizes the probability of error, when $\mathbf{H}$ and $A_1, ..., A_{T_{\mathrm{s}}}$ are known. In the following, we are going to derive the decoding rule. To express in matrix form, we define $\mathbf{A} = \mathrm{diag}\big(\big[1/\sqrt{A_1}, ..., 1/\sqrt{A_{T_{\mathrm{s}}}}\big]\big)$. Right multiplying (3.1) by $\mathbf{A}$, we obtain:

$$\mathbf{YA} = \sqrt{\rho}\mathbf{HSA} + \mathbf{WA} \tag{3.4}$$

so that the product $\mathbf{WA}$ has i.i.d. $\mathcal{CN}(0, 1)$ entries. Since the elements of $\mathbf{WA}$ are now white Gaussian and the codewords are equally likely, the optimal decision rule is to minimize the Euclidean distance:

$$\hat{\mathbf{S}} = \underset{\mathbf{S}}{\mathrm{argmin}} \|\mathbf{YA} - \sqrt{\rho}\mathbf{HSA}\|^2. \tag{3.5}$$

To express the PEP that $\mathbf{S}$ is transmitted and $\mathbf{S}'$ is received for the GAR in (3.5), we follow the derivation in the Gaussian noise case and obtain,

$$P\left(\mathbf{S} \to \mathbf{S}' | \mathbf{H}, \mathbf{A}\right) = Q\left(\sqrt{\frac{\rho \|\mathbf{H}\left(\mathbf{S} - \mathbf{S}'\right)\mathbf{A}\|^2}{2}}\right). \tag{3.6}$$

Using (3.6) and Craig's representation of the Q function,

$$Q(x) = \frac{1}{\pi}\int_0^{\frac{\pi}{2}} \exp\left(-\frac{x^2}{2\sin^2\theta}\right)\, \mathrm{d}\theta, \tag{3.7}$$

(3.6) can be expressed as follows:

$$P\left(\mathbf{S}\to\mathbf{S}'|\mathbf{H},\mathbf{A}\right)=\frac{1}{\pi}\int_0^{\frac{\pi}{2}}\exp\left(\frac{\rho\|\mathbf{H}\left(\mathbf{S}-\mathbf{S}'\right)\mathbf{A}\|^2}{4\sin^2\theta}\right)\,\mathrm{d}\theta. \tag{3.8}$$

Taking expectation with respect to $\mathbf{H}$ and $\mathbf{A}$, we get

$$E_{\mathbf{H},\mathbf{A}}P\left(\mathbf{S}\to\mathbf{S}'|\mathbf{A}\right)=\frac{1}{\pi}\int_0^{\frac{\pi}{2}}E_{\mathbf{A}}\left[\prod_{i=1}^{N_\mathrm{t}}\left(\frac{1}{1+\frac{\rho}{4\sin^2\theta}\lambda_i(\mathbf{B})}\right)^{N_\mathrm{r}}\right]\,\mathrm{d}\theta \tag{3.9}$$

where $\mathbf{B}:=(\mathbf{S}-\mathbf{S}')\mathbf{A}\mathbf{A}^H(\mathbf{S}-\mathbf{S}')^H$. Using (3.9), we can show that the code design criterion under SαS noise remains the same as the Gaussian noise case as follows. To obtain the maximum diversity order, we need $\mathbf{B}$ to be a full rank matrix for any realization of $\mathbf{A}$ in (3.9). Since $\mathbf{A}$ is diagonal with nonzero diagonal elements, it is a full rank matrix. Therefore, if the codeword different matrix $\mathbf{S}-\mathbf{S}'$ is full rank, $\mathbf{B}$ is guaranteed to be a full rank matrix.

When $\mathbf{S}-\mathbf{S}'$ is square and unitary which is satisfied by e.g., the Alamouti code [70], the eigenvalues satisfy $\lambda_i(\mathbf{B})=1/A_i$. Since $\{A_i\}_{i=1,\ldots,N_\mathrm{t}}$ are i.i.d., each term of the product in (3.9) has the same expected value, which results in

$$E_{\mathbf{H},\mathbf{A}}P\left(\mathbf{S}\to\mathbf{S}'|\mathbf{A}\right)=\frac{1}{\pi}\int_0^{\frac{\pi}{2}}\left(E_{\mathbf{A}}\left[\left(\frac{1}{1+\frac{\rho}{4\sin^2\theta}\frac{1}{A}}\right)^{N_\mathrm{r}}\right]\right)^{N_\mathrm{t}}\,\mathrm{d}\theta \tag{3.10}$$

where A represents any of the random variables A_i. To simplify the expectation in the RHS of (3.10), recall that $A\sim S_{\alpha/2}([\cos(\pi\alpha/4)]^{2/\alpha},1,0)$, so that

$$E_{\mathbf{A}}\left[\left(\frac{1}{1+\frac{\rho}{4\sin^2\theta}\frac{1}{A}}\right)^{N_\mathrm{r}}\right]=\int_0^\infty\left(\frac{4A\sin^2\theta}{4A\sin^2\theta+\rho}\right)^{N_\mathrm{r}}f_{\alpha/2}(A)\,\mathrm{d}A. \tag{3.11}$$

The PDF $f_{\alpha/2}(A)$ as suggested by the asymptotic expansion for the PDF of α-stable distribution in (2.15) as $A\to\infty$ is given by

$$f_{\alpha/2}(A)=\alpha\cos(\pi\alpha/4)C_{\alpha/2}A^{-(1+\alpha/2)}+O\left(A^{-(1+\alpha)}\right). \tag{3.12}$$

Substituting (3.12) in (3.11), we get

$$\begin{aligned}
&\int_0^{\infty} \left(\frac{4A\sin^2\theta}{4A\sin^2\theta+\rho}\right)^{N_{\mathrm{r}}} \left[\alpha C_{\alpha/2}\cos\left(\frac{\pi\alpha}{4}\right)A^{-\left(1+\frac{\alpha}{2}\right)}+O\left(A^{-(1+\alpha)}\right)\right]\,\mathrm{d}A \\
&= \left(\frac{\alpha}{2}\frac{\Gamma\left(\frac{\alpha}{2}\right)\Gamma\left(N_{\mathrm{r}}-\frac{\alpha}{2}\right)}{\Gamma\left(1-\frac{\alpha}{2}\right)\Gamma(N_{\mathrm{r}})}\right)\left(\frac{\rho}{4\sin^2\theta}\right)^{-\frac{\alpha}{2}}+O\left(\rho^{-\alpha}(4\sin^2\theta)^{\alpha}\right) \\
&= \left(\frac{\Gamma\left(1+\frac{\alpha}{2}\right)\Gamma\left(N_{\mathrm{r}}-\frac{\alpha}{2}\right)}{\Gamma\left(1-\frac{\alpha}{2}\right)\Gamma(N_{\mathrm{r}})}\right)\left(\frac{\rho}{4\sin^2\theta}\right)^{-\frac{\alpha}{2}}+O\left(\rho^{-\alpha}\right). \qquad (3.13)
\end{aligned}$$

Plugging (3.13) in (3.10), and using the binomial expansion, we get

$$\begin{aligned}
P\left(\mathbf{S}\to\mathbf{S}'\right) &= \frac{1}{\pi}\int_0^{\frac{\pi}{2}}\left[\left(\frac{\Gamma\left(1+\frac{\alpha}{2}\right)\Gamma\left(N_{\mathrm{r}}-\frac{\alpha}{2}\right)}{\Gamma\left(1-\frac{\alpha}{2}\right)\Gamma(N_{\mathrm{r}})}\right)\left(\frac{\rho}{4}\right)^{-\frac{\alpha}{2}}\right]^{N_{\mathrm{t}}}\sin^{\alpha N_{\mathrm{t}}} \\
&\quad +O\left(\rho^{-\frac{\alpha}{2}(N_{\mathrm{t}}+1)}\right)\sin^{\alpha(N_{\mathrm{t}}-1)}\theta\,\mathrm{d}\theta. \qquad (3.14)
\end{aligned}$$

Solving the integral in (3.14), we get

$$\begin{aligned}
P\left(\mathbf{S}\to\mathbf{S}'\right) &= \Bigg[\underbrace{\left(\frac{1}{2\sqrt{\pi}}\frac{\Gamma\left(\frac{\alpha N_{\mathrm{t}}+1}{2}\right)}{\Gamma\left(\frac{\alpha N_{\mathrm{t}}}{2}+1\right)}\right)^{-\frac{2}{\alpha N_{\mathrm{t}}}}\left(\frac{\Gamma\left(1+\frac{\alpha}{2}\right)\Gamma\left(N_{\mathrm{r}}-\frac{\alpha}{2}\right)}{\Gamma\left(1-\frac{\alpha}{2}\right)\Gamma(N_{\mathrm{r}})}4^{\frac{\alpha}{2}}\right)^{-\frac{2}{\alpha}}}_{=:G_{\mathrm{GAR}}(N_{\mathrm{t}},N_{\mathrm{r}},\alpha)}\ \rho\Bigg]^{-\frac{\alpha N_{\mathrm{t}}}{2}} \\
&\quad +O\left(\rho^{-\frac{\alpha}{2}(N_{\mathrm{t}}+1)}\right). \qquad (3.15)
\end{aligned}$$

Using $(G_{\mathrm{c}}\cdot\rho)^{-G_{\mathrm{d}}}$ expression to present PEP, we can define the diversity order, G_{d}, and the coding gain, G_{c}, from the PEP. The coding gain is defined as the amount that bit energy or signal-to-noise power ratio can be reduced under the coding technique for a given bit error rate. In (3.15), the G_{c} is $G_{\mathrm{GAR}}(N_{\mathrm{t}},N_{\mathrm{r}},\alpha)$ and the G_{d} is $\alpha N_{\mathrm{t}}/2$. The implications of (3.15) are interesting, because it suggests that the diversity order depends on the number of transmit antennas, N_{t}, and the noise parameter, α. However, the number of receive antennas, N_{r}, does not contribute to the diversity order. This is due to the fact that the noise is not i.i.d. across antennas in Model I.

In order to investigate the behavior of the coding gain as a function of N_{r}, by differentiating the natural logarithm of the coding gain with respect to N_{r}, we get

$$\frac{\partial}{\partial N_{\mathrm{r}}}\log G_{\mathrm{GAR}} = -\frac{1}{\alpha}\left[\psi\left(N_{\mathrm{r}}-\frac{\alpha}{2}\right)-\psi\left(N_{\mathrm{r}}\right)\right] \qquad (3.16)$$

where $\psi(x) := \frac{\mathrm{d}\log\Gamma(x)}{\mathrm{d}x}$ is the digamma function as defined in [71, pp. 258-259]. In (3.16), since $\psi(x)$ is a monotonically increasing function for $x > 0$, the term inside the brackets is negative $\forall \alpha \in (0, 2)$. Therefore, the coding gain is a monotonically increasing function of N_{r}. So, even though N_{r} does not contribute to diversity, it does improve the coding gain.

Regarding the analysis of $G_{\mathrm{GAR}}(N_{\mathrm{t}}, N_{\mathrm{r}}, \alpha)$ in (3.15) with respect to N_{t} as explained next. To prove the coding gain, $G_{\mathrm{GAR}}(N_{\mathrm{t}}, N_{\mathrm{r}}, \alpha)$, is a monotonically decreasing and convex function with respect to N_{t}, we will show a stronger statement which states that the coding gain is a logarithmically completely monotonic (c.m.) function which means that the derivatives of the logarithm satisfy:

$$(-1)^n \left(\frac{\partial}{\partial N_{\mathrm{t}}}\right)^n \log G_{\mathrm{GAR}}(N_{\mathrm{t}}, N_{\mathrm{r}}, \alpha) \geq 0 \tag{3.17}$$

for $n \in \mathbb{Z}^+$. Letting $\alpha N_{\mathrm{t}}/2 = x$ in the coding gain of (3.15), it suffices to show that

$$h(x) := \frac{(2\sqrt{\pi})^{\frac{1}{x}} \Gamma(x+1)^{\frac{1}{x}}}{\Gamma\left(x+\frac{1}{2}\right)^{\frac{1}{x}}} \tag{3.18}$$

is a logarithmically c.m. function. Taking logarithm in (3.18), we get

$$f(x) = \log h(x) = \frac{1}{x}\log 2\sqrt{\pi} + \frac{1}{x}\log\Gamma(x+1) - \frac{1}{x}\log\Gamma\left(x+\frac{1}{2}\right). \tag{3.19}$$

Using Leibnitz' rule, $[u(x)v(x)]^{(n)} = \sum_{k=0}^{n} \binom{n}{k} u^{(k)}(k) v^{(n-k)}(k)$, in each of the last two terms in (3.19), we obtain

$$\begin{aligned} f^{(n)}(x) &= (-1)^n \frac{n!}{x^{n+1}} \log 2\sqrt{\pi} + \sum_{k=0}^{n} \binom{n}{k} \left(\frac{1}{k}\right)^{(n-k)} \\ &\quad \times \left[[\log\Gamma(x+1)]^{(k)} - \left[\log\Gamma\left(x+\frac{1}{2}\right)\right]^{(k)} \right] \\ &= \frac{(-1)^n n!}{x^{n+1}} g(x) \end{aligned} \tag{3.20}$$

where

$$g(x) := \log 2\sqrt{\pi} + \log\Gamma(x+1) - \log\Gamma(x+\frac{1}{2}) + \sum_{k=1}^{n} \frac{(-1)^k x^k}{k!}\psi^{(k-1)}(x+1) - \sum_{k=1}^{n} \frac{(-1)^k x^k}{k!}\psi^{(k-1)}\left(x+\frac{1}{2}\right) \quad (3.21)$$

and $\psi^{(n)}(x)$ is the polygamma function as defined follows [71, pp. 260]:

$$\psi^{(n)}(x) = (-1)^{n+1}\int_0^\infty \frac{t^n}{1-e^{-t}} e^{-xt}\,\mathrm{d}t. \quad (3.22)$$

The proof will be complete when we show $g(x) \geq 0$ for $x > 0$ since that would make (3.20) positive. The first derivative of $g(x)$ can be expressed as follows:

$$g'(x) = \frac{(-1)^n x^n}{n!}\left[\psi^{(n)}(x+1) - \psi^{(n)}\left(x+\frac{1}{2}\right)\right]. \quad (3.23)$$

Using (3.22), we conclude

$$\frac{1}{x^n}g'(x) = \frac{1}{n!}\int_0^\infty \left(\frac{e^{-\frac{t}{2}} - e^{-t}}{1-e^{-t}}\right) t^n e^{-xt}\,\mathrm{d}t > 0, \quad (3.24)$$

since $\left(\frac{e^{-\frac{t}{2}}-e^{-t}}{1-e^{-t}}\right) > 0$ for $t > 0$. Thus, the function $g(x)$ is increasing and $g(x) > g(0) > 0$ on $(0,\infty)$, which implies $(-1)^n f^{(n)}(x) > 0$ and $n = 0, 1, 2, \ldots$. Thus, $h(x)$ is a logarithmically c.m. function. Since a logarithmically c.m. function is also c.m. [72], $h(x)$ is a c.m. function, which in turn has convex and decreasing functions as a special case. Therefore, it is proved the coding gain is a monotonically decreasing and convex function with respect to N_t.

For Model II the GAR can also be derived by using the Hadamard product with $\mathbf{A}$ which is a matrix with (j,k) element $1/\sqrt{A_{j,k}}$. However, its performance is not tractable.

3.3.2 Minimum Distance Receiver

The MDR, which is optimal over Gaussian noise minimizes the Euclidean distance:

$$\hat{\mathbf{S}} = \underset{\mathbf{S}}{\operatorname{argmin}} \|\mathbf{Y} - \sqrt{\rho}\mathbf{H}\mathbf{S}\|^2. \quad (3.25)$$

Note that unlike the GAR in (3.5), the MDR does not depend on $\mathbf{A}$. We now derive the PEP for the MDR. Define $\mathbf{E} := \mathbf{H}(\mathbf{S}-\mathbf{S}')/\|\mathbf{H}(\mathbf{S}-\mathbf{S}')\|$, and let $e_{j,k}$ be the (j,k) element of $\mathbf{E}$. The PEP and its upper bound for the MDR are given by:

$$\begin{aligned} P\left(\mathbf{S}\to\mathbf{S}'|\mathbf{H},\mathbf{A}\right) &= Q\left(\sqrt{\frac{\rho\|\mathbf{H}\left(\mathbf{S}-\mathbf{S}'\right)\|^2}{2\sum_{k=1}^{T_\mathrm{s}}A_k\sum_{j=1}^{N_\mathrm{r}}|e_{j,k}|^2}}\right) && (3.26)\\ &\leq Q\left(\sqrt{\frac{\rho\|\mathbf{H}\left(\mathbf{S}-\mathbf{S}'\right)\|^2}{2A_{\max}\sum_{k=1}^{T_\mathrm{s}}\sum_{j=1}^{N_\mathrm{r}}|e_{j,k}|^2}}\right) && (3.27)\\ &= Q\left(\sqrt{\frac{\rho\|\mathbf{H}\left(\mathbf{S}-\mathbf{S}'\right)\|^2}{2A_{\max}}}\right) && (3.28)\\ &= \frac{1}{\pi}\int_0^{\frac{\pi}{2}}\exp\left(\frac{\rho\|\mathbf{H}\left(\mathbf{S}-\mathbf{S}'\right)\|^2}{4\sin^2\theta A_{\max}}\right)\,\mathrm{d}\theta && (3.29)\end{aligned}$$

where $A_{\max} := \max_k A_k$ is the maximum value among $A_1,...,A_{T_\mathrm{s}}$. In (3.28) we used the fact that $\|\mathbf{E}\|=1$, and in (3.29) we used (3.7). Taking expectation with respect to $\mathbf{H}$ and $A_{\max}$, the following upper bound on the average PEP is obtained:

$$E_{\mathbf{H},A_{\max}}P\left(\mathbf{S}\to\mathbf{S}'|A_{\max}\right)\leq\frac{1}{\pi}\int_0^{\frac{\pi}{2}}E_{A_{\max}}\left[\prod_{i=1}^{N_\mathrm{t}}\left(\frac{1}{1+\frac{\rho}{4\sin^2\theta}\frac{\lambda_i(\mathbf{C})}{A_{\max}}}\right)^{N_\mathrm{r}}\right]\,\mathrm{d}\theta \qquad (3.30)$$

where $\mathbf{C} := (\mathbf{S}-\mathbf{S}')(\mathbf{S}-\mathbf{S}')^H$. When $\mathbf{S}-\mathbf{S}'$ is square and unitary, we can rewrite (3.30) as follows:

$$E_{\mathbf{H},A_{\max}}P\left(\mathbf{S}\to\mathbf{S}'|A_{\max}\right)\leq\frac{1}{\pi}\int_0^{\frac{\pi}{2}}E_{A_{\max}}\left[\left(\frac{1}{1+\frac{\rho}{4\sin^2\theta}\frac{1}{A_{\max}}}\right)^{N_\mathrm{r}N_\mathrm{t}}\right]\,\mathrm{d}\theta. \qquad (3.31)$$

Using the asymptotic CCDF of α-stable distribution in (2.16) and order statistics, we can find the PDF of $A_{\max}$ as follows:

$$\begin{aligned} f_{A_{\max}}(x) &= \frac{\alpha}{2}T_\mathrm{s}2C_{\alpha/2}\cos\left(\frac{\pi\alpha}{4}\right)x^{-\left(1+\frac{\alpha}{2}\right)}\left(1-2C_{\alpha/2}\cos\left(\frac{\pi\alpha}{4}\right)x^{-\frac{\alpha}{2}}\right)^{T_\mathrm{s}-1}\\ &\quad +O\left(x^{-\frac{\alpha}{2}(T_\mathrm{s}+1)-1}\right). && (3.32)\end{aligned}$$

If $T_{\mathrm{s}} \geq 2$ and is equal to N_{t}, plugging (3.32) in (3.31) and using binomial expansion, we can get as follows:

$$\begin{aligned}
&\int_0^{\infty} \left(\frac{4x\sin^2\theta}{4x\sin^2\theta+\rho}\right)^{N_{\mathrm{r}}N_{\mathrm{t}}} \left(\frac{\alpha N_{\mathrm{t}}}{2}\sum_{k=0}^{N_{\mathrm{t}}-1}(-1)^k\left(2C_{\alpha/2}\cos\left(\frac{\pi\alpha}{4}\right)\right)^{k+1} x^{-\left(1+\frac{\alpha}{2}+\frac{\alpha k}{2}\right)}\right. \\
&\qquad \left.+O\left(x^{-\frac{\alpha}{2}(N_{\mathrm{t}}+1)-1}\right)\right)\mathrm{d}x \\
&= \frac{\alpha N_{\mathrm{t}}}{2}\sum_{k=0}^{N_{\mathrm{t}}-1}\left[(-1)^k\left(\frac{\Gamma\left(\frac{\alpha(1+k)}{2}\right)\Gamma\left(N_{\mathrm{r}}N_{\mathrm{t}}-\frac{\alpha(1+k)}{2}\right)}{\left(\Gamma\left(1-\frac{\alpha}{2}\right)\right)^{(k+1)}\Gamma(N_{\mathrm{r}}N_{\mathrm{t}})}\right)\left(\frac{\rho}{4\sin^2\theta}\right)^{-\frac{\alpha(1+k)}{2}}\right] \\
&\qquad +O\left(\rho^{-\frac{\alpha(N_{\mathrm{t}}+1)}{2}}\right) \\
&= \left(\frac{\alpha N_{\mathrm{t}}}{2}\frac{\Gamma\left(\frac{\alpha}{2}\right)\Gamma\left(N_{\mathrm{r}}N_{\mathrm{t}}-\frac{\alpha}{2}\right)}{\Gamma\left(1-\frac{\alpha}{2}\right)\Gamma(N_{\mathrm{r}}N_{\mathrm{t}})}\right)\left(\frac{\rho}{4\sin^2\theta}\right)^{-\frac{\alpha}{2}} + O\left(\rho^{-\alpha}(4\sin^2\theta)^{\alpha}\right)+\cdots \\
&\qquad +O\left(\rho^{-\frac{\alpha(N_{\mathrm{t}}+1)}{2}}\right) \\
&= \left(\frac{N_{\mathrm{t}}\Gamma\left(1+\frac{\alpha}{2}\right)\Gamma\left(N_{\mathrm{r}}N_{\mathrm{t}}-\frac{\alpha}{2}\right)}{\Gamma\left(1-\frac{\alpha}{2}\right)\Gamma(N_{\mathrm{r}}N_{\mathrm{t}})}\right)\left(\frac{\rho}{4\sin^2\theta}\right)^{-\frac{\alpha}{2}} + O\left(\rho\right)^{-\alpha}. \qquad (3.33)
\end{aligned}$$

Plugging (3.33) in (3.31), we get

$$P\left(\mathbf{S}\to\mathbf{S}'\right) = \frac{1}{\pi}\int_0^{\frac{\pi}{2}}\left(\frac{N_{\mathrm{t}}\Gamma\left(1+\frac{\alpha}{2}\right)\Gamma\left(N_{\mathrm{r}}N_{\mathrm{t}}-\frac{\alpha}{2}\right)}{\Gamma\left(1-\frac{\alpha}{2}\right)\Gamma(N_{\mathrm{r}}N_{\mathrm{t}})}\right)\left(\frac{\rho}{4}\right)^{-\frac{\alpha}{2}}\sin^{\alpha}\theta + O\left(\rho\right)^{-\alpha}\ \mathrm{d}\theta. \qquad (3.34)$$

Solving the integral in (3.34), we get

$$P\left(\mathbf{S}\to\mathbf{S}'\right) \leq \left[\underbrace{\left(\frac{N_{\mathrm{t}}}{2\sqrt{\pi}}\frac{\Gamma\left(\frac{1+\alpha}{2}\right)\Gamma\left(N_{\mathrm{r}}N_{\mathrm{t}}-\frac{\alpha}{2}\right)}{\Gamma\left(1-\frac{\alpha}{2}\right)\Gamma(N_{\mathrm{r}}N_{\mathrm{t}})}4^{\frac{\alpha}{2}}\right)^{-\frac{2}{\alpha}}}_{=:G_{\mathrm{MDR}}(N_{\mathrm{t}},N_{\mathrm{r}},\alpha)}\ \rho\right]^{-\frac{\alpha}{2}} + O\left(\rho^{-\alpha}\right). \qquad (3.35)$$

Equation (3.35) suggests that the diversity order is always $\alpha/2$ regardless the number of antennas which is reduced compared to the GAR where it was $\alpha N_{\mathrm{t}}/2$.

The behavior of the coding gain as a function of N_{r} can be obtained from the derivative given by

$$\frac{\partial}{\partial N_{\mathrm{r}}}\log G_{\mathrm{MDR}} = -\frac{2N_{\mathrm{t}}}{\alpha}\left[\psi\left(N_{\mathrm{r}}N_{\mathrm{t}}-\frac{\alpha}{2}\right)-\psi\left(N_{\mathrm{r}}N_{\mathrm{t}}\right)\right]. \qquad (3.36)$$

In (3.36), since $\psi(x)$ is a monotonically increasing function for $x > 0$, we can verify the term inside the brackets is negative $\forall \alpha \in (0, 2)$. Therefore, the coding gain is a monotonically increasing function of N_{r}. Next, by differentiating the log-coding gain with respect to N_{t}, we get

$$\frac{\partial}{\partial N_{\mathrm{t}}} \log G_{\mathrm{MDR}} = -\frac{2}{\alpha} \left[\frac{1}{N_{\mathrm{t}}} + N_{\mathrm{r}} \left[\psi \left(N_{\mathrm{r}} N_{\mathrm{t}} - \frac{\alpha}{2} \right) - \psi \left(N_{\mathrm{r}} N_{\mathrm{t}} \right) \right] \right]. \tag{3.37}$$

It can be shown numerically that the $G_{\mathrm{MDR}}(N_{\mathrm{t}}, N_{\mathrm{r}}, \alpha)$ monotonically decreases with N_{t} when $\alpha \in (0, \alpha_0)$ for some constant α_0. Unlike the GAR, in case of the MDR the number of transmit antennas, N_{t}, does not contribute to the diversity order. Hence when $\alpha \in (0, \alpha_0)$ the performance of MDR will be worse as N_{t} increases. Intuitively, the reason for the deterioration in performance is that when α is small, the sum of independent noise samples do not "average out" like it does when the noise has a finite variance. In other words, when α is small enough the performance bound of MDR suffers from increased transmit antennas! On the other hand, the coding gain is a monotonically increasing function of N_{t} when $\alpha \in (\alpha_1, 2)$ for some constant α_1. In other words, when $\alpha \in (\alpha_1, 2)$ the coding gain increases as the number of transmit antennas increase. When $\alpha \in (\alpha_0, \alpha_1)$, the coding gain is a concave function of N_{t}. The values of α_0 and α_1 depend on N_{r} (e.g. when $N_{\mathrm{r}} = 1$, $\alpha_0 \approx 1.333$ and $\alpha_1 \approx 1.799$).

For Model II the PEP of MDR can be derived by using $A_{\max} := \max_{j,k} A_{j,k}$ in (3.27). Following the same derivation, the PEP of MDR for Model II is obtained by multiplying $G_{\mathrm{MDR}}(N_{\mathrm{t}}, N_{\mathrm{r}}, \alpha)$ in (3.35) with $N_{\mathrm{r}}^{-2/\alpha}$ which implies less coding gain and the same diversity order. This is in contrast with the GAR which will be shown in the simulations to have better performance under Model II compared to Model I. In conclusion, for SαS noise environments the conventional MDR receiver has poor performance especially for small α.

3.3.3 Maximum Likelihood Receiver

We introduce the optimal ML receiver for Model I and II. Firstly, the optimal ML receiver for Model I is given by

$$\hat{\mathbf{S}} = \underset{\mathbf{S}}{\operatorname{argmax}} \prod_{k=1}^{T_{\mathrm{s}}} f_\alpha \left(\|\mathbf{y}_k - \sqrt{\rho}\mathbf{H}\mathbf{s}_k\| \right) \tag{3.38}$$

$$= \underset{\mathbf{S}}{\operatorname{argmax}} \sum_{k=1}^{T_{\mathrm{s}}} \log f_\alpha \left(\|\mathbf{y}_k - \sqrt{\rho}\mathbf{H}\mathbf{s}_k\| \right) \tag{3.39}$$

where $f_\alpha(\|\mathbf{x}\|)$ is a probability density function of amplitude distribution of d-dimensional multivariate isotropic stable random variables and is given by [73]:

$$f_\alpha(r) = \frac{2}{2^{d/2}\Gamma(d/2)} \int_0^\infty (rt)^{d/2} J_{d/2-1}(rt) e^{\sigma^\alpha t^\alpha} dt \tag{3.40}$$

where $r = \|\mathbf{x}\| = \sqrt{X_1^2 + \cdots + X_d^2}$ and $J_\nu(\cdot)$ is the Bessel function of order ν.

In case of Model II, complex symmetric α-stable random variables are independent in both space and time. Thus, we can modify the optimal ML receiver for Model II as follows:

$$\hat{\mathbf{S}} = \underset{\mathbf{S}}{\operatorname{argmax}} \sum_{k=1}^{T_{\mathrm{s}}} \sum_{j=1}^{N_{\mathrm{r}}} \log f_\alpha(\|[\mathbf{Y}]_{j,k} - \sqrt{\rho}[\mathbf{HS}]_{j,k}\|). \tag{3.41}$$

Since $f_\alpha(r)$ cannot be expressed in terms of closed-form elementary functions, these ML receivers are seen to be computationally complex, and dependent on the noise parameters σ and α. We now consider receivers that perform nearly optimally, with the advantage of reduced complexity and not requiring knowledge of noise parameters, when compared to the ML receivers.

3.3.4 Asymptotically Optimal Receiver

To simplify (3.38), we use the expression for the tail of $f_\alpha(\cdot)$ in [73]

$$f_\alpha(r) = \alpha 2^\alpha \frac{\sin(\pi\alpha/2)}{\pi\alpha/2} \frac{\Gamma((\alpha+2)/2)\Gamma((\alpha+d)/2)}{\Gamma(d/2)} r^{-(\alpha+1)} + O(r^{-(2\alpha+1)}) \tag{3.42}$$

as $r \to \infty$, where we note that $\alpha 2^{\alpha} \frac{\sin(\pi\alpha/2)}{\pi\alpha/2} \frac{\Gamma((\alpha+2)/2)\Gamma((\alpha+d)/2)}{\Gamma(d/2)} > 0$. Now, using the dominant term of (3.42) in (3.38) and simplifying, we get

$$\hat{\mathbf{S}} = \underset{\mathbf{S}}{\operatorname{argmin}} \prod_{k=1}^{T_{\mathrm{s}}} \|\mathbf{y}_k - \sqrt{\rho}\mathbf{H}\mathbf{s}_k\| \tag{3.43}$$

$$= \underset{\mathbf{S}}{\operatorname{argmin}} \sum_{k=1}^{T_{\mathrm{s}}} \log\|\mathbf{y}_k - \sqrt{\rho}\mathbf{H}\mathbf{s}_k\|. \tag{3.44}$$

Using same approach as Model I, we can modify the asymptotically optimal receiver for Model II as follows:

$$\hat{\mathbf{S}} = \underset{\mathbf{S}}{\operatorname{argmin}} \sum_{k=1}^{T_{\mathrm{s}}} \sum_{j=1}^{N_{\mathrm{r}}} \log\|[\mathbf{Y}]_{j,k} - \sqrt{\rho}[\mathbf{HS}]_{j,k}\|. \tag{3.45}$$

The resulting receivers are asymptotically optimal at high SNR and relatively simple.

A few comments about complexity of the ML receiver and AOR follow. In (3.39) and (3.44), we need to evaluate matrix norms. The only difference between (3.39) and (3.44) is that the equation (3.39) needs to evaluate the metric in (3.40) additionally. In (3.40), it is needed to evaluate an elementary function, a special function (i.e., the Bessel function) and an integration of these functions for each candidate codeword $\mathbf{S}$. Instead of evaluation of (3.40), we can alternatively use a lookup table for the numerical values of (3.40). Such a lookup table would have sizable memory requirements since a lookup table would contain values for each of the α and σ values corresponding to the noise parameters. For example, if the sizes of quantized α and σ values are N_α and N_σ respectively, we need the $N_\alpha \cdot N_\sigma$ entries in the table. In addition to these kinds of high computational complexity, the ML receiver also requires to estimate α and σ values of SαS noise. However in case of the AOR which performs within a tenth of a dB of the ML receiver which will be shown in Section 3.4, we do not need to evaluate the equation (3.40) and estimate the α and σ values.

Therefore we propose to use the AOR for impulsive noise due to its relatively low complexity and its reasonable performance. Though our analysis is based on

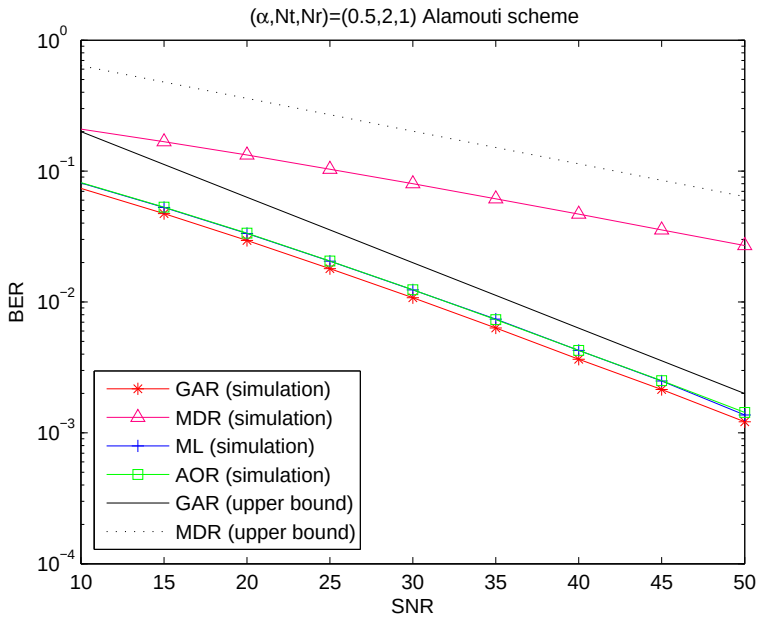

Figure 3.2: Performance comparison of GAR, MDR, ML receiver, and AOR over a channel with highly impulsive noise ($\alpha = 0.5$) with $N_{\mathrm{t}} = 2$ and $N_{\mathrm{r}} = 1$

the receivers for Model I, it will be similar in case of Model II. We note that the asymptotically optimal receivers in (3.44) and (3.45) are additive and therefore can be used in conjunction with the Viterbi algorithm when $\mathbf{S}$ is a codeword on a trellis.

3.4 Simulations

In this section, we verify our results through Monte Carlo simulations. In our simulations, we assume that $\alpha = 1.43$, which corresponds to the value estimated in [74] for modeling radio frequency interference in laptop receivers. We also consider a "highly impulsive" scenario, with $\alpha = 0.5$, which corresponds to a path loss exponent of $2/\alpha = 4$ in an environment where the interfering nodes are scattered according to a PPP on a two-dimensional plane [43].

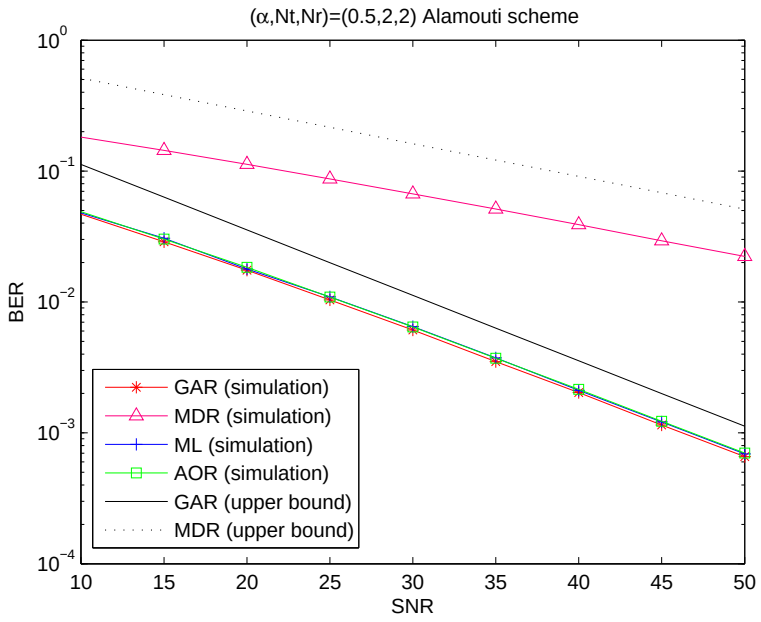

Figure 3.3: Performance comparison of GAR, MDR, ML receiver, and AOR over a channel with highly impulsive noise ($\alpha = 0.5$) with $N_{\mathrm{t}} = 2$ and $N_{\mathrm{r}} = 2$

3.4.1 Performance Results under Model I

We show in Fig. 3.2 the performance bound of GAR for Alamouti code with $N_{\mathrm{t}} = 2, N_{\mathrm{r}} = 1$ over highly impulsive noise with BPSK. We calculate the BER union bound using the PEP of GAR in (3.15). We also plot the upper bounds for the MDR obtained using (3.35). In Fig. 3.2, we also show the simulated BER results of Alamouti code for GAR, MDR, ML receiver, and AOR. Comparing between theoretical and simulated results, we observe the diversity orders of GAR and MDR are $\alpha N_{\mathrm{t}}/2$ and $\alpha/2$. We also observe the performance gap between ML receiver and GAR is about 1.3 dB at 10^{-2} BER. We also found the performance for AOR which does not need the noise parameters shows a difference less than a tenth of a dB to the ML receiver.

In Fig. 3.3, we show the performance of Alamouti code with $N_{\mathrm{t}} = 2, N_{\mathrm{r}} = 2$. It

is noted that the diversity orders do not change even though the number of receiver antennas increases in accordance with our theoretical result. In this case, the ML receiver and AOR are seen to be within 0.6 dB of the GAR.

In the following, we show the performance of Alamouti code over impulsive noise with $\alpha = 1.43$. In Fig. 3.4, we show the theoretical and simulated BER with $N_{\mathrm{t}} = 2, N_{\mathrm{r}} = 1$. The performances with $N_{\mathrm{t}} = 2, N_{\mathrm{r}} = 2$ are shown in Fig. 3.5. Under the less impulsive noise environment with $\alpha = 1.43$, we observe that the diversity orders of GAR and MDR are also $\alpha N_{\mathrm{t}}/2$ and $\alpha/2$ which are in line with our theoretical results. It is also observed the performances for ML receiver and AOR are within 2.5 dB of the GAR at 10^{-3} BER, as suggested by Fig. 3.4. In Fig. 3.5, the ML receiver and AOR are seen to be within 1 dB of the GAR.

In Fig. 3.6 and 3.7, we show the performances of OSTBC with $N_{\mathrm{t}} = 4$ which is a

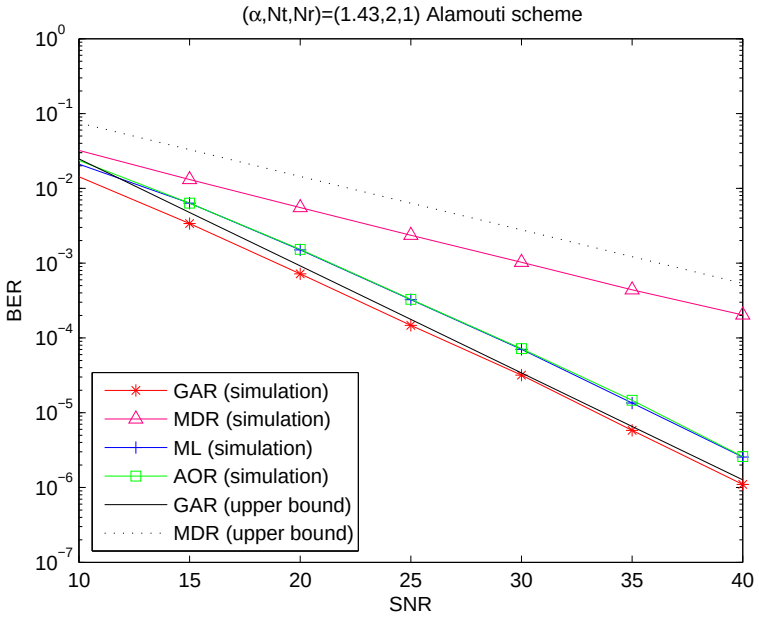

Figure 3.4: Performance comparison of GAR, MDR, ML receiver, and AOR over a channel with moderately impulsive noise ($\alpha = 1.43$) with $N_{\mathrm{t}} = 2$ and $N_{\mathrm{r}} = 1$

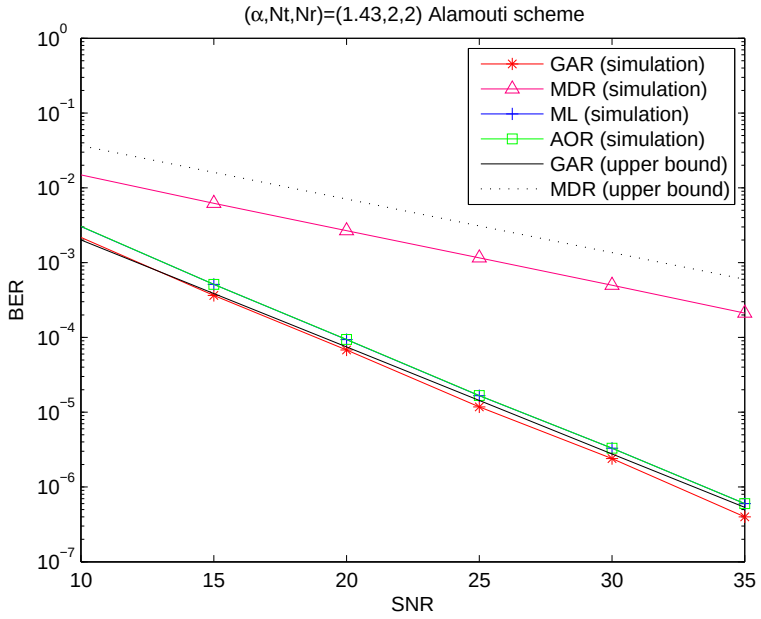

Figure 3.5: Performance comparison of GAR, MDR, ML receiver, and AOR over a channel with moderately impulsive noise ($\alpha = 1.43$) with $N_{\mathrm{t}} = 2$ and $N_{\mathrm{r}} = 2$

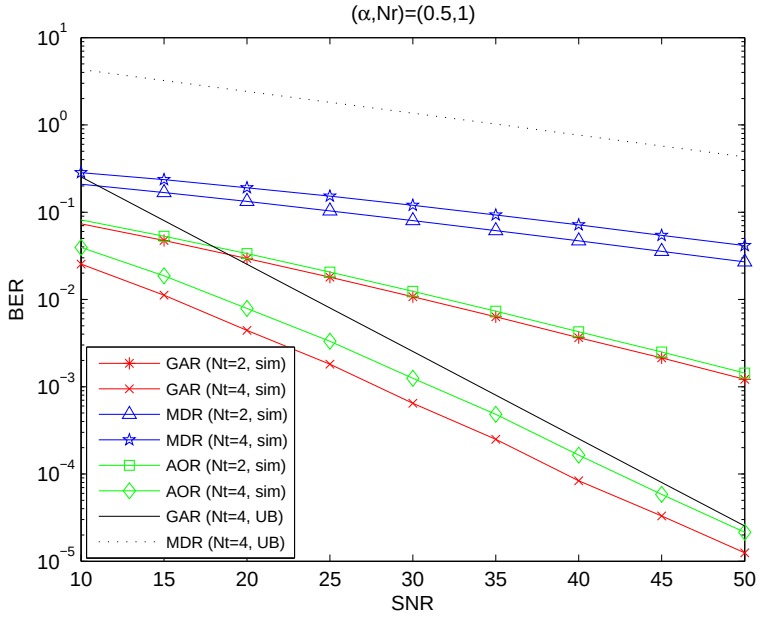

Figure 3.6: Performance comparison of GAR, MDR and AOR over a channel with highly impulsive noise ($\alpha = 0.5$) with $N_{\mathrm{r}} = 1$

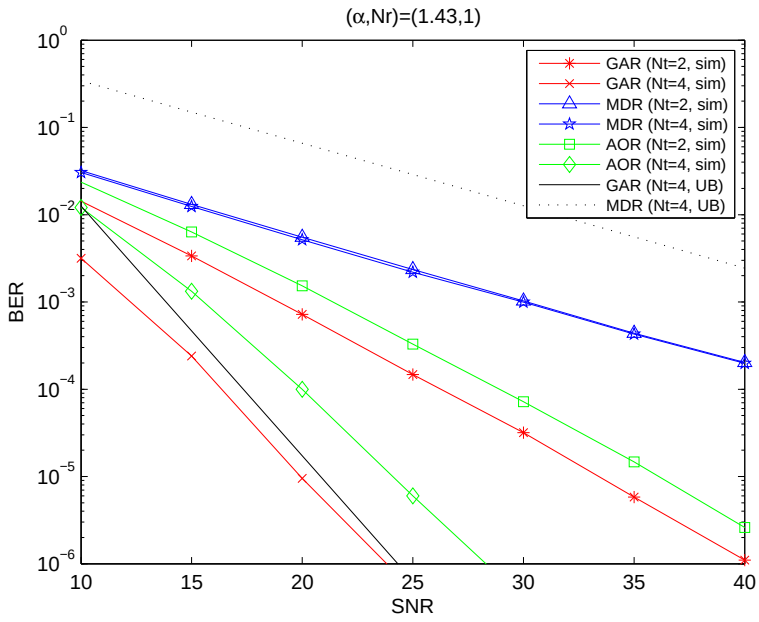

Figure 3.7: Performance comparison of GAR, MDR and AOR over a channel with moderately impulsive noise ($\alpha = 1.43$) with $N_{\mathrm{r}} = 1$

space-time code borrowed from [70]. In Fig. 3.6, we show the performance of OSTBC with $N_{\mathrm{t}} = 4$ over highly impulsive noise under Model I. Comparing the theoretical and simulated results, we observe the diversity orders of GAR and MDR are $\alpha N_{\mathrm{t}}/2$ and $\alpha/2$ as expected from our results. It is noted that the diversity order of GAR with $N_{\mathrm{t}} = 4$ is larger than that with $N_{\mathrm{t}} = 2$ in accordance with our theoretical result. We also observe the performance gap between AOR and GAR is about 3 dB at 10^{-3} BER. The diversity of MDR does not change regardless the number of antennas, and the MDR performance is worse as N_{t} increases for small α as predicted from our theoretical result.

In Fig. 3.7, we show the performance of OSTBC with $N_{\mathrm{t}} = 4$ over impulsive noise with $\alpha = 1.43$. We observe the diversity orders of GAR and MDR with $N_{\mathrm{t}} = 4$ are also $\alpha N_{\mathrm{t}}/2$ and $\alpha/2$ which are larger than that with $N_{\mathrm{t}} = 2$.

3.4.2 Performance Comparison between Model I and II

In Fig. 3.8, we compare the simulated performances of Alamouti code over highly impulsive noise under Model I and II. Under Model II, we can observe that the diversity order of GAR will be larger than that of Model I, because additional diversity can be obtained due to the independence of the noise in the space domain. However, the diversity order of MDR does not change even under Model II. We can also observe the performance difference for AOR and ML receiver is less than a tenth of a dB. Additionally, we show the simulated performances over impulsive noise with $\alpha = 1.43$ under Model I and II in Fig. 3.9 where we observe the diversity order of GAR of Model II is larger than that of Model I and the diversity orders of MDR are always $\alpha/2$. It is also observed the performance difference for AOR and ML receiver is less than a tenth of a dB.

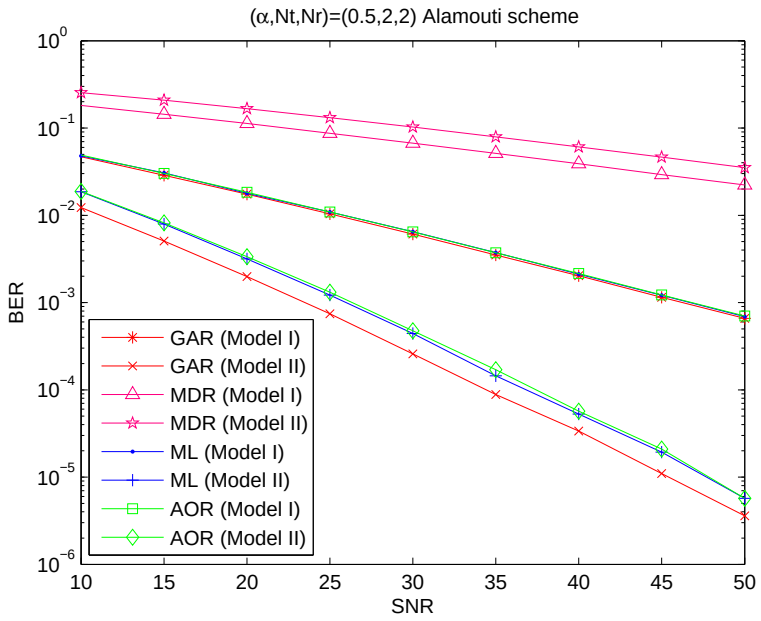

Figure 3.8: Performance comparison of GAR, MDR, ML receiver, and AOR over a channel with highly impulsive noise ($\alpha = 0.5$) with $N_{\mathrm{t}} = 2$ and $N_{\mathrm{r}} = 2$ under Model I and II

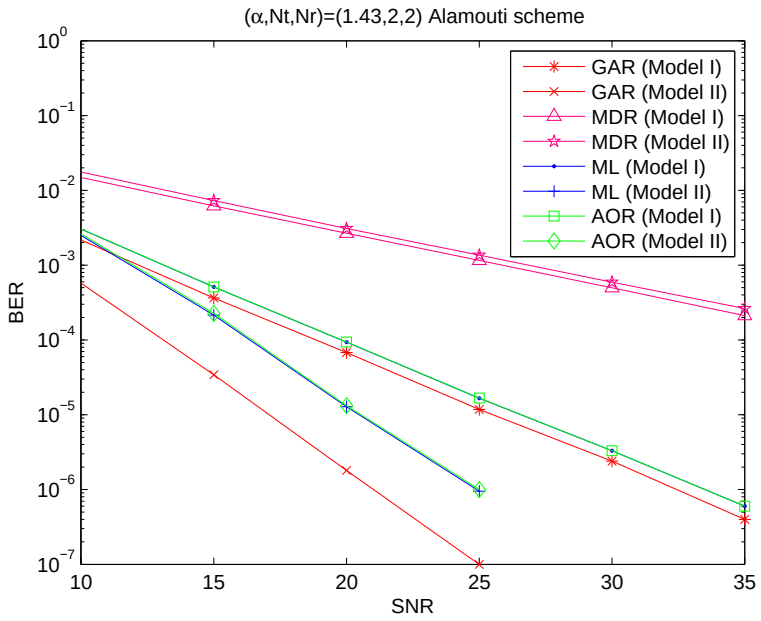

Figure 3.9: Performance comparison of GAR, MDR, ML receiver, and AOR over a channel with moderately impulsive noise ($\alpha = 1.43$) with $N_{\mathrm{t}} = 2$ and $N_{\mathrm{r}} = 2$ under Model I and II

Chapter 4

DISTRIBUTED DETECTION IN COEXISTING LARGE-SCALE SENSOR NETWORKS

4.1 Literature Survey and Motivation

A homogeneous Poisson point process is widely used in the literature to model large-scale wireless sensor networks (WSNs) [75, 76, 77]. It is a natural model to use when little is known about the spatial distribution of the network, aside from the area it is spread over, and the spatial density of nodes. The complete spatial randomness or independence property makes the Poisson point process easy to analyze. A number of studies about network interference have been reported in the literature when the interfering nodes are scattered according to a spatial Poisson point process. In [53, 54, 55, 56, 57, 43], a multi-user network is considered with power-law path loss, where the multiple access interference follows a symmetric α-stable distribution.

As unlicensed band utilization increases, it becomes important to understand how different wireless services, operating in the same band, may affect each other. In an effort to understand the effect of coexistence between networks, the network performance was investigated in the presence of interference from a coexisting network in [78]. Coexistence issues such as congestion control and interference between WSNs and other wireless applications have been studied in [79, 80]. In [81] the authors proposed a multiple access control (MAC) scheme to avoid interference between coexisting WSNs. Most WSNs may not have a sophisticated MAC scheme which requires high complexity and exchange of information. Consequently when two WSNs coexist in the same unlicensed band, the WSNs interfere with each other.

In this dissertation, we consider signal detection in coexisting WSNs. The spatial distribution of sensors is modeled as a Poisson point process. The sensors measure the phenomenon of interest and transmit their local binary decisions via wireless channel to a central site for global processing. We also assume there is a coexisting sensor network which causes interference to the desired sensor network and also is modeled as an independent Poisson point process. As a result, we consider the detection of the aggregate sensing signal from the desired network in the presence of aggregate interference from the interfering network. To the best of our knowledge, in the literature, there is no study on the signal detection with interference in coexisting WSNs. In this dissertation, we show that the problem becomes a binary hypothesis testing problem of detecting α-stable random signals in α-stable random noise, which has not been considered in the literature. In the literature on detection in α-stable noise, the signal has always assumed to be deterministic [82, 83, 84, 85]. We design simple and robust detectors for α-stable signal in the presence of α-stable interference which arises naturally from a Poisson network interference context where the signal is also from a set of Poisson sensors.

4.2 Preliminaries

Since the brief sketch of the α-stable distribution was introduced in Section 2.4, we show the derivation of the characteristic function of the aggregate signal from nodes which are distributed according to a homogeneous Poisson point process in the two-dimensional infinite plane. Let Y denote the aggregate signal from the Poisson distributed network, such that

$$Y = \sum_{i=1}^{\infty} \frac{X_i}{r_i^{\delta}} \tag{4.1}$$

where X_i are independent and identically distributed (i.i.d.) random sensor emissions which are used to model various propagation effects such as fading channel, trans-

mitting power and/or shadowing; r_i is the distance between the receiver and sensor i, and δ is a power loss exponent. The characteristic function of Y follows immediately from Campbell's theorem [86] and is given by

$$\varphi_{_Y}(t) = \exp\left(-2\pi\lambda \int_0^\infty \left[1 - \varphi_{_X}\left(\frac{t}{r^\delta}\right)\right] r\mathrm{d}r\right) \tag{4.2}$$

where λ is the spatial density of nodes and $\varphi_{_X}(\cdot)$ is the characteristic function of X_i. The following theorem which follows from (4.2) gives the characteristic function of the aggregate signal Y and depends on characteristic functions of random variables X_i.

Theorem 4.2.1. *When $\{X_i\}_{i=1}^\infty$ are i.i.d. sequence of symmetric random variables, the characteristic function of the aggregate signal Y in* (4.1) *is given by* [43]

$$\varphi_{_Y}(t) = \exp\left(-\sigma^\alpha |t|^\alpha\right) \tag{4.3}$$

where $\alpha = \frac{2}{\delta}$, $\sigma^\alpha = \lambda\frac{\pi}{2}C_\alpha^{-1}E\left[|X_i|^\alpha\right]$ and $C_\alpha = \frac{1-\alpha}{\Gamma(2-\alpha)2\cos(\pi\alpha/2)}$.

Proof. Let $\{r_i\}_{i=1}^\infty$ denote the sequence of distances between the origin and random points of a two-dimensional Poisson process with spatial density λ and $\{X_i\}_{i=1}^\infty$ be a sequence of spherically symmetric[1] random variables, i.i.d. in i, independent of the sequence $\{r_i\}$. Let Y denote the aggregate signal at the origin generated by the nodes scattered in the infinite plane, such that

$$Y = \sum_{i=1}^\infty \frac{X_i}{r_i^\delta} \tag{4.4}$$

for $\delta > 1$. If the random variable X has a spherically symmetric pdf, its characteristic function is also spherically symmetric, i.e., $\varphi_{_X}(t) = \varphi_0(|t|)$ for some $\varphi_0(\cdot)$. Using this property of spherically symmetric random variable and (4.2), we can get

$$\varphi_{_Y}(t) = \exp\left(-2\pi\lambda \int_0^\infty \left[1 - \varphi_0\left(\left|\frac{t}{r^\delta}\right|\right)\right] r\mathrm{d}r\right) \tag{4.5}$$

[1]A random variable X is said to be spherically symmetric if its pdf $f_X(x)$ depends only on $|x|$.

which, using the change of variable $|t|r^{-\delta} = s$, can be written as

$$\varphi_{_Y}(t) = \exp\left(-\pi\lambda|t|^{2/\delta}\frac{2}{\delta}\int_0^\infty \frac{1-\varphi_{_0}(s)}{s^{2/\delta+1}}\mathrm{d}s\right) \tag{4.6}$$

The characteristic function $\varphi_{_0}(s)$ in (4.6) can be rewritten as follows

$$\begin{aligned}
\varphi_{_0}(s) &= \varphi_{_{X_i}}(s) && (4.7)\\
&= E\left[e^{jsX_i}\right] && (4.8)\\
&= E\left[\cos(sX_i)\right] + j\underbrace{E\left[\sin(sX_i)\right]}_{=0} && (4.9)\\
&= E\left[\cos(sX_i)\right] && (4.10)
\end{aligned}$$

Using the elementary integral [87, Eq. 3.823], we can write

$$\int_0^\infty \frac{1-\cos(zs)}{s^{\alpha+1}}\mathrm{d}s = \frac{\Gamma(1-\alpha)\cos\left(\frac{\pi\alpha}{2}\right)}{\alpha}|z|^\alpha \tag{4.11}$$

for any real constants z and $0 < \alpha < 2$. For $z = X_i$ and taking expectations with respect to X_i on both sides, we obtain

$$\int_0^\infty \frac{1-\varphi_{_0}(s)}{s^{\alpha+1}}\mathrm{d}s = \frac{\Gamma(1-\alpha)\cos\left(\frac{\pi\alpha}{2}\right)}{\alpha}E\left[|z|^\alpha\right] \tag{4.12}$$

Noting that $\Gamma(1-\alpha) = \Gamma(2-\alpha)/(1-\alpha)$ for $\alpha \neq 1$, we can rewrite (4.12) as

$$\int_0^\infty \frac{1-\varphi_{_0}(s)}{s^{\alpha+1}}\mathrm{d}s = \frac{C_\alpha^{-1}}{\alpha}E\left[|z|^\alpha\right] \tag{4.13}$$

where C_α is defined in (4.17). By setting $2/\delta = \alpha$ and substituting (4.13) in (4.6), we can get the characteristic function $\varphi_{_Y}(t) = E[e^{jtY}]$ as follow

$$\varphi_{_Y}(t) = \exp\left(-\gamma|t|^\alpha\right) \tag{4.14}$$

where

$$\alpha = \frac{2}{\delta} \tag{4.15}$$

$$\gamma = \lambda\frac{\pi}{2}C_\alpha^{-1}E\left[|X_i|^\alpha\right] \tag{4.16}$$

and C_α is defined as

$$C_\alpha \triangleq \begin{cases} \frac{1-\alpha}{\Gamma(2-\alpha)2\cos(\pi\alpha/2)}, & \alpha \neq 1 \\ \frac{2}{\pi}, & \alpha = 1 \end{cases} \tag{4.17}$$

with $\Gamma(\cdot)$ denoting the gamma function. □

Random variables with characteristic function of the form of $\varphi_{_Y}(t)$ in (4.3) belong to the class of *symmetric α-stable random variables*. In the following, we consider the case that $\{X_i\}_{i=1}^{\infty}$ is a sequence of real nonnegative random variables.

Theorem 4.2.2. *When $\{X_i\}_{i=1}^{\infty}$ are i.i.d. sequence of real nonnegative random variables, the characteristic function of the aggregate signal Y in* (4.1) *is given by* [43]

$$\varphi_{_Y}(t) = \exp\left(-\sigma^\alpha |t|^\alpha \left[1 - j\beta \text{sign}(t) \tan\left(\frac{\pi\alpha}{2}\right)\right]\right) \tag{4.18}$$

where $\alpha = \frac{2}{\delta}$, $\beta = 1$, $\sigma^\alpha = \lambda \frac{\pi}{2} C_\alpha^{-1} E\left[X_i^\alpha\right]$ and $C_\alpha = \frac{1-\alpha}{\Gamma(2-\alpha)2\cos(\pi\alpha/2)}$.

Proof. Let $\{r_i\}_{i=1}^{\infty}$ denote the sequence of distances between the origin and random points of a two-dimensional Poisson process with spatial density λ same as Symmetric case. Let $\{X_i\}_{i=1}^{\infty}$ be a sequence of i.i.d. real nonnegative random variables and independent of the sequence $\{r_i\}$. Let Y denote the aggregate signal at the origin generated by the nodes scattered in the infinite plane, such that

$$Y = \sum_{i=1}^{\infty} \frac{X_i}{r_i^\delta} \tag{4.19}$$

for $\delta > 2$. Using (4.2), we can get

$$\varphi_{_Y}(t) = \exp\left(-2\pi\lambda \int_0^\infty \left[1 - \varphi_{_X}\left(\frac{t}{r^\delta}\right)\right] r \mathrm{d}r\right) \tag{4.20}$$

where $\varphi_{_X}(t)$ is the characteristic function of X_i. Using the change of variable $|t|r^{-\delta} = s$, can be written as

$$\varphi_{_Y}(t) = \exp\left(-\pi\lambda|t|^{2/\delta} \frac{2}{\delta} \int_0^\infty \frac{1 - E\left[e^{j\text{sign}(t)X_i s}\right]}{s^{2/\delta+1}} \mathrm{d}s\right) \tag{4.21}$$

Using the elementary integral [88, Eq. (4.11), p. 542], we can write

$$\int_0^\infty \frac{1-e^{jzs}}{s^{\alpha+1}}\mathrm{d}s = \frac{\Gamma(1-\alpha)}{\alpha}|z|^\alpha \left[\cos\left(\frac{\pi\alpha}{2}\right) - j\mathrm{sign}(z)\sin\left(\frac{\pi\alpha}{2}\right)\right] \tag{4.22}$$

for any real constants z and $0 < \alpha < 1$. For $z = \mathrm{sign}(t)X_i$ and taking expectations on both sides, we obtain

$$\int_0^\infty \frac{1-E\left[e^{j\mathrm{sign}(t)X_i s}\right]}{s^{\alpha+1}}\mathrm{d}s = E\left[X_i^\alpha\right]\frac{\Gamma(1-\alpha)\cos\left(\frac{\pi\alpha}{2}\right)}{\alpha}\left[1 - j\mathrm{sign}(t)\tan\left(\frac{\pi\alpha}{2}\right)\right] \tag{4.23}$$

Noting that $\Gamma(1-\alpha) = \Gamma(2-\alpha)/(1-\alpha)$, we can rewrite (4.23) as

$$\int_0^\infty \frac{1-E\left[e^{j\mathrm{sign}(t)X_i s}\right]}{s^{\alpha+1}}\mathrm{d}s = E\left[X_i^\alpha\right]\frac{C_\alpha^{-1}}{\alpha}\left[1 - j\mathrm{sign}(t)\tan\left(\frac{\pi\alpha}{2}\right)\right] \tag{4.24}$$

where C_α is defined in (4.17). By setting $2/\delta = \alpha$ and substituting (4.24) in (4.21), we can get the characteristic function $\varphi_{_Y}(t) = E[e^{jtY}]$ as follow

$$\varphi_{_Y}(t) = \exp\left(-\gamma|t|^\alpha\left[1 - j\beta\mathrm{sign}(t)\tan\left(\frac{\pi\alpha}{2}\right)\right]\right) \tag{4.25}$$

where

$$\alpha = \frac{2}{\delta} \tag{4.26}$$

$$\beta = 1 \tag{4.27}$$

$$\gamma = \lambda\frac{\pi}{2}C_\alpha^{-1}E\left[X_i^\alpha\right] \tag{4.28}$$

and C_α is defined in (4.17). □

Random variables with characteristic function of the form of $\varphi_{_Y}(t)$ in (4.18) belong to the class of *totally positive skewed α-stable random variables*. Note that only when $\beta = 1$ each realization of Y is positive.

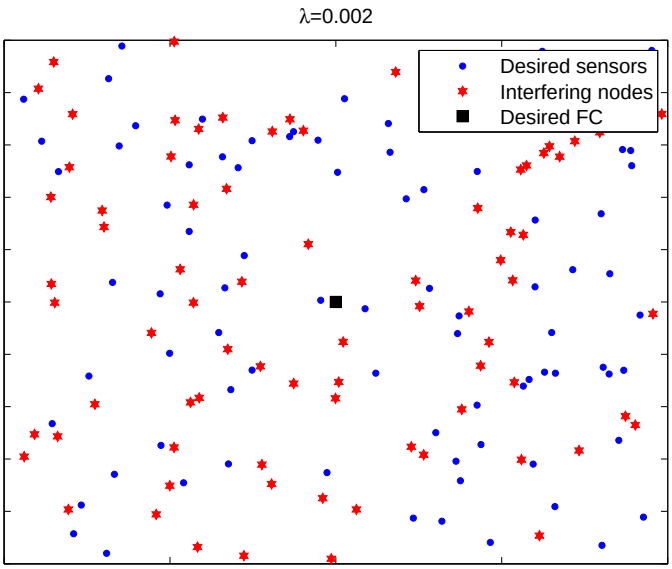

Figure 4.1: Realization of the spatial distribution of two networks according to the homogeneous Poisson point process ($\lambda = 0.002$)

4.3 System Model

We consider the coexistence of two WSNs which are distributed according to Poisson point process as shown in Fig. 4.1. We assume one is a desired network where active sensors transmit their measurements to the Fusion Center (FC), and the other is a interfering network which causes interference to the desired network. The interfering network also may have a FC which is not shown in Fig. 4.1. It is also assumed that the spatial density of the Poisson point process for the desired network is λ_{D} and the spatial density of interfering network is λ_{I} respectively. Under these assumptions, we will consider the distributed detection and data fusion problem with channel knowledge to be transmitted at each sensor [89] and show that both aggregate signal and interference converge to the class of α-stable distributions with different parameters. We will also consider imperfect local detection error at each sensor and

study how this error affects the detection performance.

4.3.1 Decision Fusion

In the desired sensor network, we can consider a binary hypothesis testing problem with two hypotheses $\mathcal{H}_0, \mathcal{H}_1$ where P_0, P_1 are their respective prior probabilities. In this dissertation, we assume the two hypotheses equally likely ($P_0 = P_1 = 1/2$). Let the sensed signal at the i^{th} sensor be,

$$x_i = \theta + n_i, \tag{4.29}$$

where $\theta = 1$ under $\mathcal{H}_1$ and $\theta = 0$ under $\mathcal{H}_0$, is a deterministic parameter whose presence or absence has to be detected, and n_i is the noise sample at the i^{th} sensor. We consider a setting where the i^{th} sensor transmits its measurement using a distributed detection scheme. It is also assumed that h_i is a symmetric real-valued fading channel coefficient from the i^{th} sensor to the FC satisfying $\mathbb{E}[|h|^2] = 1$.

In the system, each local sensor makes a decision based on its decision rule

$$\gamma(x_i) = M_i = \begin{cases} 1 & \text{under } \mathcal{H}_1 \\ \\ 0 & \text{under } \mathcal{H}_0 \end{cases}, \tag{4.30}$$

where the function $\gamma(\cdot)$ is the local decision rule that minimizes the error probability at the local i^{th} sensor and M_i is the local decision at the i^{th} local sensor. Therefore, the transmitting signal at the local sensor is sent to the FC as follows:

$$f(x_i) = h_i \gamma(x_i), \tag{4.31}$$

At the desired FC, the received signal at a sample time is given by

$$Y = \sum_{i=1}^{\infty} h_i \frac{f(x_i)}{r_i^{\delta}} + W \tag{4.32}$$

where W is the interference from interfering network which will be shown to have a symmetric α-stable distribution as explained later in this section. By substituting (4.31) in (4.32), we obtain

$$Y = \sum_{i=1}^{\infty} \frac{|h_i|^2}{r_i^{\delta}} M_i + W \tag{4.33}$$

where $\{|h_i|^2\}_{i=1}^{\infty}$ is a sequence of real non-negative random variables. In (4.33), $|h_i|^2$ corresponds to X_i in (4.1). Using Theorem 4.2.2 in (4.33), we can show that $S = \sum_{i=1}^{\infty} |h_i|^2 M_i / r_i^{\delta}$ converges to the totally positive skewed α-stable distribution as follows:

$$S \sim S_{\alpha}\left(\sigma_S, \beta_S, 0\right) \tag{4.34}$$

where $\alpha = \frac{2}{\delta}$, $\sigma_S^{\alpha} = \lambda_{\mathrm{D}} \frac{\pi}{2} C_{\alpha}^{-1} M^{\alpha} E[|h|^{2\alpha}]$, and $\beta_S = 1$.

In the following, we will show the interference from the interfering network, W in (4.33), can be modeled as a symmetric α-stable distribution. Similar to the signal part in (4.32), we assume that the nodes in interfering network transmit their measurements with channel information between the nodes and *their* FC. Then the aggregate interference at the desired FC at a sample time is as follows:

$$W = \sum_{i=1}^{\infty} h_i g_i \frac{w_i}{r_i^{\delta}} \tag{4.35}$$

where g_i is the channel coefficient between the interfering node and its FC, h_i is the channel between the interfering node and the desired FC, and w_i is the emission at the interfering node i. The random variable $h_i g_i w_i$ is a symmetric regardless w_i is a constant or any random variable depending on a transmission scheme of interfering network [90]. Using Theorem 4.2.1, we can show that (4.35) converges to a symmetric α-stable distribution as follows:

$$W \sim S_{\alpha}\left(\sigma_W, 0, 0\right) \tag{4.36}$$

where $\alpha = \frac{2}{\delta}$ and $\sigma_W^{\alpha} = \lambda_{\mathrm{I}} \frac{\pi}{2} C_{\alpha}^{-1} E[|hgw|^{\alpha}]$.

By using the property of α-stable random variable in Section 2.4.2, we can define the binary hypothesis testing problem as a positive α-stable random signal detection in a symmetric α-stable random noise. It is given as follows:

$$Y = \begin{cases} S + W \sim S_\alpha(\sigma_{\mathrm{H}_1}, \beta_{\mathrm{H}_1}, 0) & \text{under } \mathcal{H}_1 \\ W \sim S_\alpha(\sigma_{\mathrm{H}_0}, 0, 0) & \text{under } \mathcal{H}_0 \end{cases} \tag{4.37}$$

where $\sigma_{\mathrm{H}_1} = (\sigma_S^\alpha + \sigma_W^\alpha)^{1/\alpha}$, $\beta_{\mathrm{H}_1} = \frac{(\beta_S \sigma_S^\alpha)}{(\sigma_S^\alpha + \sigma_W^\alpha)}$ and $\sigma_{\mathrm{H}_0} = \sigma_W^\alpha$. Note that $0 < \beta_{\mathrm{H}_1} < 1$ since $\sigma_S > 0$, $\sigma_W > 0$, and $\beta_S = 1$.

4.3.2 Detection Error at a Local Sensor

Each local sensor makes a decision and forwards its decision to the FC. In Section 4.3.1, we assume each local sensor can detect the phenomenon of interest perfectly. In this section, we consider the effect of detection error at the local sensor. We define the error probability for detection at a local sensor as $P_{\mathrm{L,e}} < 1$. It is also assumed that the detection error at a local sensor occurs independently across sensors. The detecting error will reduce the number of sensors which transmit their detection message to the FC. Therefore the spatial density of actual transmitting nodes will be $\lambda_{\mathrm{D,e}} = \lambda_{\mathrm{D}} P_{\mathrm{L,e}}$ by the thinning property of Poisson point process [3]. As a result, σ_S^α in (4.34) will be reduced to $\sigma_{S,\mathrm{e}}^\alpha = \lambda_{\mathrm{D,e}} \frac{\pi}{2} C_\alpha^{-1} M^\alpha E[|h|^{2\alpha}]$ due to the detection error at a local sensor. This is related with the following SNR definition.

The usual SNR definition using the variance of the noise process is not suitable when the additive noise is α-stable random noise since α-stable random variables do not have finite variance when $\alpha < 2$. Therefore, we propose the modified SNR definition as follows [83, 84]:

$$SNR_{\mathrm{m}} = 10 \log_{10} \frac{\sigma_S^\alpha}{\sigma_W^\alpha} (\mathrm{dB}) \tag{4.38}$$

where σ_S is the scale parameter of the signal, σ_W is the scale parameter of the noise and α is the characteristic exponent. Since $\sigma_{S,e}^{\alpha} < \sigma_S^{\alpha}$, the SNR defined in (4.38) will decrease due to the detection error at each local sensor. Consequently, the performance will be degraded due to the detection error at a local sensor as expected.

4.4 Signal Detection

In this section, we will introduce the Maximum Likelihood (ML) detector for α-stable signal detection in α-stable interference which has considerable computational complexity. To surmount the complexity of the ML detector, we will also propose several simple detectors. For the signal detection, it is assumed that the desired FC observes $\{Y_j\}_{j=1}^{L}$ which are L independent measurements across time.

4.4.1 Maximum Likelihood Detector

The optimal ML detector computes the following test statistics:

$$T_{\mathrm{ML}} = \sum_{j=1}^{L} \log \frac{f_\alpha(Y_j, \sigma_{\mathrm{H}_1}, \beta_{\mathrm{H}_1}, 0; \mathcal{H}_1)}{f_\alpha(Y_j, \sigma_{\mathrm{H}_0}, \beta_{\mathrm{H}_0}, 0; \mathcal{H}_0)} \underset{\mathrm{H}_0}{\overset{\mathrm{H}_1}{\gtrless}} 0 \tag{4.39}$$

where $f_\alpha(Y, \sigma, \beta, \mu)$ is a probability density function of α-stable random variable whose characteristic function is introduced in Section 2.4.1. Because there is no closed form expression for the PDF of α-stable random variables, the PDF can be obtained by taking inverse Fourier transform numerically! Instead of numerical integration, we can alternatively use a lookup table for the numerical values of α-stable random variables. Such a lookup table would have sizable memory requirements since a lookup table would contain values for each of the α, σ, and β values corresponding to the noise parameters. Therefore, the ML detector requires high computational complexity. Thus, we propose several simple detectors in following sections.

4.4.2 Fractional Lower Order Moments (FLOM) Detector

Although the second-order moment of a α-stable random variable with $0 < \alpha < 2$ does not exist, all moments of order less than α do exist and are called the *Fractional Lower-Order Moments* or FLOMs. The FLOMs of a α-stable random variable $Y \sim S_\alpha(\sigma, \beta, 0)$ are given by [91]:

$$E[|Y|^p] = \frac{\Gamma\left(1-\frac{p}{\alpha}\right)}{\Gamma(1-p)\cos\left(\frac{p\pi}{2}\right)}\left(1+\beta^2\tan^2\frac{\alpha\pi}{2}\right)^{\frac{p}{2\alpha}}\cos\left(\frac{p}{\alpha}\arctan\left(\beta\tan\left(\frac{\alpha\pi}{2}\right)\right)\right)\sigma^p \quad (4.40)$$

for $p < \alpha$. The FLOM in (4.40) is an even function of β and increases with $|\beta|$. Now $|Y|^p$ has a finite mean from (4.40) and a finite variance as follows:

$$\text{var}[|Y|^p] = E[|Y|^{2p}] - E[|Y|^p]^2, \quad p < \alpha/2, \quad (4.41)$$

which can be computed using (4.40). Since $|Y|^p$ has a finite mean and a finite variance, by the central limit theorem the mean of $|Y_j|^p, j = 1, 2, ..., L$ will be approximately normally distributed as follows:

$$Z = \frac{1}{L}\sum_{j=1}^{L}|Y_j|^p = \begin{cases} \mathcal{N}(\mu_{\text{H}_1}, \sigma^2_{\text{G,H}_1}) & \text{under } \mathcal{H}_1 \\ \mathcal{N}(\mu_{\text{H}_0}, \sigma^2_{\text{G,H}_0}) & \text{under } \mathcal{H}_0 \end{cases} \quad (4.42)$$

where μ_{H_k} and $\sigma^2_{\text{G,H}_k}$ are the means and variances of Gaussian random variables under hypotheses $\mathcal{H}_k, k = 0, 1$. The mean μ_{H_k} can be calculated from (4.40), and $\sigma^2_{\text{G,H}_k} = \text{var}[|Y|^p]/L$ using (4.41). The suboptimal FLOM detector computes the following test statistics:

$$T_{\text{FLOM}}(Z) = \log\frac{\frac{1}{\sqrt{2\pi\sigma^2_{\text{G,H}_1}}}\exp\left(-\frac{(Z-\mu_{\text{H}_1})^2}{2\sigma^2_{\text{G,H}_1}}\right)}{\frac{1}{\sqrt{2\pi\sigma^2_{\text{G,H}_0}}}\exp\left(-\frac{(Z-\mu_{\text{H}_0})^2}{2\sigma^2_{\text{G,H}_0}}\right)} \underset{\text{H}_0}{\overset{\text{H}_1}{\gtrless}} 0 \quad (4.43)$$

The theoretical detection performance can be approximated as

$$P_{\text{e,FLOM}} = \frac{1}{2}\left[Q\left(\frac{t_1-\mu_{\text{H}_0}}{\sigma_{\text{G,H}_0}}\right) - Q\left(\frac{t_2-\mu_{\text{H}_0}}{\sigma_{\text{G,H}_0}}\right)\right] + \frac{1}{2}\left[1 - Q\left(\frac{t_1-\mu_{\text{H}_1}}{\sigma_{\text{G,H}_1}}\right) + Q\left(\frac{t_2-\mu_{\text{H}_1}}{\sigma_{\text{G,H}_1}}\right)\right]$$

where t_1 and t_2 are thresholds to decide $\mathcal{H}_1$ if $t_1 \leq Z \leq t_2$ and otherwise $\mathcal{H}_0$. These thresholds can be obtained by solving the quadratic equation arising from $T_{\mathrm{FLOM}}(Z) = 0$ in (4.43). By numerical computation, it is easy to see (4.44) is an increasing function of p. Thus, the detection performance becomes better as $p \to 0$. The FLOM of α-stable random variable has been used for the estimation of the parameters of α-stable random variables [91]. In this dissertation, the FLOM is used for the detection problem. For radar systems, the FLOM detector for the detection of distorted known signal sequence due to α-stable clutter with α-stable noise has been studied in [92]. However, it is different from our system which is α-stable random signal detection in α-stable noise. The FLOM detector is not the best detector among multiple candidates we propose in this dissertation, and is improved next.

4.4.3 Signed-FLOM Detector

In this section, we propose a simple detector for the α-stable random signal detection in α-stable noise. We denote the signed p^{th} power of a number x by

$$x^{<p>} := \mathrm{sign}(x)|x|^p \tag{4.44}$$

The signed FLOMs of a α-stable random variable can be found as follows [91]:

$$E[Y^{<p>}] = \frac{\Gamma\left(1-\frac{p}{\alpha}\right)}{\Gamma(1-p)\sin\left(\frac{p\pi}{2}\right)}\left(1+\beta^2\tan^2\frac{\alpha\pi}{2}\right)^{\frac{p}{2\alpha}}\sin\left(\frac{p}{\alpha}\arctan\left(\beta\tan\left(\frac{\alpha\pi}{2}\right)\right)\right)\sigma^p. \tag{4.45}$$

The variance of $Y^{<p>}$ can be defined by

$$\mathrm{var}[Y^{<p>}] = E[Y^{<2p>}] - E[Y^{<p>}]^2, \quad p < \alpha/2. \tag{4.46}$$

Using same approach with the FLOM detector, we can define the binary hypothesis test and its test statistics same as (4.42) and (4.43) with different means and variances which can be calculated using (4.45) and (4.46). The theoretical performance also can be approximated using the Q-function. It is numerically observed that the

performance of the signed-FLOM detector is a convex function of p. Therefore, one can find the optimal p value numerically. This signed-FLOM of α-stable random variable has also been used for estimation problem of the parameters of the random variable [91].

4.4.4 Logarithm Detector

In this section, we propose the another simple detector. We define $\log|Y|$ as a new random variable and a following relationship.

$$E[|Y|^p] = E[e^{p\log|Y|}] = M_{\log|Y|}(p) \tag{4.47}$$

where $E[e^{p\log|Y|}]$ can be regarded as the moment generating function of $\log|Y|$. Then, moment of $\log|Y|$ of any order can be obtained by

$$E[\log|Y|^k] = \frac{\mathrm{d}^k M_{\log|Y|}(0)}{\mathrm{d}p^k}. \tag{4.48}$$

Using (4.48) $\log|Y|$ has a mean and a finite variance as follows [91]:

$$E[\log|Y|] = -C_{\mathrm{e}} + \frac{C_{\mathrm{e}}}{\alpha} + \log\sigma + \frac{\log(1+\beta^2\tan(\frac{\alpha\pi}{2})^2)}{2\alpha}, \tag{4.49}$$

$$\mathrm{var}[\log|Y|] = \frac{\pi^2}{4} - \frac{\pi^2}{6} + \frac{\pi^2}{6\alpha^2} - \frac{\arctan^2(\beta\tan(\frac{\alpha\pi}{2}))}{\alpha^2} \tag{4.50}$$

where C_{e} is the Euler constant. Since $\log|Y|$ has a mean and a finite variance, using same approach with the previous two detectors we can define the binary hypothesis test and its test statistics same as (4.42) and (4.43) with different means and variances which can be calculated from (4.49) and (4.50). The theoretical performance also can be approximated using the Q-function and it does not depend on any parameter unlike FLOM-based detectors. Like previous FLOM-based methods, the log method has also been used for parameter estimation of the parameters of α-stable random variable [91].

4.4.5 Mixed-FLOM Detector

Even though we proposed several simple detectors in previous sections, the detectors have moderate performances compared with the ML detector which will be shown in Section 4.5. Therefore, we propose the novel mixed-FLOM detector which combines the FLOM and the signed-FLOM detectors with better performance and without any serious increase of computational complexity. Since $|Y|^{p_1}$ and $Y^{<p_2>}$ are functions of same random variable Y, there is a dependence between two random variables. The covariance between $|Y|^{p_1}$ and $Y^{<p_2>}$ is derived by

$$\mathrm{cov}[|Y|^{p_1}, Y^{<p_2>}] = E[Y^{<p_1+p_2>}] - E[|Y|^{p_1}]E[Y^{<p_2>}], \quad p_1 + p_2 < \alpha/2. \tag{4.51}$$

By using these two random variables, the binary hypothesis test can be approximated as follows:

$$\mathbf{Z} = \begin{bmatrix} Z_1 \\ Z_2 \end{bmatrix} = \begin{bmatrix} \frac{1}{L}\sum_{j=1}^{L} |Y_j|^{p_1} \\ \frac{1}{L}\sum_{j=1}^{L} Y_j^{<p_2>} \end{bmatrix} = \begin{cases} \mathcal{N}(\boldsymbol{\mu}_{\mathrm{H}_1}, \mathbf{C}_{\mathrm{H}_1}) & \text{under } \mathcal{H}_1 \\ \mathcal{N}(\boldsymbol{\mu}_{\mathrm{H}_0}, \mathbf{C}_{\mathrm{H}_0}) & \text{under } \mathcal{H}_0 \end{cases} \tag{4.52}$$

where $\boldsymbol{\mu}_{\mathrm{H}_k} = [\mu_{1,k}\ \mu_{2,k}]^T, k = 0, 1$ can be calculated by using (4.40) and (4.45). In covariance matrix $\mathbf{C}_{\mathrm{H}_k} = [c_{11,k}\ c_{12,k}; c_{21,k}\ c_{22,k}], k = 0, 1$, the diagonal terms are $c_{11,k} = \mathrm{var}[|Y|^{p_1}]/L$ and $c_{22,k} = \mathrm{var}[Y^{<p_2>}]/L$ which can be calculated using (4.41) and (4.46). The covariance between Z_1 and Z_2 is $c_{12,k} = c_{21,k} = \mathrm{cov}[|Y|^{p_1}, Y^{<p_2>}]/L$ from (4.51). The covariance can be computed by using (4.40) and (4.45). The suboptimal mixed-FLOM detector computes the following test statistics:

$$T_{\text{mixed-FLOM}}(\mathbf{Z}) = \log \frac{\frac{1}{2\pi \det|\mathbf{C}_{\mathrm{H}_1}|} \exp\left(-(\mathbf{Z}-\boldsymbol{\mu}_{\mathrm{H}_1})^T \mathbf{C}_{\mathrm{H}_1}^{-1}(\mathbf{Z}-\boldsymbol{\mu}_{\mathrm{H}_1})\right)}{\frac{1}{2\pi \det|\mathbf{C}_{\mathrm{H}_0}|} \exp\left(-(\mathbf{Z}-\boldsymbol{\mu}_{\mathrm{H}_0})^T \mathbf{C}_{\mathrm{H}_0}^{-1}(\mathbf{Z}-\boldsymbol{\mu}_{\mathrm{H}_0})\right)} \underset{\mathrm{H}_0}{\overset{\mathrm{H}_1}{\gtrless}} 0 \tag{4.53}$$

The theoretical detection performance can be approximated as

$$P_{\mathrm{e,mixed-FLOM}} = \frac{1}{2}\left(P_{\mathrm{e},\mathrm{H}_1} + P_{\mathrm{e},\mathrm{H}_0}\right) \tag{4.54}$$

where

$$P_{\mathrm{e,H_0}} = \int_{s_1}^{s_2} \left[Q\left(\frac{t_1(Z_1) - \mu_{2,0}}{\sqrt{c_{22,0}}} \right) - Q\left(\frac{t_2(Z_1) - \mu_{2,0}}{\sqrt{c_{22,0}}} \right) \right] \frac{1}{\sqrt{2\pi c_{11,0}}} \exp\left(-\frac{(Z_1 - \mu_{1,0})^2}{2c_{11,0}} \right) \mathrm{d}Z_1,$$

and

$$P_{\mathrm{e,H_1}} = \int_{s_1}^{s_2} \left[1 - Q\left(\frac{t_1(Z_1) - \mu_{2,1}}{\sqrt{c_{22,1}}} \right) + Q\left(\frac{t_2(Z_1) - \mu_{2,1}}{\sqrt{c_{22,1}}} \right) \right] \frac{1}{\sqrt{2\pi c_{11,1}}} \exp\left(-\frac{(Z_1 - \mu_{1,1})^2}{2c_{11,1}} \right) \mathrm{d}Z_1,$$

where $t_1(Z_1) = (-b_\mathrm{t} + \sqrt{b_\mathrm{t}^2 - a_\mathrm{t}c_\mathrm{t}})/a_\mathrm{t}$ and $t_2(Z_1) = (-b_\mathrm{t} - \sqrt{b_\mathrm{t}^2 - a_\mathrm{t}c_\mathrm{t}})/a_\mathrm{t}$ are thresholds that are functions of Z_1 as seen in (4.55) to decide $\mathcal{H}_1$ if $t_1(Z_1) \leq Z_2 \leq t_2(Z_1)$ and otherwise $\mathcal{H}_0$. In order for the thresholds $t_1(Z_1)$ and $t_2(Z_1)$ to have real values, the ranges for Z_1 are defined as $s_1 := (-b_\mathrm{s} + \sqrt{b_\mathrm{s}^2 - a_\mathrm{s}c_\mathrm{s}})/a_\mathrm{s}$ and $s_2 := (-b_\mathrm{s} - \sqrt{b_\mathrm{s}^2 - a_\mathrm{s}c_\mathrm{s}})/a_\mathrm{s}$. We have also defined

$$\begin{aligned}
a_\mathrm{t} &= [\mathbf{A}]_{2,2} \\
b_\mathrm{t} &= [\mathbf{A}]_{1,2} Z_1 + [\mathbf{b}^T]_{1,2} \\
c_\mathrm{t} &= [\mathbf{A}]_{1,1} Z_1^2 + 2[\mathbf{b}^T]_{1,1} Z_1 + c \\
a_\mathrm{s} &= [\mathbf{A}]_{1,2}^2 - [\mathbf{A}]_{2,2}[\mathbf{A}]_{1,1} \\
b_\mathrm{s} &= [\mathbf{A}]_{1,2}[\mathbf{b}^T]_{1,2} - [\mathbf{A}]_{2,2}[\mathbf{b}^T]_{1,1} \\
c_\mathrm{s} &= [\mathbf{b}^T]_{1,2}^2 - c[\mathbf{A}]_{2,2},
\end{aligned} \tag{4.55}$$

where $\mathbf{A} = \mathbf{C}_{\mathrm{H}_0}^{-1} - \mathbf{C}_{\mathrm{H}_1}^{-1}$, $\mathbf{b}^T = \boldsymbol{\mu}_{\mathrm{H}_1}^T \mathbf{C}_{\mathrm{H}_1}^{-1} - \boldsymbol{\mu}_{\mathrm{H}_0}^T \mathbf{C}_{\mathrm{H}_0}^{-1}$, $c = \boldsymbol{\mu}_{\mathrm{H}_0}^T \boldsymbol{\mu}_{\mathrm{H}_0} - \boldsymbol{\mu}_{\mathrm{H}_1}^T \boldsymbol{\mu}_{\mathrm{H}_1} + \log \frac{\det |\mathbf{C}_{\mathrm{H}_0}|}{\det |\mathbf{C}_{\mathrm{H}_1}|}$, and $[\mathbf{D}]_{i,j}$ is the $(i,j)^{\mathrm{th}}$ element of matrix $\mathbf{D}$. Using (4.54), we can obtain optimal p_1 and p_2 values which guarantee the best theoretical performance numerically.

The mixed-FLOM detector requires the mean $\boldsymbol{\mu}_{\mathrm{H}_k}$ and covariance matrix $\mathbf{C}_{\mathrm{H}_k}$, $k = 0, 1$ which can be calculated using (4.40), (4.41), (4.45), and (4.46) with the parameters of α-stable random variable. The mixed-FLOM detector has close performance to the ML detector and is more robust to uncertainties in the knowledge of parameters of α-stable random variables than the ML detector which will be shown in the next Section 4.5.

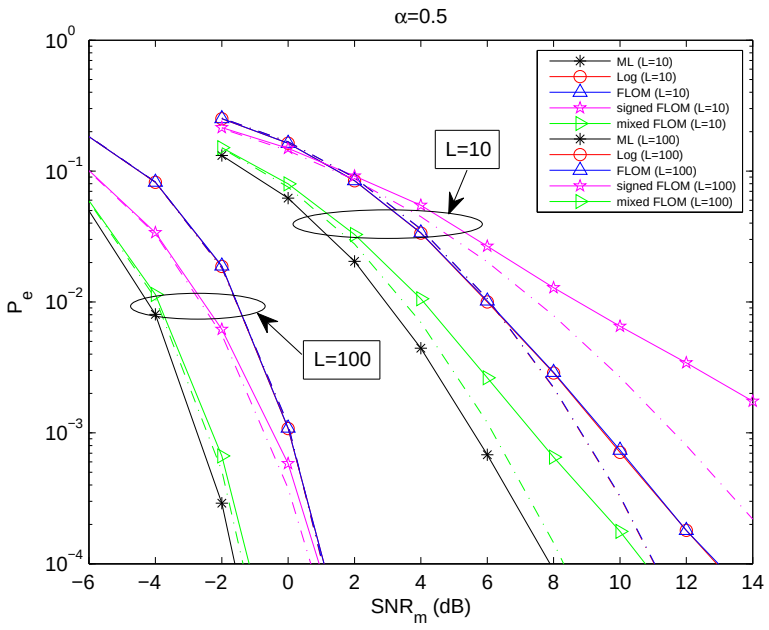

Figure 4.2: Performance comparison of ML and proposed simple detectors with $\alpha = 0.5$. The dotted lines are the theoretical results using (4.44) and (4.54) with different means and variances according to the proposed detectors.

4.5 Simulations

In this section, we will show the detection performances for proposed detectors. Since signal and interference models are already verified mathematically in Section 4.3, we will generate totally positive skewed α-stable random variables and symmetric α-stable random variables as the signal and noise instead of aggregate signal and interference from Poisson networks.

In Fig. 4.2, we show the detection performance of proposed detectors with $\alpha = 0.5$ which implies the path-loss exponent is $\delta = 4$. We also show the performance of the ML detector for comparison using numerical integration. The number of received time samples for detection is L. For the FLOM detector, $p = 0.001$ is used since the theoretical performance of the FLOM detector is an increasing function of p. In

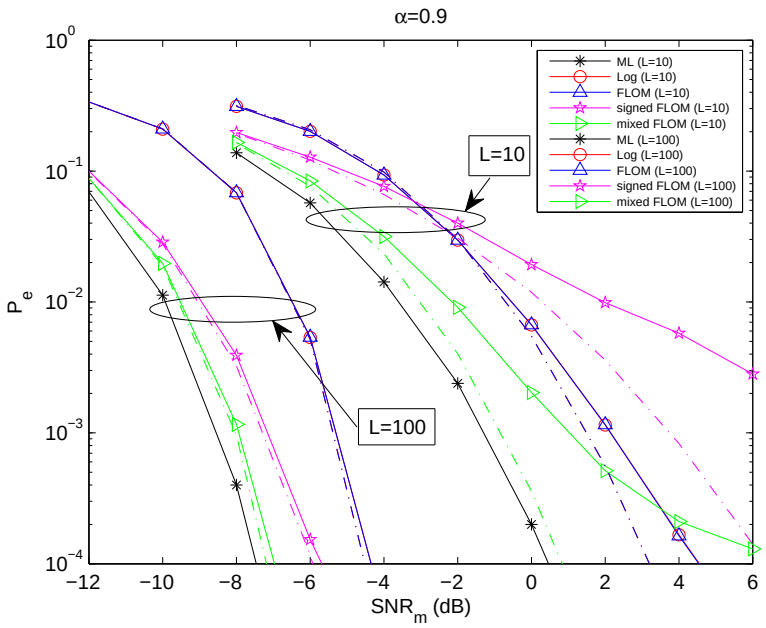

Figure 4.3: Performance comparison of ML and proposed simple detectors with $\alpha = 0.9$. The dotted lines are the theoretical results using (4.44) and (4.54) with different means and variances according to the proposed detectors.

case of the signed-FLOM detector, we used the optimal p values which are obtained numerically and guarantee the minimum theoretical performance. The log detector does not depend on p. The simulated performances of proposed detectors become close to their theoretical performances as L increases due to the central limit theorem. The mixed-FLOM detector shows the best performance over other proposed detectors. When the number of samples for detection is small ($L = 10$), the gap between the mixed-FLOM detector and the ML detector is about 2 dB at 10^{-3} error rate. Meanwhile, the performance gaps between the ML and the other proposed detectors are more than 3 dB. The gap between the ML and the mixed-FLOM detector decreases to less than 0.5 dB when the number of samples for detection is relatively large ($L = 100$).

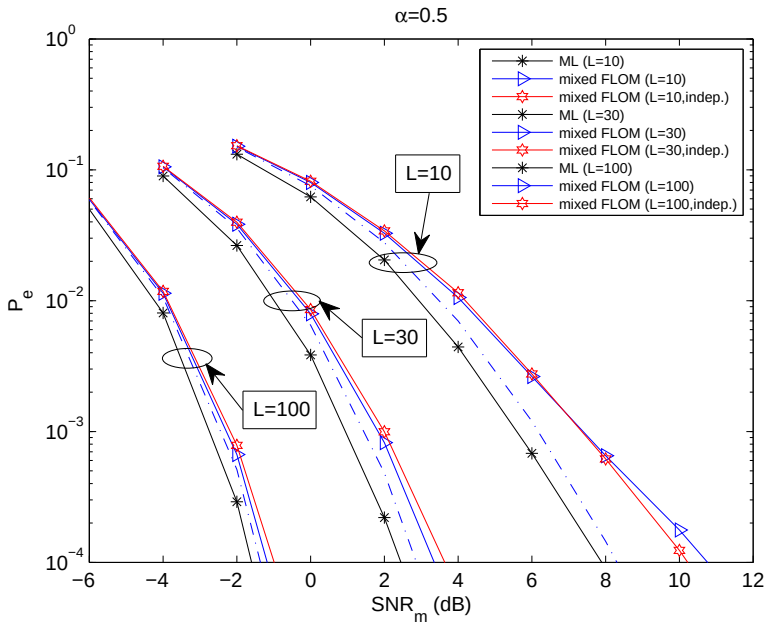

Figure 4.4: Performance comparison of mixed-FLOM detector with its simply modified detector with $\alpha = 0.5$ The dotted lines are the theoretical results using (4.54).

In the following, we show the performances with $\alpha = 0.9$ corresponding to the path-loss exponent $\delta = 2.222$ which is close to the path-loss exponent in free space. In Fig. 4.3, the mixed-FLOM detector is seen to be within 0.7 dB of the ML detector at 10^{-3} error rate when the number of samples for detection is sufficiently large ($L = 100$).

Even though the complexity of mixed-FLOM detector is much less than the ML detector, it still requires the inverse of a 2×2 covariance matrix (4.53). If it is assumed that Z_1 and Z_2 are independent in (4.52), the mixed-FLOM detector does not require the inverse matrix operation with negligible performance loss as shown in Fig. 4.4. It is noted that the mixed-FLOM detector with this assumption has a better performance than the mixed-FLOM detector without the assumption at high SNR regime when the small number of L is used for detection ($L = 10$). The reason

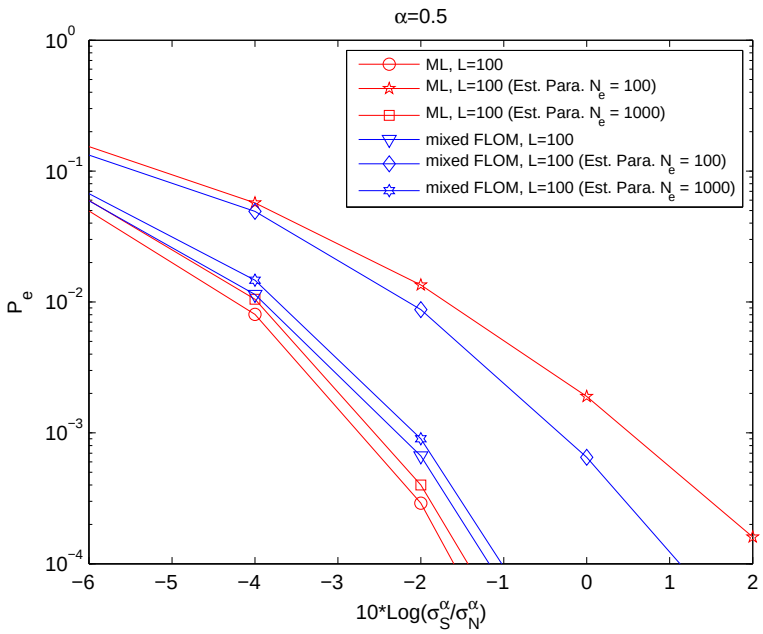

Figure 4.5: Performance comparison of ML and mixed-FLOM detector with parameter estimation error.

is that positive α-stable random variables will be generated more likely than negative values under H_1 since β_{H_1} is close to 1 at high SNR $\sigma_S^\alpha \gg \sigma_W^\alpha$. In this case, if L is small, Z_1 and Z_2 have strong correlation even though p_1 and p_2 have different values. The strong correlation can cause the covariance matrix to be ill-conditioned. By independence assumption between Z_1 and Z_2, the ill-conditioning can be avoided. However, except for the small number of samples for detection ($L = 10$), a small loss of performances is seen due to disregarding the dependency between two random variables, Z_1 and Z_2, in Fig. 4.4.

Fig. 4.5 shows the performances when the detectors use the estimated parameters of α-stable random variables, α, σ, and β. In order to investigate the effect of parameter estimation error, we assume the parameters are estimated periodically under both hypotheses using existing estimation schemes [91] and then used for the signal detec-

tion. When the number of samples for estimation is relatively large ($N_{\mathrm{e}} = 1000$), the ML detector is slightly better than the mixed-FLOM detector similar with the case that the exact knowledge of the parameters is assumed. However, the ML detector is worse than the mixed-FLOM detector when the number of samples for estimation is relatively small ($N_{\mathrm{e}} = 100$). The mixed-FLOM detector not only takes a advantage of the low computational complexity, but also possesses robustness to the parameter estimation error.

Chapter 5

STOCHASTIC ORDERING OF INTERFERENCES IN LARGE-SCALE WIRELESS NETWORKS

5.1 Literature Survey and Motivation

Since interference is the main performance-limiting factor in most wireless networks, it is crucial to characterize its statistics. The interference mainly depends on the fading channel (interfering power distribution), the path-loss model (signal attenuation with distance), and network geometry (spatial distribution of concurrently transmitting nodes). The spatial location of the interferers can be modeled either deterministically or stochastically. Deterministic models include square, triangular, and hexagonal lattices [1, 2], which are applicable when the location of the nodes in the network is constrained to a regular structure. On the other hand, only a statistical description of the location of the nodes is available in some scenarios. In both cases, the locations of transmitting nodes in the network are seen as the realizations of some point processes [3, 4, 5]. For certain classes of node distributions, most notably Poisson point processes, and certain attenuation laws, closed-form results are available for the interference distribution which determine the network performance [54, 43] (and the references therein). However the interference distribution is not tractable in most other cases.

Successful transmission probability in the presence of interference can be calculated by determining the Laplace transform of interference [93, 94, 5]. However, closed-form expressions for the Laplace transform of interference are not tractable in many cases. We approach this problem from a stochastic ordering perspective,

which is a partial order on random variables [7, 40]. Concepts of stochastic ordering have been applied to scenarios of interest in wireless communications in [41]. We will use these concepts to understand the interference in large scale wireless networks. In [40, 95, 96], the application of this set of tools in communication networks can be found. In [40, 95], the stochastic ordering has been used in studying a class of queueing networks. Directionally convex ordering of different point processes and its integral shot noise fields which are inherent from the point processes has been studied in [96]. To the best of our knowledge, there is no study of conditions on fading channels and path-loss models for stochastic ordering of network interference in the literature. In this dissertation, we use stochastic ordering theory to compare network performance under conditions of differing fading on the interference link, and different path-loss models for the establishment of stochastic ordering of interference from different point processes. Using the conditions, we compare performance without having to obtain closed-form results for a wide range of performance metrics. We also compare different point processes which are commonly used in the literature using stochastic orders, and advocate Laplace functional ordering of point processes over directional convex ordering when interferences due to these point processes are compared.

5.2 Preliminaries

In what follows, we briefly introduce several basic point processes which are commonly used to model large-scale networks [5, 43, 44, 45, 8, 38, 46, 47]. In this dissertation, we focus on stationary and isotropic point processes which are introduced in . A point process Φ is stationary if its distribution is invariant under translation through any vector $v \in \mathbb{R}^d$ and a point process Φ is isotropic if its distribution is invariant to rotations. The details for these point processes can be found in [42, 3, 44].

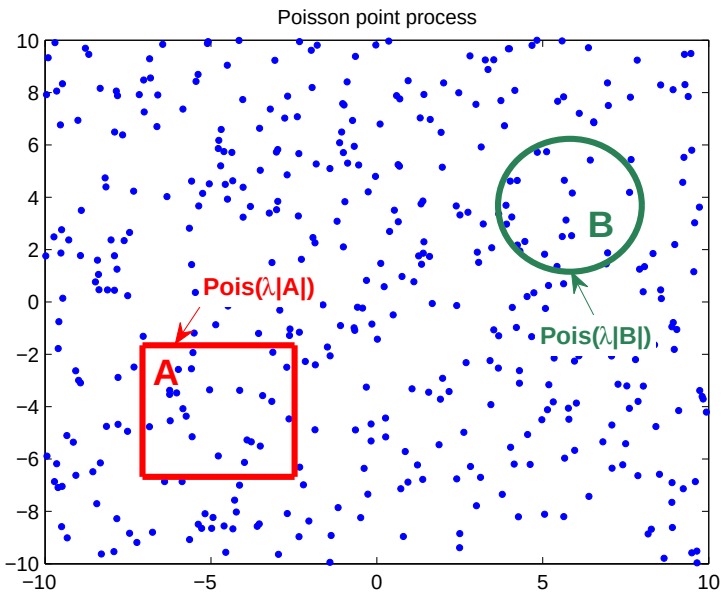

Figure 5.1: Illustration of a Poisson point process.

Homogeneous Poisson Point Processes: A homogeneous *Poisson point process* is characterized by two fundamental properties. The first is that the number of points of Φ in a bounded subset B of $\mathbb{R}^d$ has a Poisson distribution of mean $\lambda|B|$, where $|\cdot|$ denote n-dimensional volume and the constant λ is called the intensity of the Poisson point process. The second is that the numbers of points of Φ in k disjoint subsets of $\mathbb{R}^d$ form k independent random variables, for arbitrary k as shown in Fig. 5.1. A homogeneous Poisson point process is stationary and isotropic.

Doubly Stochastic Poisson Processes: A generalization of a Poisson process is made by supposing that the intensity measure is itself random, with the point process being Poisson conditional on the realization of the intensity measure. Such a process is called a *doubly stochastic Poisson process* or *Cox process*. A Cox process Φ can be thought of as arising from a two-step random mechanism, hence the term "doubly stochastic". The first step generates a measure $\Lambda(\cdot)$ on $\mathbb{R}^d$ according to the

driving random measure distribution Q. Given $\Lambda(\cdot)$, $\Phi(B)$ is Poisson distribution with parameter $\Lambda(B)$ for any bounded subset $B \subset \mathbb{R}^d$. For any finite collection of disjoint subsets $B_1, ..., B_n$ and conditioned on $\Lambda(B_1), ..., \Lambda(B_n)$, we have $\Phi(B_1), ..., \Phi(B_n)$ are independent.

Mixed Poisson Processes: The *mixed Poisson process* is a simple instance of a Cox process. It can be thought of as a homogeneous Poisson point process with randomized intensity parameter. The deriving random measure is $\Lambda(B) = X|B|$ where the randomized intensity X is a non-negative random variable. Every sample of such a process looks like a sample of some homogeneous Poisson point process. In this dissertation, $\mathbb{E}[X] = \lambda$ is assumed.

Poisson Cluster Processes: A Poisson cluster process results from homogeneous independent clustering applied to a stationary Poisson process. The parent points form a stationary Poisson process $\Phi_{\mathrm{p}} = \{x_1, x_2, \dots\}$ of intensity λ_{p}. The clusters are of the form $N_{x_i} = x_i + N_i$ for each point $x_i \in \Phi_{\mathrm{p}}$. The daughter points $N_i = \{y_1, y_2, ..., y_L\}$ are random in number and are scattered independently and with identical distribution $f(y)$ which follows an arbitrary distribution (e.g., a uniform distribution for Martérn cluster process or a symmetric normal distribution for Thomas cluster process). The complete point process Φ is given by

$$\Phi = \bigcup_{x \in \Phi_{\mathrm{p}}} N_x. \tag{5.1}$$

The intensity of the process is $\lambda = \lambda_{\mathrm{p}} \bar{c}$ where $\bar{c}$ is the mean number of daughter points per parent. In this dissertation, we assume the number of daughter points per cluster has a Poisson distribution with parameter $\bar{c}$. Fig. 5.2 shows a realization of Poisson cluster process.

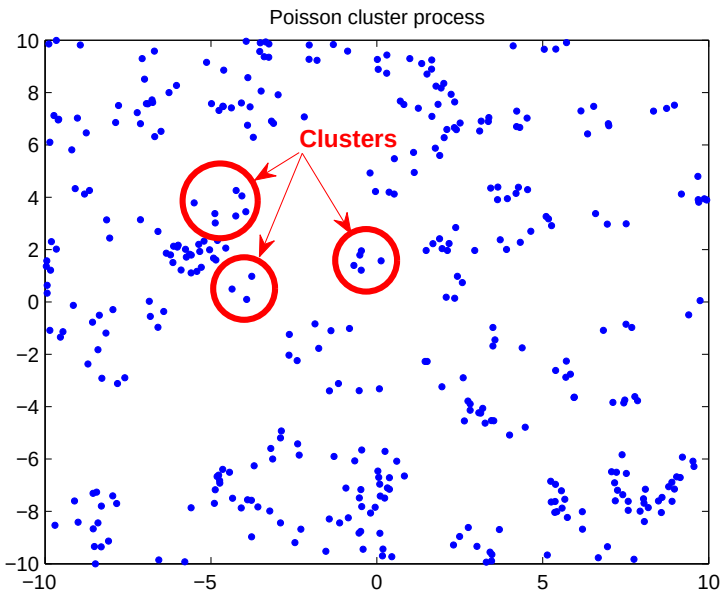

Figure 5.2: Illustration of a Poisson cluster process.

Binomial Point Processes: A Binomial Point Process (BPP) is generally used to model the location of a fixed number of wireless nodes in a bounded domain. It is a simple point process obtained by placing n points $\Phi = \{x_1, ..., x_n\} \subset \mathbb{R}^d$ independently and uniformly in a closed and bounded set $B \subset \mathbb{R}^d$. The probability that there are $k < n$ nodes in $A \subset B$ of a BPP is

$$P\left(\Phi(A) = k\right) = \binom{n}{k} \left(\frac{|A|}{|B|}\right)^k \left(1 - \frac{|A|}{|B|}\right)^{n-k}. \tag{5.2}$$

where $|A|$ represents the volume of A.

Deterministic Lattice Processes: Let $\mathbb{L} \subset \mathbb{R}^d$ be a d-dimensional lattice, i.e.,

$$\mathbb{L} \triangleq \{x = \mathbf{G}u : u \in \mathbb{Z}^d\} \tag{5.3}$$

where $\mathbf{G} \in \mathbb{R}^{d \times d}$ is the generator matrix. It is assumed that $\det \mathbf{G} \neq 0$ to exclude degenerate cases. Important cases include the square integer and the triangular lattice

in two dimensions, both with nearest-neighbor distance 1:

$$\mathbf{G}_{\text{sq}} = \begin{bmatrix} 1 & 0 \\ 0 & 1 \end{bmatrix}, \qquad \mathbf{G}_{\text{tri}} = \begin{bmatrix} 1 & 1/2 \\ 0 & \sqrt{3}/2 \end{bmatrix} \tag{5.4}$$

The lattice $\mathbb{L}$ has the property that each lattice point is centered in its Voronoi cell. The volume of each Voronoi cell is $V = |\det \mathbf{G}|$, and the density of the lattice (points per unit volume) is $\lambda = V^{-1}$.

5.3 System Model

As shown in Fig. 1.2 of Section 1.1, we assume a transmit/receive pair communicating over a wireless channel. The receiver is being interfered by interference sources distributed as stationary and isotropic point process. As introduced in Section 1.1, The accumulated interference to the receiver is given by

$$I = \sum_{x \in \Phi} h_{\text{I}}^{(x)} g(\|x\|) \tag{5.5}$$

where Φ denotes the set of all interfering nodes which is modeled as a point process on $\mathbb{R}^d$ and $h_{\text{I}}^{(x)}$ is a random variable capturing the fading coefficient between the receiver and the x^{th} interfering node. Here, typically $d = 2$ or $d = 3$, though this assumption is not necessary. Moreover, $\{h_{\text{I}}^{(x)}\}_x$ are i.i.d. random variables and independent of the point process. The path-loss is captured by a function $g(\cdot) : \mathbb{R}^+ \to \mathbb{R}^+$ which is a continuous, positive, non-increasing function of $\|x\|$ and assumed to depend only on the Euclidean distance $\|x\|$ from the node x to the receiver at the origin. In this chapter, we consider the following general path-loss model [54, 5, 43, 4]:

$$g(\|x\|) = (a + b\|x\|^{\delta})^{-1} \tag{5.6}$$

for some $b > 0$, $\delta > d$ and $a \in \{0, 1\}$, where δ is called the path-loss exponent, a determines whether the path-loss model belongs to a singular path-loss model ($a = 0$)

or a non-singular path-loss model ($a = 1$), and b is a compensation parameter to keep the total receive power normalized which will be discussed in detail in Section 5.6. It is noted that from Campbell's theorem in Section 2.3.2 and the aggregated interference model in (5.5), any two stationary point processes with the same intensity have equal mean power of interferences (when the expectation of (5.5) exists).

Assuming the effective channel power between the desired receiver and its transmitter is h_{S} which can be a non-negative constant or a RV, the signal to interference ratio (SIR) is given by

$$SIR = \frac{h_{\mathrm{S}}}{I} \tag{5.7}$$

where I is the interference power given by (5.5). If there is additive noise with power W which can be a non-negative constant or RV as well, then the signal to interference plus noise ratio (SINR) is given by [5, 57, 4]

$$SINR = \frac{h_{\mathrm{S}}}{W + I}. \tag{5.8}$$

In this dissertation, the LT ordering of two interference distributions will be mainly discussed. The Laplace transform of interference plus noise is $\mathbb{E}[\exp(-s(W+I))] = \mathcal{L}_W(s)\mathcal{L}_I(s)$. Clearly the LT ordering of two interference distributions is not affected by a common noise power W. Therefore, we focus on interference distributions hereafter.

5.4 Ordering of Outage Probability and Ergodic Capacity Metric

In this section we introduce performance metrics involving the stochastic ordering of interference. Firstly, we study the SIR-based outage probability. It has been shown in [5] that when h_{S} is exponentially distributed, the LT ordering of the interference can be related to the outage defined in terms of SINR. We generalize this result to a broader class of distributions for the effective channel RV h_{S}.

Theorem 5.4.1. *Let I_1 and I_2 denote the interferences from point process Φ_1 and Φ_2 respectively. Also, let h_{S} be the effective fading channel between the desired receiver and its transmitter and has a CCDF $\bar{F}_{h_{\mathrm{S}}}(x) := 1 - F_{h_{\mathrm{S}}}(x)$, which is a c.m. function. Under these assumptions, if $I_1 \leq_{\mathrm{Lt}} I_2$, then $SIR_2 \leq_{\mathrm{st}} SIR_1$.*

Proof. Let $\bar{F}_{h_{\mathrm{S}}}(x)$ be the c.m. CCDF of h_{S}. Then we have

$$P(SIR_1 > x) = \mathbb{E}_{I_1}\left[P(h_{\mathrm{S}} > xI_1)\right] = \mathbb{E}_{I_1}\left[\bar{F}_{h_{\mathrm{S}}}(xI_1)\right] \tag{5.9}$$

$$\geq \quad \mathbb{E}_{I_2}\left[\bar{F}_{h_{\mathrm{S}}}(xI_2)\right] = \mathbb{E}_{I_2}\left[P(h_{\mathrm{S}} > xI_2)\right] = P(SIR_2 > x), \tag{5.10}$$

where the inequality is due to $I_1 \leq_{\mathrm{Lt}} I_2$ and equation (2.5). Recalling the definition of $\leq_{\mathrm{st}}$ in (2.3), Theorem 5.4.1 is proved. □

Theorem 5.4.1 enables us to conclude the usual stochastic ordering of SIRs whenever LT ordering of interferences are established. In the sequel, we will show many examples of how LT ordering between two interference distributions can be established which can be used with Theorem 5.4.1 to establish the "usual stochastic" ordering of outage as in (2.3) of Section 2.2.1. Illustrations of Theorem 5.4.1 are shown in our numerical results in Section 5.8. Note that if two interferences have the usual stochastic ordering $I_1 \leq_{\mathrm{st}} I_2$ (a stronger assumption than in Theorem 5.4.1), then we can have $SIR_2 \leq_{\mathrm{st}} SIR_1$ with any arbitrary distribution for h_{S} and not just those with a c.m. CCDF.

Now consider the expression

$$C = \mathbb{E}\left[\log_2\left(1 + \frac{h_{\mathrm{S}}}{W + I}\right)\right], \tag{5.11}$$

which is the bandwidth-normalized capacity in the weak interference regime [5, 97, 57]. The expectation in (5.11) is with respect to the arbitrary positive random variable h_{S}, as well as the interference I given in (5.5). The noise power $W \geq 0$ is fixed, and h_{S}, I are independent.

We would like to compare two regimes (h_{S_1}, I_1) with capacity C_1, and (h_{S_2}, I_2) with capacity C_2, where $h_{\mathrm{S}_2} \leq_{\mathrm{Lt}} h_{\mathrm{S}_1}$, and $I_1 \leq_{\mathrm{Lt}} I_2$. Since $\log(1+h_{\mathrm{S}})$ is c.m.d. with respect to h_{S} and $\log(1+1/(W+I))$ is c.m. with respect to I, by using (2.5) and (2.6) successively, we have $C_1 \geq C_2$. Therefore the LT ordering of interferences and the LT ordering of effective channels together lead to ordering of ergodic capacities. Unlike in Theorem 5.4.1, in this case, we can compare the ergodic capacity *regardless of the distribution* of fading channel, h_{S}. Section 5.5.1 has examples of fading distributions that are LT ordered.

Having emphasized the impact of LT ordering on outage and capacity metrics, in what follows, we will investigate the conditions for the presence of LT ordering of interference distributions. The three factors which affect the interference distribution are the fading channel from the interfering nodes to the receiver $h_{\mathrm{I}}^{(x)}$, the path-loss model $g(\cdot)$, and the point process of interfering nodes Φ as shown in the interference model in (5.5). We derive the conditions on fading channels and path-loss models and the underlying point processes for the LT ordering of interferences. We also identify the LT ordering of interference distributions in commonly used point processes.

5.5 Comparison of Fading Channels on the Interference Link

In the previous section we mentioned that the effective channels between the transmitter and receiver, h_{S_1} and h_{S_2}, can be compared. In this section, we find the conditions on the distribution of $h_{\mathrm{I}}^{(x)}$ on the *interference link* for the interference in (5.5) to be LT ordered. Since $h_{\mathrm{I}}^{(x)}$ are assumed as i.i.d., we will drop the node index x for convenience hereafter, when we refer to its distribution.

Theorem 5.5.1. *Let I_1 and I_2 denote the interferences both with the same path-loss model $g(\|x\|)$, from a stationary point process Φ as in* (5.5)*. Also, let h_{I_1} and h_{I_2} be RVs whose distributions capture the fading channels between the receiver and*

interferers under the two scenarios that are compared. Under these assumptions, if $h_{\mathrm{I}_1} \leq_{\mathrm{Lt}} h_{\mathrm{I}_2}$, *then* $I_1 \leq_{\mathrm{Lt}} I_2$.

Proof. The Laplace transform of aggregated interference $I := \sum_{x\in\Phi} h_{\mathrm{I}}^{(x)} g(\|x\|)$ is a Laplace functional (2.8) evaluated at $u(x) = sh_{\mathrm{I}} g(\|x\|), s \geq 0, h_{\mathrm{I}} \geq 0$ and $g(\|x\|) \geq 0$ where h_{I} is the effective fading channel between the receiver and interferers and $g(\|x\|)$ is a path-loss model. $\mathcal{L}_I(s)$ can be expressed as follows:

$$\mathcal{L}_I(s) = \mathbb{E}\left[e^{-sI}\right] = \mathbb{E}\left[e^{-sh_{\mathrm{I}} \int_{\mathbb{R}^d} g(\|x\|)\Phi(\mathrm{d}x)}\right], \tag{5.12}$$

where the expectation is to be taken over both Φ and h_{I}. Let $Z = \int_{\mathbb{R}^d} g(\|x\|)\Phi(\mathrm{d}x)$ in (5.12). From [7, Theorem 5.A.7 (b)], if $\mathbb{E}\left[\exp\left(-sI_1\right)|Z=z\right] \geq \mathbb{E}\left[\exp\left(-sI_2\right)|Z=z\right]$ for all z in the support of Z, then $I_1 \leq_{\mathrm{Lt}} I_2$. Therefore, it is sufficient to show the following equation regardless of a point process Φ in order to satisfy the LT ordering between interferences,

$$\mathbb{E}_{h_{\mathrm{I}_1}}\left[e^{-szh_{I_1}}|Z=z\right] \geq \mathbb{E}_{h_{\mathrm{I}_2}}\left[e^{-szh_{I_2}}|Z=z\right]. \tag{5.13}$$

But (5.13) follows from the assumption $h_{\mathrm{I}_1} \leq_{\mathrm{Lt}} h_{\mathrm{I}_2}$. Thus, we conclude that if $h_{\mathrm{I}_1} \leq_{\mathrm{Lt}} h_{\mathrm{I}_2}$, then $I_1 \leq_{\mathrm{Lt}} I_2$. □

The interference in a stationary point process depends on the fading channel between the receiver and interferers. Intuitively a bigger LT ordering indicates a fading channel that is more like AWGN (i.e., "less fading"). Therefore, the interference arising from it indicates interference adding up more coherently, giving rise to a "bigger" interference in the LT ordering sense.

As mentioned in Section 5.3, we assumed the interferers are distributed on an infinite region due to the stationarity of the point process. However, receivers in many wireless networks may experience interference from finite-area regions [98]. Theorem 5.5.1 is also valid for the interference in finite area. Moreover, when guard zones

around the receiver occur due to sophisticated MAC protocols [99, 100], Theorem 5.5.1 still holds.

5.5.1 Parametric Fading on the Interference Link

In this section, we show the interference distributions are monotonic in line of sight (LoS) parameter of the fading channels with respect to the LT order for commonly used parametric fading distributions such as Nakagami-m and Ricean fading. By Theorem 5.5.1 this implies LT ordering of interferences, which, by Theorem 5.4.1 establishes stochastic ordering of SIRs.

Consider Nakagami fading model, where the envelope $\sqrt{h_{\mathrm{I}}}$ is Nakagami and the effective channel h_{I} follows the distribution

$$f_{h_{\mathrm{I}}}(x) = \frac{m^m}{\Gamma(m)} x^{m-1} \exp(-mx),\ x \geq 0. \tag{5.14}$$

Since $\mathbb{E}[-sh_{\mathrm{I}}] = (1 + s/m)^{-m}$ is a decreasing function of m for each s, it follows that if the m parameters of two channel distributions satisfy $m_1 \leq m_2$ then, $h_{\mathrm{I}_1} \leq_{\mathrm{Lt}} h_{\mathrm{I}_2}$ where h_{I_1} and h_{I_2} have normalized Gamma distributions with parameter m_1 and m_2 respectively. From Theorem 5.5.1, it follows that $I_1 \leq_{\mathrm{Lt}} I_2$, if $m_1 \leq m_2$.

Similarly, the envelope $\sqrt{h_{\mathrm{I}}}$ is Ricean and the distribution of effective channel h_{I} is given by

$$f_{h_{\mathrm{I}}}(x) = (K+1) \exp\left[-(K+1)x - K\right] I_0(2\sqrt{K(K+1)x}),\ x \geq 0, \tag{5.15}$$

where K is the LoS parameter of Ricean fading channel and $I_0(t) := \sum_{m=0}^{\infty} (t/2)^{2m}/(m!\,\Gamma(m+1))$ is the modified Bessel function of the first kind of order zero. The Laplace transform of (5.15) decreases with K for all $s \geq 0$. Thus, similar to the Nakagami case, if $K_1 \leq K_2$ are the Ricean parameters of two channels, then $h_{\mathrm{I}_1} \leq_{\mathrm{Lt}} h_{\mathrm{I}_2}$ which by Theorem 5.5.1 imply that $I_1 \leq_{\mathrm{Lt}} I_2$.

In addition to the Nakagami-m and Ricean fading cases, it can be shown through a procedure similar to the discussion that the interference distribution corresponding to Nakagami-q (Hoyt) fading [101] also satisfies LT ordering with respect to the shape parameter.

5.5.2 Interference in Combined Multipath Fading and Shadowing

The effect of shadow fading on the interference power distribution can be modeled as a product of a shadowing random variable with a multipath fading random variable. Let $h_{\mathrm{I}_1} \leq_{\mathrm{Lt}} h_{\mathrm{I}_2}$ be the two effective multipath fading distributions, and $X_1 \leq_{\mathrm{Lt}} X_2$ be the two shadowing distributions. Then, from [7, Theorem 5.A.7 (d)], it follows that the composite RV satisfies $h_{\mathrm{I}_1} X_1 \leq_{\mathrm{Lt}} h_{\mathrm{I}_2} X_2$, since $l(x, y) = xy$ has a c.m. derivative in each variable. We conclude that if $h_{\mathrm{I}_1} \leq_{\mathrm{Lt}} h_{\mathrm{I}_2}$ and $X_1 \leq_{\mathrm{Lt}} X_2$, then $I_1 \leq_{\mathrm{Lt}} I_2$ from Theorem 5.5.1. Such conclusions are especially useful even when the composite distribution of $h_{\mathrm{I}_1} X_1$ or $h_{\mathrm{I}_2} X_2$ cannot be written in closed-form.

5.6 Comparison of Path-loss Models

Here, we show the ordering of mean power of interferences in a stationary point process with different path-loss models. Generally, the mean power of interference is an important factor to determine a system performance. For example, by considering the mean power of interferences as noise power, the average error rate can be approximated. Thus, we are interested in comparison the mean power of interferences. In what follows, we show the condition on the mean power of interferences with non-singular path-loss models with different path-loss exponents under which this ordering holds:

Theorem 5.6.1. *Let I_1 and I_2 denote the interferences both with identical fading distribution h_{I} in a stationary point process Φ. Also, let $g_1(\|x\|)$ and $g_2(\|x\|)$ be*

the non-singular path-loss models with $a = 1$ and $b = 1$ in (5.6) and with different path-loss exponents δ_1 and δ_2, respectively. If $\delta_1 \leq \delta_2$, then $\mathbb{E}[I_2] \leq \mathbb{E}[I_1]$.

Proof. In order to prove $\mathbb{E}[I_1] \geq \mathbb{E}[I_2]$, using Campbell's theorem in Section 2.3.2 with $u(x) = h_{\mathrm{I}} g(\|x\|)$ where h_{I} is the (power) fading coefficient and $g(\|x\|)$ is the non-singular path-loss model in (5.6), we need to show the following:

$$\lambda \int_{\mathbb{R}^d} h_{\mathrm{I}} g_1(\|x\|) \mathrm{d}x \geq \lambda \int_{\mathbb{R}^d} h_{\mathrm{I}} g_2(\|x\|) \mathrm{d}x. \tag{5.16}$$

Since h_{I} is independent from the point process and $g(\|x\|)$ can be expressed as $g(r), r = \|x\|$ under polar coordinates, after expectation with respect to h_{I} and change to polar coordinates, the following condition needs to be satisfied to prove Theorem 5.6.1:

$$\mathbb{E}\left[h_{\mathrm{I}}\right] \lambda c_d d \int_0^{\infty} g_1(r) r^{d-1} \mathrm{d}r \geq \mathbb{E}\left[h_{\mathrm{I}}\right] \lambda c_d d \int_0^{\infty} g_2(r) r^{d-1} \mathrm{d}r. \tag{5.17}$$

where c_d is the volume of the d-dimensional unit ball and h_{I} is the (power) fading coefficient between the receiver and interferers. Using a change of variables, we get

$$\int_{g_1(\infty)}^{g_1(0)} u \left(g_1^{-1}(u)\right)^{d-1} \frac{\partial}{\partial u} \left(g_1^{-1}(u)\right) \mathrm{d}u \geq \int_{g_2(\infty)}^{g_2(0)} u \left(g_2^{-1}(u)\right)^{d-1} \frac{\partial}{\partial u} \left(g_2^{-1}(u)\right) \mathrm{d}u. \tag{5.18}$$

where d is the dimension of point process, $g^{-1}(\cdot)$ is the inverse function of $g(\cdot)$ and $I[u \in S] = 1$, if $u \in S$, and 0 otherwise, is the indicator function. Substituting the non-singular path-loss models $g_1(r)$ and $g_2(r)$ with $a = 1$ and $b = 1$ in (5.6) into (5.18), we get

$$\int_0^1 u \left(\frac{\left(\frac{1}{u} - 1\right)^{\frac{d}{\delta_1} - 1}}{\delta_1 u^2} - \frac{\left(\frac{1}{u} - 1\right)^{\frac{d}{\delta_2} - 1}}{\delta_2 u^2} \right) \mathrm{d}u = \frac{\Gamma\left(1 - \frac{d}{\delta_1}\right) \Gamma\left(\frac{d}{\delta_1}\right)}{\delta_1} - \frac{\Gamma\left(1 - \frac{d}{\delta_2}\right) \Gamma\left(\frac{d}{\delta_2}\right)}{\delta_2} \geq 0, \tag{5.19}$$

since $\frac{\Gamma\left(1-\frac{d}{\delta}\right)\Gamma\left(\frac{d}{\delta}\right)}{\delta}$ is a decreasing function with δ for a fixed d and $\delta_1 \leq \delta_2$. The proof for Theorem 5.6.1 is complete. □

Theorem 5.6.1 compares the mean power of interference for two different path-loss models and identical fading. It is clear from the proof of Theorem 5.6.1 that if the fading is different with $\mathbb{E}[h_{\mathrm{I}_1}] \geq \mathbb{E}[h_{\mathrm{I}_2}]$, the conclusion would still hold.

Under a stationary Poisson point process, we can establish the stronger stochastic ordering, LT ordering of interferences, because if $I_1 \geq_{\mathrm{Lt}} I_2$, then $\mathbb{E}[I_1] \geq \mathbb{E}[I_2]$. In what follows, we find the conditions on the interference distributions with non-singular path-loss models with different path-loss exponents under which this stochastic ordering holds:

Theorem 5.6.2. *Let I_1 and I_2 denote the interferences both with identical fading distribution h_{I} in a stationary Poisson point process Φ_{PPP}. Also let $g_1(\|x\|)$ and $g_2(\|x\|)$ be the non-singular path-loss models with $a = 1$ and $b = 1$ in (5.6) and with different path-loss exponents δ_1 and δ_2, respectively. If $\delta_1 \leq \delta_2$, then $I_2 \leq_{\mathrm{Lt}} I_1$.*

Proof. The Laplace transform of interference power in a stationary Poisson point process with path-loss model $g_j(r), j = 1, 2$ in (5.6) and intensity λ can be expressed as follows:

$$\mathcal{L}_{I_j}(s) = \exp\left\{-\lambda c_d d \int_0^\infty \left[1 - \exp\left(-s h_{\mathrm{I}} g_j(r)\right)\right] r^{d-1} \mathrm{d}r\right\} \tag{5.20}$$

where c_d is the volume of the d-dimensional unit ball and h_{I} is the (power) fading coefficient between the receiver and interferers. From [7, Theorem 5.A.7 (b)], it is sufficient to show $\mathcal{L}_{I_1}(s) \geq \mathcal{L}_{I_2}(s)$ in (5.20) regardless of a distribution of h_{I} in order to satisfy the LT ordering between interferences. To do so, the following condition needs to be satisfied after change of variables:

$$\begin{aligned} &\int_{g_1(\infty)}^{g_1(0)} \left[1 - \exp\left(-s h_{\mathrm{I}} u\right)\right] \left(g_1^{-1}(u)\right)^{d-1} \frac{\partial}{\partial u}\left(g_1^{-1}(u)\right) \mathrm{d}u \\ &\quad \geq \int_{g_2(\infty)}^{g_2(0)} \left[1 - \exp\left(-s h_{\mathrm{I}} u\right)\right] \left(g_2^{-1}(u)\right)^{d-1} \frac{\partial}{\partial u}\left(g_2^{-1}(u)\right) \mathrm{d}u. \end{aligned} \tag{5.21}$$

Substituting the same non-singular path-loss models into (5.21), it follows

$$\int_0^1 \left(1-\exp\left(-sh_{\mathrm{I}}u\right)\right)\left(\frac{\left(\frac{1}{u}-1\right)^{\frac{d}{\delta_1}-1}}{\delta_1 u^2}-\frac{\left(\frac{1}{u}-1\right)^{\frac{d}{\delta_2}-1}}{\delta_2 u^2}\right)\mathrm{d}u \tag{5.22}$$

$$\geq \left(1-\exp\left(-sh_{\mathrm{I}}\right)\right)\int_0^1 u\left(\frac{\left(\frac{1}{u}-1\right)^{\frac{d}{\delta_1}-1}}{\delta_1 u^2}-\frac{\left(\frac{1}{u}-1\right)^{\frac{d}{\delta_2}-1}}{\delta_2 u^2}\right)\mathrm{d}u \tag{5.23}$$

$$= \left(1-\exp\left(-sh_{\mathrm{I}}\right)\right)\underbrace{\left(\frac{\Gamma\left(1-\frac{d}{\delta_1}\right)\Gamma\left(\frac{d}{\delta_1}\right)}{\delta_1}-\frac{\Gamma\left(1-\frac{d}{\delta_2}\right)\Gamma\left(\frac{d}{\delta_2}\right)}{\delta_2}\right)}_{A}\geq 0. \tag{5.24}$$

(5.23) follows from $(1-\exp(-c))u \leq 1-\exp(-cu)$ for $c \geq 0$ and $0 \leq u \leq 1$ and (5.24) follows from $1-\exp(-sh_{\mathrm{I}}) \geq 0$ for $sh_{\mathrm{I}} \geq 0$ and $A \geq 0$ from (5.19). Theorem 5.6.2 is proved. □

For the non-singular path-loss model $g(\|x\|)$ with $a=1$ and $b=1$ is assumed, however, the mean power of interference with $g_1(\|x\|)$ is greater than that with $g_2(\|x\|)$ from Theorem 5.6.1. Thus, for more fair comparison of LT ordering of the interferences, we set the parameter b in (5.6) for $g_2(\|x\|)$ to have a equal mean power of interference as that of $g_1(\|x\|)$, using Campbell's Theorem as follows:

$$b=\left(\frac{\delta_2\Gamma\left(1-\frac{d}{\delta_1}\right)\Gamma\left(\frac{d}{\delta_1}\right)}{\delta_1\Gamma\left(1-\frac{d}{\delta_2}\right)\Gamma\left(\frac{d}{\delta_2}\right)}\right)^{-\frac{\delta_2}{d}}, \tag{5.25}$$

where $b \leq 1$. It is noted that the interferences, I_1 and I_2, with path-loss models, $g_1(\|x\|)$ with $a=1$ and $b=1$ and $g_2(\|x\|)$ with $a=1$ and b is set the value in (5.25) and with different path-loss exponents δ_1 and δ_2 in (5.6) in a stationary point process Φ have same mean power of interference, even if $\delta_1 \leq \delta_2$. Then, with (5.25), we can establish additional LT ordering of interferences as follows:

Corollary 5. *Let I_1 and I_2 denote the interferences both with identical fading distribution h_{I} in a stationary Poisson point process Φ_{PPP}. Also let $g_1(\|x\|)$ be the non-singular*

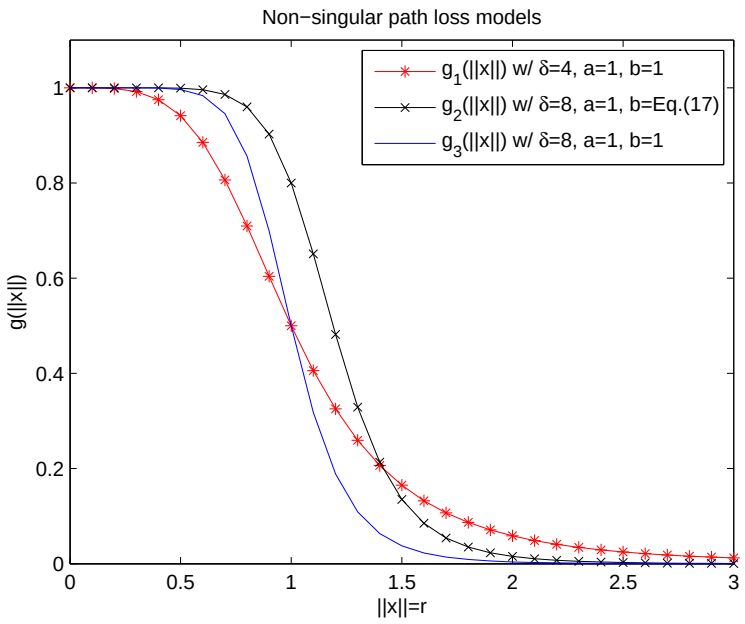

Figure 5.3: Non-singular path-loss models with different path-loss exponents, δ_1 and δ_2

path-loss model in (5.6) *with* δ_1, $a = 1$ *and* $b = 1$ *and* $g_2(\|x\|)$ *be the non-singular path-loss models with* δ_2, $a = 1$ *and* b *is set the value in* (5.25). *If* $\delta_1 \leq \delta_2$, *then* $I_2 \leq_{\mathrm{Lt}} I_1$.

Proof. The proof is the same as the proof for Corollary 5.6.2 with setting the value of b for $g_2(\|x\|)$ is (5.25) instead of $b = 1$. □

From Corollary 5, it is seen that the interference distributions with non-singular path-loss models in stationary Poisson point process are monotonic in the path-loss exponent with respect to the LT order. Indeed, the parameter b in (5.25) was set to ensure the mean interference powers are equal. Hence, the better performance in SIR-based outage probability or ergodic capacity with increased path-loss exponent δ is not due to an improvement of average interference power.

Theorem 5.6.1, 5.6.2 and Corollary 5 show that one path-loss model need not

dominate the other pointwise to get an ordering in interference in the case of the non-singular path-loss model. Indeed, if $g_1(r) \geq g_2(r), \forall r \in \mathbb{R}^+$ (for example, a comparison of singular and non-singular path-loss model), it is obvious that $\mathbb{E}[I_1] \geq \mathbb{E}[I_2]$ since the aggregated interference power with $g_1(r)$ is always greater than that with $g_2(r)$. For a stationary Poisson point process, we can also easily observe when $g_1(r) \geq g_2(r)$, $I_1 \geq_{\mathrm{Lt}} I_2$ from (5.20). However, from Theorem 5.6.1, 5.6.2 and Corollary 5, we can establish the stochastic orderings of interferences even in the case that $g_1(r) < g_2(r)$ in some range of r and $g_1(r) > g_2(r)$ in another range of r as shown in Fig. 5.3. The simulation result to verify these theorems will be shown in Section 5.8.

For the singular path-loss model ($a = 0$ and $b > 0$) in (5.6), a finite mean of interference power does not exist in a stationary point process since (5.16) does not converge. Thus the means of interferences cannot be compared. In case of a stationary Poisson point process, we have a closed-form expression for Laplace transform of interference with the singular path-loss model in a stationary Poisson point process as follows [57]:

$$\mathcal{L}_I(s) = \exp(-\lambda c_d \mathbb{E}[h_{\mathrm{I}}^{\alpha}]\Gamma(1-\alpha)s^{\alpha}), \tag{5.26}$$

where $\alpha = d/\delta$ and c_d is the volume of the d-dimensional unit ball. $\mathbb{E}[h_{\mathrm{I}}^{\alpha}]$ is a fractional moment of h_{I} with $0 < \alpha < 1$. Unlike the non-singular path-loss model, however, the LT ordering does not hold between two different interferences corresponding to path-loss exponents $\delta_1 \leq \delta_2$ in case of the singular path-loss model since (5.26) is not a decreasing function of δ.

5.7 Comparison of Different Point Processes

In [96] directionally convex ordering (DCX) is used to order point processes. In this section, we define a new stochastic ordering between point processes and state some results involving the ordering of point processes. We first define a new stochastic

ordering of point processes based on the well-known Laplace functional:

Definition 5.7.1. *Let Φ_1 and Φ_2 be two stationary point processes such that*

$$L_{\Phi_1}(u) = \mathbb{E}\left[e^{-\sum_{x\in\Phi_1} u(x)}\right] \geq \mathbb{E}\left[e^{-\sum_{x\in\Phi_2} u(x)}\right] = L_{\Phi_2}(u) \tag{5.27}$$

where $u(\cdot)$ runs over the set $\mathcal{U}$ of all non-negative functions on $\mathbb{R}^d$. Then Φ_1 is said to be smaller than Φ_2 in the Laplace functional (LF) order (denoted by $\Phi_1 \leq_{\mathrm{Lf}} \Phi_2$).

It can be shown that LF ordering follows from dcx ordering, which makes LF ordering easier to verify and easier to relate to interference metrics. Note that the LT ordering in (2.4) is for RVs, whereas the LF ordering in (5.27) is for point processes. They can be connected in the following way:

$$\Phi_1 \leq_{\mathrm{Lf}} \Phi_2 \Longleftrightarrow \sum_{x\in\Phi_1} u(x) \leq_{\mathrm{Lt}} \sum_{x\in\Phi_2} u(x),\ \forall u \in \mathcal{U} \tag{5.28}$$

Hence, it is possible to think of LF ordering of point processes as the LT ordering of their interferences in the absence of fading, for all non-negative path-loss functions. But as we will see, LT ordering of their interferences in the presence of fading can be proved when two point processes are LF ordered. We next prove a generalization of Theorem 5.5.1 where the two point processes are different and LF ordered.

Theorem 5.7.1. *Let Φ_1 and Φ_2 be two stationary point processes and h_{I_1} and h_{I_2} be RVs whose distributions capture the fading channels between the receiver and interferers under the two scenarios that are compared. Also let I_1 and I_2 denote the interferences with same path-loss model $g(\|x\|)$ in Φ_1 and Φ_2 respectively. If $\Phi_1 \leq_{\mathrm{Lf}} \Phi_2$ and $h_{\mathrm{I}_1} \leq_{\mathrm{Lt}} h_{\mathrm{I}_2}$, then $I_1 \leq_{\mathrm{Lt}} I_2$.*

Proof. Theorem 5.7.1 follows from Theorem 5.5.1 and equation (5.28) with $u(x) = h_{\mathrm{I}} g(\|x\|)$. □

Note that in Theorem 5.7.1, h_{I} does not only capture a fading distribution, but also can capture a random thinning property of point process.

5.7.1 Laplace Functional Ordering between Specific Point Processes

Here, we compare the LF order between different point processes which are commonly used. These are Poisson point process and Neyman-Scott process with Poisson distributed number of points in each cluster which is one of example of Poisson cluster process. The Neyman-Scott process results from homogeneous independent clustering applied to a stationary Poisson point process. The details for these point processes can be found in [3, 44].

Theorem 5.7.2. *If Φ_{PPP} and Φ_{PCP} denote Poisson point process and Neyman-Scott process with Poisson distributed number of daughter points respectively and both point processes have same intensity λ, then $\Phi_{\text{PCP}} \leq_{\text{Lf}} \Phi_{\text{PPP}}$.*

Proof. Let $u(\cdot) \in \mathcal{U}$ be all non-negative functions on $\mathbb{R}^d$. The Laplace functional of Neyman-Scott process with Poisson distributed number of daughter points and with the distribution $f(\cdot)$ for locations of daughter points can be expressed as follows[3, 5]:

$$\begin{aligned} L_{\Phi_{\text{PCP}}}(u) &= \exp\left\{-\lambda_{\text{p}} \int_{\mathbb{R}^d} \left[1 - \exp\left(-\bar{c}\left(1 - \int_{\mathbb{R}^d} \exp(-u(x+y)) f(y)\mathrm{d}y\right)\right)\right] \mathrm{d}x\right\} \\ &\geq \exp\left\{-\lambda_{\text{p}} \bar{c} \int_{\mathbb{R}^d} \left[1 - \int_{\mathbb{R}^d} \exp(-u(x+y)) f(y)\mathrm{d}y\right] \mathrm{d}x\right\} \qquad (5.29) \\ &= \exp\left\{-\lambda \int_{\mathbb{R}^d} [1 - \exp(-u(x))]\, \mathrm{d}x\right\} \qquad (5.30) \\ &= L_{\Phi_{\text{PPP}}}(u) \end{aligned}$$

where the inequality in (5.29) follows from the fact that $1-\exp(-ax) \leq ax,\ a \geq 0$ and (5.30) follows from change of variables, interchanging integrals and using $\int f(y)\mathrm{d}y = 1$ [44]. □

We consider another point process, the mixed Poisson process which is a simple instance of a Cox process. It can be thought of as a stationary Poisson point process with randomized intensity parameter X which has the averaged intensity measure

$\mathbb{E}_X[X] = \lambda$. Every sample of such a process looks like a sample of some stationary Poisson point process. We compare the LF ordering of this point process with that of stationary Poisson point process as follows:

Theorem 5.7.3. *If Φ_{PPP} and Φ_{MPP} denote Poisson point process and mixed Poisson process respectively and both point processes have same average intensity λ, then $\Phi_{\text{MPP}} \leq_{\text{Lf}} \Phi_{\text{PPP}}$.*

Proof. Let $u(\cdot) \in \mathcal{U}$ be all non-negative functions on $\mathbb{R}^d$. The Laplace functional of the mixed Poisson process process with a random intensity measure X which has the averaged intensity measure $\mathbb{E}_X[X] = \lambda$ can be expressed as follows [102]:

$$\begin{aligned} L_{\Phi_{\text{MPP}}}(u) &= \mathbb{E}_X\left[\exp\left\{-X\int_{\mathbb{R}^d}[1-\exp(-u(x))]\,\mathrm{d}x\right\}\right] && (5.31)\\ &\geq \exp\left\{-\mathbb{E}_X[X]\int_{\mathbb{R}^d}[1-\exp(-u(x))]\,\mathrm{d}x\right\} && (5.32)\\ &= \exp\left\{-\lambda\int_{\mathbb{R}^d}[1-\exp(-u(x))]\,\mathrm{d}x\right\} && (5.33)\\ &= L_{\Phi_{\text{PPP}}}(u) \end{aligned}$$

where the inequality in (5.32) follows from Jensen's inequality since the term inside the brackets in (5.31) is a convex function of X. □

The aggregated interference from Poisson cluster process or mixed Poisson process is always less than that from Poisson point process in LT order by Theorem 5.7.1. This means that the orderings of SIR-based outage probabilities or ergodic capacities are established depending on a point process by the performance metrics in Section 5.4. It is noted that from Campbell's theorem in Section 2.3.2, any two stationary point processes with same intensity have equal mean power of interferences (when the expectation in (5.5) exists). Hence, the better performance in SIR-based outage probability or ergodic capacity in specific point process is not due to an improvement of average interference power.

The above point processes are less than Poisson point process in LF order. In what follows, we show the point process which has larger LF ordering than Poisson point process even though it is non-stationary and non-isotropic. In binomial point processes, there are a total of N transmitting nodes uniformly distributed in a d-dimensional ball of radius r centered at the origin, denoted as $B_{\rm o}(r)$. The density of the process is given by $\lambda = N/(c_d r^d)$ where c_d is the volume of the d-dimensional unit ball [103]. In this case, we can compare the LF ordering of point processes in bounded area as follows:

Theorem 5.7.4. *Let $\Phi_{\rm PPP}(r)$ be a Poisson point process over $B_{\rm o}(r)$. If $\Phi_{\rm PPP}(r)$ and $\Phi_{\rm BPP}$ denote Poisson point process and binomial point process respectively in finite area and both point processes have same intensity λ, then $\Phi_{\rm PPP}(r) \leq_{\rm Lf} \Phi_{\rm BPP}$.*

Proof. Let $u(\cdot) \in \mathcal{U}$ be all non-negative functions on $\mathbb{R}^d$. The Laplace functional of the binomial point process consisting N points with a density λ can be expressed as follows [103]:

$$\begin{aligned} L_{\Phi_{\rm BPP}}(u) &= \left(1 - \frac{\lambda}{N}\int_{B_{\rm o}(r)} [1-\exp(-u(x))]\,{\rm d}r\right)^N && (5.34)\\ &\leq \exp\left\{-\lambda \int_{B_{\rm o}(r)} [1-\exp(-u(x))]\,{\rm d}x\right\} && (5.35)\\ &= L_{\Phi_{\rm PPP}(r)}(u) \end{aligned}$$

where the inequality in (5.35) is due to $(1-c/n)^n \leq e^{-c}$ for $0 \leq c \leq n$. Thus, Theorem 5.7.4 is followed since $0 \leq \lambda \int_{B_{\rm o}(r)} [1-\exp(-u(x))]\,{\rm d}x \leq N$ always holds with $\lambda = N/(c_d r^d)$ and $0 \leq [1-\exp(-u(x))] \leq 1$. □

In a finite area $B_{\rm o}(r)$, the aggregated interference at the origin from a binomial point process is always larger than that from Poisson point process in LT order from Theorem 5.7.1.

5.7.2 Laplace Transform Ordering of Interferences in Heterogeneous Networks

As unlicensed band utilization increases, the unlicensed wireless network may experience adverse interference from collocated wireless devices that are transmitting in the same unlicensed band. Such a heterogeneous network scenario can be modeled as a superposition of mutually independent point processes [104]. Let $\Phi_1 = \bigcup_{i=1}^{M} \Phi_{1,i}$ and $\Phi_2 = \bigcup_{i=1}^{M} \Phi_{2,i}$ for $i = 1, ..., M$ be the heterogeneous networks which are modeled as superpositions of mutually independent point processes. Since the Laplace functional of superposition of mutually independent point processes is $L_{\Phi}(u) = \prod_{i=1}^{M} L_{\Phi_i}(u)$ [105], if $\Phi_{1,i} \leq_{\text{Lf}} \Phi_{2,i}$ for $i = 1, ..., M$, then $\Phi_1 \leq_{\text{Lf}} \Phi_2$. Therefore, $I_1 \leq_{\text{Lt}} I_2$ from Theorem 5.7.1.

5.8 Numerical Results

In this section, we verify our theoretical results through Monte Carlo simulations. Since the LT ordering between two interference scenarios cannot be verified directly from its probability distributions such as PDF and CDF, we will verify the LT ordering between interferences by the ordering of SIR-based outage probabilities or ergodic capacities as mentioned in Section 5.4.

5.8.1 Comparison of Fading Channels on the Interference Link

In many practical scenarios, different links in wireless networks can experience asymmetric fading conditions. If the interferer's channel is Nakagami-m fading, while the desired link is Rayleigh fading which has an effective channel CCDF which is c.m., we can compare SIR-based outage probabilities using using Theorem 5.4.1.

In Fig. 5.4 the CDFs of interference power and SIR from Poisson cluster process with different Nakagami-m fading parameters and with the non-singular path-loss

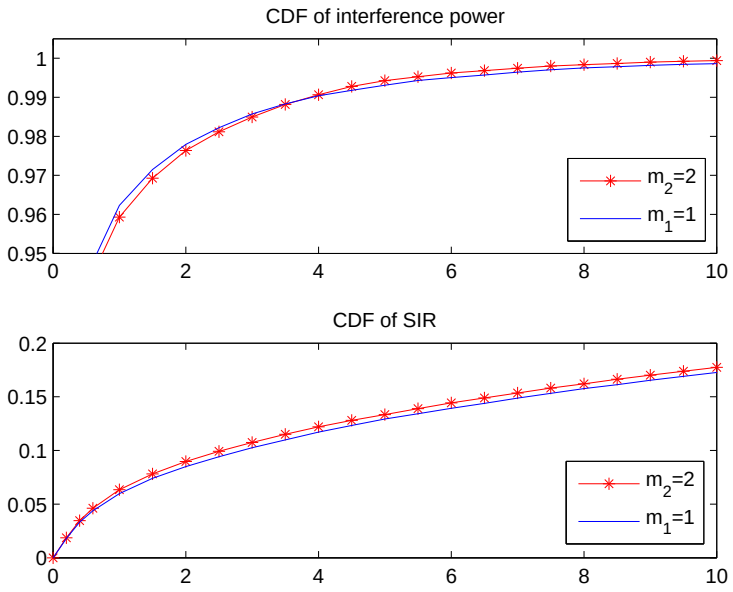

Figure 5.4: CDFs of interference and SIR for Poisson cluster process with different fading parameters and with $\lambda = 0.01$

model ($a = 1$, $b = 1$ and $\delta = 4$) in (5.6) are shown. We consider two different LoS parameters: $m_1 = 1$ and $m_2 = 2$. The choice of these parameters ensures $I_1 \leq_{\mathrm{Lt}} I_2$ from Theorem 5.5.1. Consequently, we observe $SIR_1 \geq_{\mathrm{st}} SIR_2$ in the bottom of Fig. 5.4 which agrees with Theorem 5.4.1 even though there is a crossover point between interference power distributions in the top of Fig. 5.4.

The CDFs of SIR from Poisson point process with different Nakagami-m fading parameters and with the singular path-loss model ($a = 0$, $b = 1$ and $\delta = 4$) in (5.6) are shown in Fig. 5.5. Similarly the LoS parameters $m_1 \leq m_2$ lead to $I_1 \leq_{\mathrm{Lt}} I_2$ from Theorem 5.5.1. Clearly, it is observed $SIR_1 \geq_{\mathrm{st}} SIR_2$ in Fig. 5.5 which agrees with Theorem 5.4.1.

Table 5.1 shows the ergodic capacity performances when the desired link has Ricean fading channel with $K_{\mathrm{S}} = 5$ and interfering channels follow Ricean distribu-

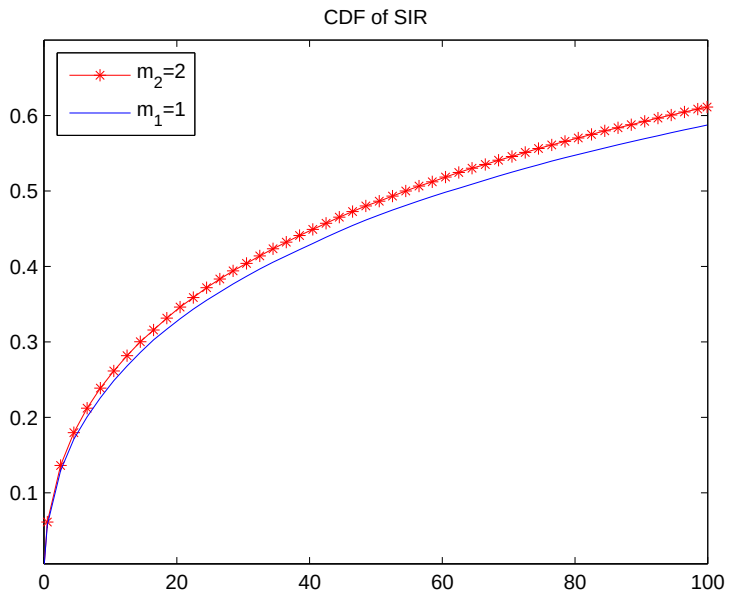

Figure 5.5: CDFs of SIR for Poisson point process with different fading parameters and with $\lambda = 0.01$

tions with $K_{\mathrm{I}_1} = 0$ and $K_{\mathrm{I}_2} = 1$ in the two scenarios compared on a Poisson cluster process. The ergodic capacity with I_1 is always better than that with I_2 as expected since the interference distributions are monotonic in LoS parameter of Ricean fading channel with respect to the LT ordering in Section 5.5.

Table 5.1: Ergodic capacities (bits/s/Hz) over Ricean fading channel with $K_{\mathrm{S}} = 5$ in Poisson cluster process

SINR (dB)	-4	-2	0	2	4	6	8	10
I_1 ($K_{\mathrm{I}_1} = 0$)	0.9433	1.2282	1.5709	1.9820	2.4538	3.0063	3.6482	4.5313
I_2 ($K_{\mathrm{I}_2} = 1$)	0.9426	1.2277	1.5707	1.9803	2.4526	3.0020	3.6449	4.5278

The ergodic capacities in Poisson point process are shown in Table 5.2. In this case, all conditions are same except for the type of point process. Therefore, the

Table 5.2: Ergodic capacities (bits/s/Hz) over Ricean fading channel with $K_{\mathrm{S}} = 5$ in Poisson point process

SINR (dB)	-4	-2	0	2	4	6	8	10
I_1 ($K_{\mathrm{I}_1} = 0$)	0.9346	1.2162	1.5485	1.9501	2.3847	2.9295	3.5491	4.3477
I_2 ($K_{\mathrm{I}_2} = 1$)	0.9342	1.2152	1.5468	1.9460	2.3816	2.9231	3.5407	4.3349

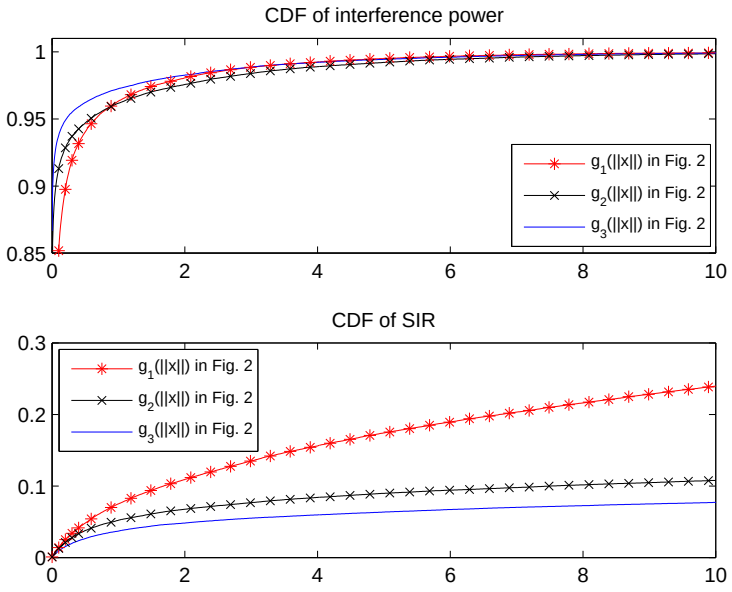

Figure 5.6: CDFs of interference and SIR for Poisson point process with non-singular path-loss models with different path-loss exponents and with $\lambda = 0.01$

ergodic capacity with I_1 is always better than that with I_2 when $I_1 \leq_{\mathrm{Lt}} I_2$.

5.8.2 Comparison of Path-loss Models

We show in Fig. 5.6 the CDFs of the interference power and CDFs of SIR from a Poisson point process with the non-singular path-loss models, $g_1(\|x\|)$ and $g_2(\|x\|)$ which are given in Fig. 5.3 and discussed in Corollary 5. It is noted the

non-singular path-loss models with two different path-loss exponents: $\delta_1 = 4$ and $\delta_2 = 8$ ensures $I_1 \geq_{\mathrm{Lt}} I_2$ from Corollary 5. We consider additional non-singular path-loss, $g_3(\|x\|)$ whose parameters are $a = 1, b = 1$, and $\delta = 8$ in Fig. 5.3. Since $g_3(\|x\|) \leq g_2(\|x\|)$ for $\|x\| \geq 0$ as shown in Fig. 5.3, it is obvious $I_2 \geq_{\mathrm{Lt}} I_3$. Thus, we observe $SIR_1 \leq_{\mathrm{st}} SIR_2 \leq_{\mathrm{st}} SIR_3$ in the bottom of Fig 5.6. By Theorem 5.4.1, when the fading channel between the desired receiver and its transmitter is Rayleigh distributed and the effective fading channel is exponentially distributed, we can observe the usual stochastic ordering of SIR distributions if the interferences are LT ordered as shown in Fig. 5.6.

5.8.3 Comparison of Different Point Processes

In the following, we compare the CDFs of interference power and CDFs of SIR from Poisson point process and Poisson cluster process. Since the interferences from Poisson point process and Poisson cluster process with the same intensity λ, the same non-singular path-loss model $g(\|x\|)$, and identical fading distribution h_{I} yield $I_{\mathrm{PCP}} \leq_{\mathrm{Lt}} I_{\mathrm{PPP}}$, which implies $SIR_{\mathrm{PCP}} \geq_{\mathrm{st}} SIR_{\mathrm{PPP}}$. This is observed in the bottom of Fig. 5.7 as predicted from our theoretical result in Theorem 5.7.2.

In addition to SIR-based outage performance, it is observed that the ergodic capacity in Poisson cluster processes is always greater than that in Poisson point processes by comparing same rows in Table 5.1 and 5.2.

5.9 Applications

The results in this chapter are useful for the system design and evaluation. We first remark on general qualitative insights that can be obtained from a stochastic ordering approach in systems with spatially distributed nodes. Then we consider a specific cognitive radio setting.

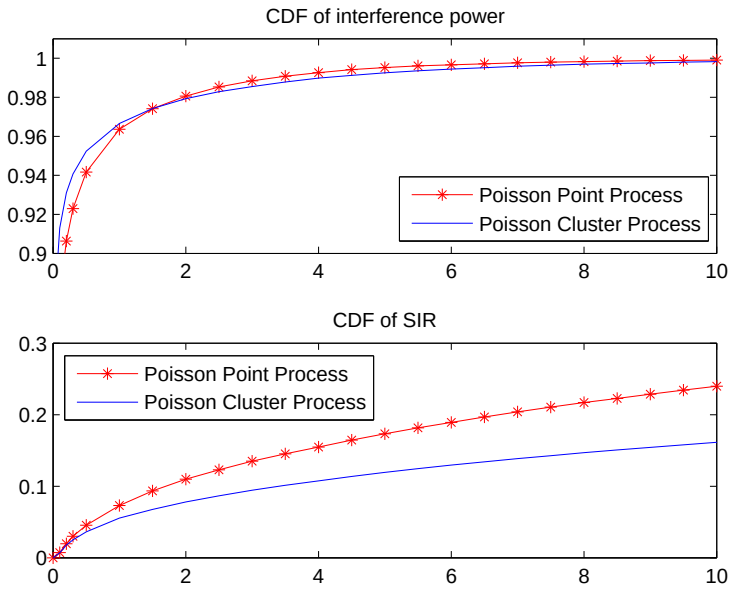

Figure 5.7: CDFs of interference and SIR for Poisson point process and Poisson cluster process with $\lambda = 0.01$

5.9.1 Insights for System Design

Using stochastic ordering, we can compare scenarios and gain qualitative insights for system design. As an example, consider the effects of clustering. The clustering of nodes "reduces" a point process in the LF order. From an interference point of view, the clustering of interfering nodes causes less interference in the LT order between interference distributions. This translates into an increased coverage probability and improved capacity for the system. As another example, by comparing between binomial point process and Poisson point process in Section 5.7.1, it is noted that a fixed number of interferers in a finite area cause more interference than Poisson random number of interferers in the same finite area in the LT ordering sense. These insights can help guide judicious deployment of nodes, which includes how to deploy the additional nodes for less interference to other systems.

The aggregate interference also depends on the fading distribution on the interfering links. Fading distributions that are smaller in the LT ordering sense causes less interference in the LT order, which implies better performance metrics such as coverage probability and achievable rate regardless of actual interference distributions. In the case of the non-singular path-loss model, less path-loss exponent guarantees better performance measured in terms of coverage probability and ergodic capacity. Thus, having the statistical knowledge of fading channels or estimating the path-loss exponent, we can get qualitative insights for system design without actual system evaluation.

5.9.2 Application to Cognitive Radios

We now discuss applications of stochastic ordering ideas to cognitive radio interference problems. We consider both overlay and underlay scenarios. We show that in each scenario, a LF comparison of two underlying point processes can help us order the interference in the LT sense.

In an *underlay* [106] cognitive network where a primary user and secondary users can transmit simultaneously, as long as the interference to the primary receiver is below a certain threshold. Suppose the secondary user's transmitters are distributed in an annular area encircling the primary user's receiver, with an inner radius (guard distance) of $R_{\min}$ and an outer radius of $R_{\max}$ as shown in Fig. 5.8 [36, 37]. The guard distance $R_{\min}$ ensures a minimum performance on the primary user. Such a guard region can be ensured through multiple access protocols of secondary users [38]. The interference from the secondary users beyond $R_{\max}$ is assumed to be negligible due to path loss. The interference at the primary receiver can be expressed as the aggregate

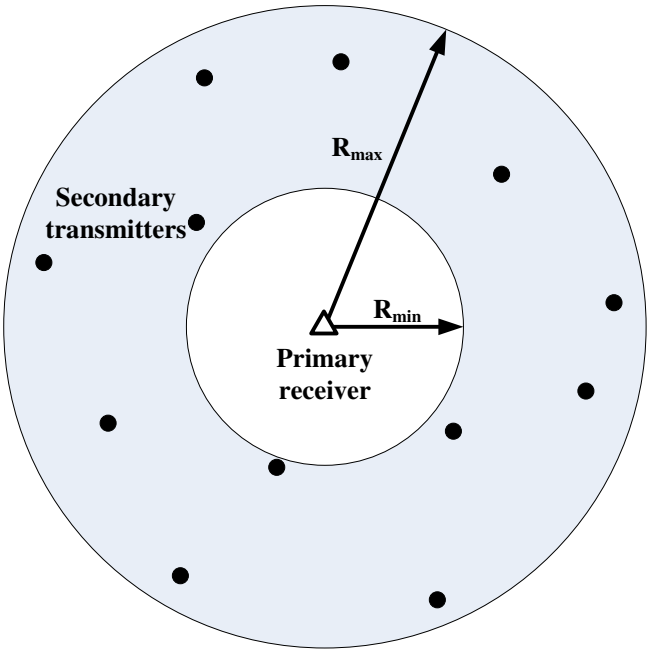

Figure 5.8: Illustration of a cognitive network. Secondary users are distributed in the shaded region around the primary user.

signal from the secondary users in the annual area surrounding the primary receiver.

$$I_{\mathrm{P}} = \sum_{x \in \Phi_{\mathrm{S}}} h_{\mathrm{I}}^{(x)} g(x) \mathbf{1}\{x \in A_{\mathrm{I}}\}, \tag{5.36}$$

where $|A_{\mathrm{I}}| = \pi(R_{\min}^2 - R_{\max}^2)$ is the total area encompassing the secondary users, and the point process for secondary users is denoted by Φ_{S}. $h_{\mathrm{I}}^{(x)}$ is a positive random variable capturing the (power) fading coefficient between a secondary user x and the primary receiver. The path-loss model $g(\cdot)$ is same as (5.6). Therefore in the underlay scenario the interference is from the point process of secondary users in the annular region.

In an *overlay* [106] cognitive network where secondary users only can transmit when a primary user does not transmit its signal, the secondary users should detect the signal from the primary user to make a decision if it can transmit. However, since a miss detection event in the detection of primary users exists in practice, the

interference from the secondary users will affect the performance of the primary user. When it is assumed that the miss detection occurs independently on the stationary point process for secondary users, the yielding point process $\Phi_{\mathrm{S,thin}}$ is also stationary with reduced intensity $P_{\mathrm{miss}}\lambda_{\mathrm{S}}$ [3] where P_{miss} is the miss detection probability. In this case, the interference at the primary user can be expressed as follows:

$$I_{\mathrm{P}} = \sum_{x \in \Phi_{\mathrm{S,thin}}} h_{\mathrm{I}}^{(x)} g(x) \mathbf{1}\{x \in A_{\mathrm{I}}\}. \tag{5.37}$$

In the overlay scenario, $R_{\min}$ will be zero since a close secondary transmitter to the primary receiver can fail to detect the primary user's signal. Therefore in the overlay scenario the interference is due to the point process of secondary users in the entire disk of the thinned point process.

In both (5.36) and (5.37), considering $\tilde{u}(x) = u(x)\mathbf{1}\{x \in A_{\mathrm{I}}\}$ as a non-negative function with x, we can compare the interference in this restricted region using the LF ordering of point processes for spatial distribution of secondary users. According to the LF ordering of point processes, the interferences in the restricted region will be LT ordered. In addition to spatial point process, fading channels affect the interference in the restricted region. The LT ordered fading distributions will cause LT ordered interferences. Consequently, the performance metrics such as coverage probability and achievable rate of the primary user will be compared according to the LT ordering of interferences. The comparisons will give some insights to design and evaluate cognitive networks.

Chapter 6

LAPLACE FUNCTIONAL ORDERING OF POINT PROCESSES IN LARGE-SCALE WIRELESS NETWORKS

6.1 Literature Survey and Motivation

Point processes have been used to describe spatial distribution of nodes in wireless networks, for example, randomly distributed nodes in wireless sensor networks or ad-hoc networks [5, 44, 45] and the spatial distributions for base stations and mobile users in cellular networks [11, 13, 107]. In the case of cognitive radio networks, locations of primary and secondary users have been modeled as point processes [36, 37, 38]. The point process with random translations has been used for modeling of mobile networks in [108]. Stationary Poisson processes provide a tractable framework, but suffer from notorious modeling issues in matching real network distributions. Stochastic ordering of point processes provide an ideal framework for comparing two deployment/usage scenarios even in cases where the performance metrics cannot be computed in closed form. These partial orders capture intuitive notions like one point process being "greater", or "more variable". Existing works on point process modeling for wireless networks have paid little attention to how two intractable scenarios can be nevertheless compared to aid in system optimization.

Recently a stochastic ordering theory has been used for performance comparison in wireless networks which are modeled as point processes [96, 109, 110, 111]. Directionally convex (DCX) ordering of point processes and its integral shot noise fields have been studied in [96]. In [109] usual stochastic ordering of carrier-to-interference ratio has been established in cellular systems. Ordering results for coverage prob-

ability and per user rate have been shown in multi-antenna heterogeneous cellular networks [110]. In Chapter 5, Laplace functional (LF) ordering of point processes has been introduced and used to study interference distributions in wireless networks. Several examples of the LF ordering of specific point processes have been also introduced in Chapter 5, including stationary Poisson, mixed Poisson, Poisson cluster, and Binomial point processes.

In this chapter, we apply the LF ordering concept to several general classes of point processes such as Cox, homogeneous independent cluster, perturbed lattice processes, and mixed binomial point processes which have been used to describe distributed nodes of wireless systems in the literature. We also investigate the preservation properties of the LF ordering of point processes with respect to independent operations such as marking, thinning, random translation, and superposition. We prove the LF ordering of original point processes still holds after applying these operations on the point processes. To the best of our knowledge, there is no study of the LF ordering of general classes of point processes and their preservation properties in the literature. Using these properties, we consider several effects of real systems such as propagation effects over wireless channels, multiple access schemes, heterogeneous network scenarios, and mobile networks and compare performances without having to obtain closed-form results for a wide range of performance metrics such as a coverage probability, an achievable rate, and a resource allocation under these real system effects. In addition to the performance comparison, the stochastic ordering of point processes provides guidelines for system design such as network deployments and user selection schemes. Comparing to [96], we also provide several advantages of the LF order over the DCX order.

6.2 Preliminaries

In this section, we introduce Laplace functional stochastic order between random measures. The new stochastic ordering of point processes based on the well-known Laplace functional has been defined in Chapter 5. It can be generalized to the stochastic ordering of random measures.

Definition 6.2.1. *Let Ψ_1 and Ψ_2 be two random measures such that*

$$L_{\Psi_1}(u) = \mathbb{E}\left[e^{-\int_{\mathbb{R}^d} u(x)\Psi_1(\mathrm{d}x)}\right] \geq \mathbb{E}\left[e^{-\int_{\mathbb{R}^d} u(x)\Psi_2(\mathrm{d}x)}\right] = L_{\Psi_2}(u) \tag{6.1}$$

where $u(\cdot)$ runs over the set $\mathfrak{U}$ of all non-negative functions on $\mathbb{R}^d$. Then Ψ_1 is said to be smaller than Ψ_2 in the Laplace functional (LF) order (denoted by $\Psi_1 \leq_{\mathrm{Lf}} \Psi_2$).

In this chapter, we focus on the LF order of point processes unless otherwise specified. As mentioned in (5.28) of Chapter 5, it is possible to think of LF ordering of point processes as the LT ordering of their aggregate processes.

6.3 Ordering of General Class of Point Processes

The examples for LF orderings of some specific point processes have been provided in Chapter 5. In this section, we introduce the LF ordering of general classes of point processes.

6.3.1 Cox Processes

A generalization of the Poisson process is to allow for the intensity measure itself being random. The resulting process is then Poisson conditional on the intensity measure. Such processes are called *doubly stochastic Poisson processes* or *Cox processes*. Consider a random measure Ψ on $\mathbb{R}^d$. Assume that for each realization $\Psi = \Lambda$, an independent Poisson point process Φ of intensity measure Λ is given. The random

measure Ψ is called the driving measure for a Cox process. The LF ordering of Cox processes depends on their driving random measures.

Theorem 6.3.1. *Let Φ_1 and Φ_2 be two Cox processes with driving random measures Ψ_1 and Ψ_2 respectively. If $\Psi_1 \leq_{\mathrm{Lf}} \Psi_2$, then $\Phi_1 \leq_{\mathrm{Lf}} \Phi_2$.*

Proof. The Laplace functional of the Cox process Φ with driving random measure Ψ can be expressed as follows [3]:

$$\begin{aligned} L_\Phi(u) &= \int_{\mathbb{M}} L_\Lambda(u)\Psi(\mathrm{d}\Lambda) && (6.2)\\ &= \int_{\mathbb{M}} \exp\left(-\int_{\mathbb{R}^d}[1-\exp(-u(x))]\right)\Psi(\mathrm{d}\Lambda) && (6.3)\\ &= L_\Psi(1-\exp(-u(x))), && (6.4) \end{aligned}$$

where L_Λ is the Laplace functional of the Poisson process of intensity measure Λ and $\mathbb{M}$ is the set of measures. Equation (6.3) follows from the definition of Laplace functional of Poisson point process in (2.8) and equation (6.4) is followed by the definition of Laplace functional of random measure in (6.1). Then, the proof follows from Definition 6.2.1. □

The mixed Poisson process is a simple instance of a Cox process. It can be thought of as a stationary Poisson point process with a randomized intensity parameter X. In mixed Poisson processes, the random measure Ψ is the constant random variable X. Therefore, if $X_1 \leq_{\mathrm{Lt}} X_2$, then $\Phi_1 \leq_{\mathrm{Lf}} \Phi_2$ from Theorem 6.3.1.

6.3.2 Homogeneous Independent Cluster Processes

A general cluster process is generated by taking a parent point process and daughter point processes, one per parent, and translating the daughter processes to the position of their parent. The cluster process is then the union of all the daughter points. Denote the parent point process by $\Phi_{\mathrm{p}} = \{x_1, x_2, \dots\}$, and let $n \in \mathbb{N} \cup \{\infty\}$

be the number of parent points. Further let $\{\Phi_i\}, i \in \mathbb{N}$, be a family of finite points sets, the untranslated clusters or daughter processes. The cluster process is then the union of the translated clusters:

$$\Phi := \bigcup_{i=1}^{n} \Phi_i + x_i. \tag{6.5}$$

If the parent process is a lattice, the process is called a *lattice cluster process*. Analogously, if the parent process is a Poisson point process, the resulting process is a *Poisson cluster process*.

If the parent process is stationary and the daughter processes are independent ($\{\Phi_i\}_i$ are independent each other and $\Phi_i, \forall i$ is independent of Φ_{p}) finite point sets and have the same distribution, the procedure is called *homogeneous independent clustering*. In this case, only the statistics of one cluster need to be specified, which is usually done by referring to the *representative cluster*, denoted by Φ_0. In this class of point processes, the LF ordering depends on the parent process Φ_{p} and the representative process Φ_0 as follows:

Theorem 6.3.2. *Let Φ_1 and Φ_2 be two homogeneous independent cluster processes having the representative clusters Φ_{0_1} and Φ_{0_2} respectively. Also, let Φ_{p_1} and Φ_{p_2} be the parent point processes of two homogeneous independent cluster processes Φ_1 and Φ_2 respectively. If $\Phi_{\mathrm{p}_1} \leq_{\mathrm{Lf}} \Phi_{\mathrm{p}_2}$ and $\Phi_{0_1} \leq_{\mathrm{Lf}} \Phi_{0_2}$, then $\Phi_1 \leq_{\mathrm{Lf}} \Phi_2$.*

Proof. Let $L_0^{(x)}$ denote the Laplace functional of $\Phi_0 + x$, i.e., the Laplace functional of the representative cluster translated by x:

$$L_0^{(x)}(u) := \mathbb{E}_{\Phi_0}\left[\prod_{y \in \Phi_0 + x} \exp(-u(y))\right] = \mathbb{E}_{\Phi_0}\left[\prod_{y \in \Phi_0} \exp(-u(y+x))\right]. \tag{6.6}$$

The Laplace functional of the homogeneous independent cluster process Φ with parent process Φ_{p} is

$$L_\Phi(u) = \mathbb{E}_{\Phi_{\mathrm{p}}}\left[\prod_{x \in \Phi_{\mathrm{p}}} L_0^{(x)}(u)\right] \text{ for all } u \in \mathcal{U}. \tag{6.7}$$

From Definition 6.2.1, if $\Phi_{\mathrm{p}_1} \leq_{\mathrm{Lf}} \Phi_{\mathrm{p}_2}$ and $\Phi_{0_1} \leq_{\mathrm{Lf}} \Phi_{0_2}$, then $\Phi_1 \leq_{\mathrm{Lf}} \Phi_2$. □

6.3.3 Perturbed Lattice Processes with Replicating Points

General lattices are defined as

$$\mathbb{L} := \{u \in \mathbb{Z}^d : \mathbf{G}u\}, \tag{6.8}$$

where $\mathbf{G} \in \mathbb{R}^{d\times d}$ is a matrix with $\det \mathbf{G} \neq 0$, the so-called generator matrix. The volume of each Voronoi cell is $V = |\det\mathbf{G}|$ and the intensity of the lattice is $\lambda = 1/V$ [112]. The perturbed lattice can be considered as the *lattice cluster process*. In each cluster, the daughter points are random in number X, independent of each other, and identically distributed. Moreover, these points are distributed by some given spatial distribution. Each cluster process is translated by the points of the lattice process, $\Phi_{\mathrm{d}}^{(x)} := \{x + y : y \in \Phi_{\mathrm{d}}\}$. The resulting point process can be seen as replicating and dispersing points from the original lattice:

$$\Phi := \bigcup_{x\in\mathbb{L}} \Phi_{\mathrm{d}}^{(x)}. \tag{6.9}$$

If the number of replicas X are Poisson random variables, the the resulting process is a Poisson point process. If moreover the points are uniformly distributed in the Voronoi cell of the original lattice, then the resulting point process is stationary Poisson point process. Now, we can define the following LF ordering of point processes according to the random variable, X.

Theorem 6.3.3. *Let Φ_1 and Φ_2 be two perturbed lattice processes with replicating points with non-negative integer valued random distribution X_1 and X_2 respectively and with same mean $\mathbb{E}[X_1] = \mathbb{E}[X_2] = 1$. The point displacement is uniform in the Voronoi cell of the original lattice. If $X_1 \leq_{\mathrm{Lt}} X_2$, then $\Phi_1 \leq_{\mathrm{Lf}} \Phi_2$.*

Proof. The Laplace functional of a perturbed lattice point z with replication points and uniform nodes displacements can be expressed as follows:

$$L_{\Phi_z}(u) = \mathbb{E}_X \left[\left(\frac{1}{\lambda |V|} \int_V \exp(-u(x)) \lambda \mathrm{d}x \right)^X \right], \tag{6.10}$$

where X is the random variable for the replication points and V is the Voronoi region of z. Since $1/(\lambda|V|) \int_V \exp(-u(x))\lambda \mathrm{d}x \leq 1$ and $X_1 \leq_{\mathrm{Lt}} X_2$, by denoting $t = 1/(\lambda|V|) \int_V \exp(-u(x))\lambda \mathrm{d}x$ and from the fact that $X_1 \leq_{\mathrm{Lt}} X_2 \iff X_1 \leq_{\mathrm{pgf}} X_2$ we have the following relation:

$$\mathbb{E}_{X_1} \left[t^{X_1} \right] \geq \mathbb{E}_{X_2} \left[t^{X_2} \right]. \tag{6.11}$$

From (6.11) the following LF-ordering is obtained,

$$\mathbb{E}_{X_1} \left[\left(\frac{1}{\lambda |V|} \int_V \exp(-u(x)) \lambda \mathrm{d}x \right)^{X_1} \right] \geq \mathbb{E}_{X_2} \left[\left(\frac{1}{\lambda |V|} \int_V \exp(-u(x)) \lambda \mathrm{d}x \right)^{X_2} \right]. \tag{6.12}$$

Since the entire point process can be considered as the superpositions of independent perturbed lattice point $z \in \mathbb{L}$, Theorem 6.3.3 is proved from Lemma 6.4.4. □

Based on Theorem 5.A.21 in [7], the *smallest* and *biggest* LT ordered random variables can be defined as follows: Let Y be a random variable such that $P\{Y = 0\} = 1 - P\{Y = 2\} = 1/2$ and let Z be a random variable degenerate at 1. Let X be a non-negative random variable with mean 1. Then

$$Y \leq_{\mathrm{Lt}} X \leq_{\mathrm{Lt}} Z. \tag{6.13}$$

From Theorem 6.3.3 and (6.13), the perturbed lattice processes with replicating points with non-negative integer valued random distribution Y and Z, and with uniform point displacement in the Voronoi cell of the original lattice will be the *smallest* and *biggest* LF ordered point processes respectively among uniformly perturbed lattice processes with the same average number of points. The smallest LF ordered perturbed

lattice process looks like cluster process since some of Voronoi cells have 2 points but other cells do not have any point. This observation is in line with our previous result that clustering diminishes point processes in the LF order in Chapter 5. In the biggest LF ordered perturbed lattice process, every Voronoi cell has the fixed number of point which is 1. Therefore, it looks like the superposition of Binomial point processes which have a fixed number of uniformly distributed points in a finite area and are bigger LF ordered point process than Poisson point process in Chapter 5.

6.3.4 Mixed Binomial Point Processes

In binomial point processes, there area total of fixed N points uniformly distributed in a bounded set $B \in \mathbb{R}^d$. The density of the process is given by $\lambda = N/|B|$ where $|B|$ is the volume of B. If the number of points N is random, the point process is called as a mixed binomial point process. As an example, with Poisson distributed N, the point process is called as a finite Poisson point process. The intensity measure of these point processes is $\Lambda(B) = \lambda|B|$. In these point processes, we can compare the LF ordering of point processes as follows:

Theorem 6.3.4. *Let Φ_1 and Φ_2 be two mixed binomial point process with non-negative integer valued random distribution N_1 and N_2 respectively. If $N_1 \leq_{\mathrm{Lt}} N_2$, then $\Phi_1 \leq_{\mathrm{Lf}} \Phi_2$.*

Proof. Similarly as the proof for Theorem 6.3.3, the Laplace functional of a mixed binomial point process with random number of points N can be expressed as follows:

$$L_{\Phi}(u) = \mathbb{E}_N \left[\left(\frac{1}{\lambda|B|} \int_B \exp(-u(x))\lambda \mathrm{d}x \right)^N \right], \tag{6.14}$$

where B is the bounded set of the point process. Since $1/(\lambda|B|) \int_B \exp(-u(x))\lambda \mathrm{d}x \leq 1$ and $N_1 \leq_{\mathrm{Lt}} N_2$, by denoting $t = 1/(\lambda|B|) \int_B \exp(-u(x))\lambda \mathrm{d}x$ and from the fact that

$N_1 \leq_{\text{Lt}} N_2 \iff N_1 \leq_{\text{pgf}} N_2$ we have the following relation:

$$\mathbb{E}_{N_1}\left[t^{N_1}\right] \geq \mathbb{E}_{N_2}\left[t^{N_2}\right]. \tag{6.15}$$

From (6.15) the following LF-ordering is obtained,

$$\mathbb{E}_{N_1}\left[\left(\frac{1}{\lambda|B|}\int_B \exp(-u(x))\lambda \mathrm{d}x\right)^{N_1}\right] \geq \mathbb{E}_{N_2}\left[\left(\frac{1}{\lambda|B|}\int_B \exp(-u(x))\lambda \mathrm{d}x\right)^{N_2}\right]. \tag{6.16}$$

□

6.4 Preservation of Stochastic Ordering of Point Processes

In what follows, we will show that the LF ordering between two point processes is preserved after applying independent operations on point processes such as marking, thinning, random translation, and superposition of point processes.

6.4.1 Marking

Consider a d dimensional Euclidean space $\mathbb{R}^d$, $d \geq 1$, as the state space of the point process. Consider a second space $\mathbb{R}^\ell$, called the space of marks. A marked point process $\widetilde{\Phi}$ on $\mathbb{R}^d \times \mathbb{R}^\ell$ (with points in $\mathbb{R}^d$ and marks in $\mathbb{R}^\ell$) is a locally finite, random set of points on $\mathbb{R}^d$, with some random vector in $\mathbb{R}^\ell$ attached to each point. A marked point process is said to be independently marked if, given the locations of the points in Φ, the marks are mutually independent random vectors in $\mathbb{R}^\ell$, and if the conditional distribution of the mark m of a point $x \in \Phi$ depends only on the location of this point x it is attached to.

Lemma 6.4.1. *Let Φ_1 and Φ_2 be two point processes in $\mathbb{R}^d$. Also let $\widetilde{\Phi}_1$ and $\widetilde{\Phi}_2$ be independently marked point processes with marks m with identical distribution in $\mathbb{R}^\ell$. If $\Phi_1 \leq_{\text{Lf}} \Phi_2$, then $\widetilde{\Phi}_1 \leq_{\text{Lf}} \widetilde{\Phi}_2$.*

Proof. The Laplace functional of marked point process $\widetilde{\Phi}$ with a non-negative function $u : \mathbb{R}^d \times \mathbb{R}^\ell \mapsto \mathbb{R}^+$ can be expressed as follows [113]:

$$
\begin{aligned}
L_{\widetilde{\Phi}}(u) &= \mathbb{E}_\Phi \left[\prod_{x \in \Phi} \int_{\mathbb{R}^\ell} \exp(-u(m,x)) F(\mathrm{d}m|x) \right] && (6.17) \\
&= \mathbb{E}_\Phi \left[\prod_{x \in \Phi} \exp\left(- \left(- \log \int_{\mathbb{R}^\ell} \exp\left(-u(m,x)\right) F(\mathrm{d}m|x) \right) \right) \right] && (6.18) \\
&= \mathbb{E}_\Phi \left[\prod_{x \in \Phi} \exp\left(-\tilde{u}(x)\right) \right] = \mathbb{E}_\Phi \left[\exp\left(- \sum_{x \in \Phi} \tilde{u}(x) \right) \right]. && (6.19)
\end{aligned}
$$

where $\tilde{u}(x) = -\log \int_{\mathbb{R}^\ell} \exp\left(-u(m,x)\right) F(\mathrm{d}m|x)$. $\tilde{u}(x)$ is a non-negative function of x since $0 \leq \int_{\mathbb{R}^\ell} \exp\left(-u(m,x)\right) F(\mathrm{d}m|x) \leq 1$, Then, the Laplace functional of marked point process $\widetilde{\Phi}$ is followed by

$$
L_{\widetilde{\Phi}}(u) = L_\Phi(\tilde{u}). \tag{6.20}
$$

Therefore, from (6.20) and the definition of LF ordering in (6.1), if $\Phi_1 \leq_{\mathrm{Lf}} \Phi_2$, then $\widetilde{\Phi}_1 \leq_{\mathrm{Lf}} \widetilde{\Phi}_2$. □

6.4.2 Thinning

A thinning operation uses a rule to delete points of a basic process Φ, thus yielding the *thinned point process* Φ_{th}, which can be considered as a subset of Φ. The simplest thinning is *p-thinning*: each point of Φ has probability $1-p$ of suffering deletion, and its deletion is independent of locations and possible deletions of any other points of Φ. A natural generalization allows the retention probability p to depend on the location x of the point. A deterministic function $p(x)$ is given on $\mathbb{R}^d$, with $0 \leq p(x) \leq 1$. A point x in Φ is deleted with probability $1-p(x)$ and again its deletion is independent of locations and possible deletions of any other points. The generalized operation is called $p(x)$*-thinning*. In a further generalization the function p is itself random. Formally, a random field $\boldsymbol{\pi} = \{0 \leq \pi(x) \leq 1 : x \in \mathbb{R}^d\}$ is given which is independent

of Φ. A realization φ_{th} of the thinned process Φ_{th} is constructed by taking a realization φ of Φ and applying $p(x)$-thinning to φ, using for $p(x)$ a sample $\{p(x) : x \in \mathbb{R}^d\}$ of the random field $\boldsymbol{\pi}$. Given $\pi(x) = p(x)$ and given $\Phi = \varphi$, the probability of x in Φ also belonging to Φ_{th} is $p(x)$.

Lemma 6.4.2. *Let Φ_1 and Φ_2 be two point processes in $\mathbb{R}^d$ and $\Phi_{\text{th},1}$ and $\Phi_{\text{th},2}$ be independently thinning point processes both with identical independent thinning operation regardless of p, $p(x)$, and $\pi(x)$-thinning. If $\Phi_1 \leq_{\text{Lf}} \Phi_2$, then $\Phi_{\text{th},1} \leq_{\text{Lf}} \Phi_{\text{th},2}$.*

Proof. If L_Φ is the Laplace functional of Φ then that of Φ_{th} is

$$L_{\Phi_{\text{th}}}(u) = L_\Phi(u_{\text{p}}) \text{ for } u \in \mathcal{U}, \tag{6.21}$$

where $u_{\text{p}} = -\log\left(\exp(-u(x))p(x) + 1 - p(x)\right)$. From Definition 6.2.1, if $\Phi_1 \leq_{\text{Lf}} \Phi_2$, then $\Phi_{\text{th},1} \leq_{\text{Lf}} \Phi_{\text{th},2}$. The p-thinning is subset of $p(x)$-thinning. Analogous formula for $\pi(x)$-thinning follows by averaging with respect to the distribution of the random process $\boldsymbol{\pi}$. Since the inequality holds under every realization $\pi(x)$, their expectations also hold the inequality. □

Since the thinned point process Φ_{th} is a locally finite random set of points on $\mathbb{R}^d$, with some random variable in $\mathbb{R}^+$ attached to each point, the independent thinning can be considered as the independent marking operation on a point process as discussed in the previous section.

6.4.3 Random Translation

In this section, the stochastic operation that we consider is random translations. Each point x in the realization of some initial point process Φ is shifted independently of its neighbors through a random vector t in $\mathbb{R}^d$ with independent elements. The resulting process is $\Phi_{\text{rt}} := \{x + t : x \in \Phi\}$. The random translation preserves the LF ordering of point process as follows:

Lemma 6.4.3. *Let Φ_1 and Φ_2 be two point processes in $\mathbb{R}^d$ and $\Phi_{\mathrm{rt},1}$ and $\Phi_{\mathrm{rt},2}$ be the translated point processes with the common distribution for the translation t. If $\Phi_1 \leq_{\mathrm{Lf}} \Phi_2$, then $\Phi_{\mathrm{rt},1} \leq_{\mathrm{Lf}} \Phi_{\mathrm{rt},2}$.*

Proof. Let $F(\cdot)$ denote the common distribution for the translations t_x. For $u \in \mathcal{U}$, the Laplace functional after random translation takes the form

$$L_{\Phi_{\mathrm{rt}}}(u) = L_{\Phi}\left(u_{\mathrm{t}}\right), \tag{6.22}$$

where $u_{\mathrm{t}} = -\log\left(\int_{\mathbb{R}^d} \exp(-u(\cdot + t))F(\mathrm{d}t)\right)$. From Definition 6.2.1, if $\Phi_1 \leq_{\mathrm{Lf}} \Phi_2$, then $\Phi_{\mathrm{rt},1} \leq_{\mathrm{Lf}} \Phi_{\mathrm{rt},2}$. □

Similarly as the independent thinning operation, since the random translated point process Φ_{rt} is a locally finite random set of points on $\mathbb{R}^d$, with some random vector in $\mathbb{R}^d$ attached to each point, the random translation can be considered as the independent marking operation on a point process.

6.4.4 Superposition

Let Φ_1 and Φ_2 be two point processes. Consider the union

$$\Phi = \Phi_1 \cup \Phi_2. \tag{6.23}$$

Suppose that with probability one the point sets Φ_1 and Φ_2 do not overlap. The set-theoretic union then coincides with the superposition operation of general point process theory. The superposition preserves the LF ordering of point processes as follows:

Lemma 6.4.4. *Let $\Phi_{1,i}$ and $\Phi_{2,i}, i = 1, ..., M$ be mutually independent point processes and $\Phi_1 = \bigcup_{i=1}^{M} \Phi_{1,i}$ and $\Phi_2 = \bigcup_{i=1}^{M} \Phi_{2,i}$ be the superposition of point processes. If $\Phi_{1,i} \leq_{\mathrm{Lf}} \Phi_{2,i}$ for $i = 1, ..., M$, then $\Phi_1 \leq_{\mathrm{Lf}} \Phi_2$.*

Proof. Let $\Phi_{1,i}$ and $\Phi_{2,i}, i = 1, ..., M$ be mutually independent point processes and $\Phi_1 = \bigcup_{i=1}^{M} \Phi_{1,i}$ and $\Phi_2 = \bigcup_{i=1}^{M} \Phi_{2,i}$ be the superposition of point processes. The Laplace function of superposition of mutually independent point processes can be expressed as follows [105]:

$$L_{\Phi}(u) = \prod_{i=1}^{M} L_{\Phi_i}(u). \tag{6.24}$$

$L_{\Phi}(u)$ converges if and only if the infinite sum of point processes is finite on bounded area $B \in \mathbb{R}^d$. Therefore, from (6.24) and the definition of LF ordering in (6.1), if $\Phi_{1,i} \leq_{\text{Lf}} \Phi_{2,i}$ for $i = 1, ..., M$, then $\Phi_1 \leq_{\text{Lf}} \Phi_2$. □

6.5 Applications to Wireless Networks

In the following discussion, we will consider the applications of stochastic orders to wireless network systems.

6.5.1 Cellular Networks

In this section, the comparisons of performance metrics will be derived from the LF ordering of point processes for spatial deployments of base stations (BSs) and mobile stations (MSs).

6.5.1.1 System Model

We consider the downlink cellular network model consists of BSs arranged according to some point process Φ_{B} in the Euclidean plane. For the deployment of BSs, a deterministic network such as lattice points or stochastic network (e.g. Poisson point process) may be considered. Consider an independent collection of MSs, located according to some point process Φ_{M} which is independent of Φ_{B}. For a traditional cellular network, assume that user associates with the closest BS, which would suffer the least path loss during wireless transmission. It is also assumed that the associ-

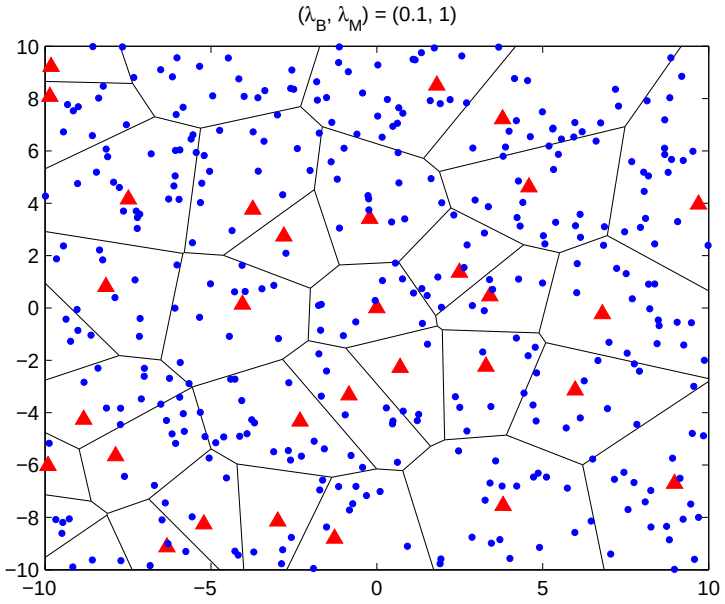

Figure 6.1: Illustration of a cellular network. The red triangles represent base stations which form a stationary Poisson point process Φ_{B} with intensity $\lambda_{\mathrm{B}} = 0.1$ and the blue dots represent users which also form a stationary Poisson point process Φ_{M} with intensity $\lambda_{\mathrm{M}} = 1.0$.

ation between a BS and a MS is carried out in a large time scale compared to the coherence time of the channel. Moreover, every cell is assumed to include only one BS and a few users. Then the cell boundary, which can be obtained by connecting the perpendicular bisector lines between each pair of BSs, splits the plane $\mathbb{R}^2$ into irregular polygons that correspond to different cell coverage areas. Such stochastic and irregular topology forms a Voronoi tessellation as shown in Fig. 6.1. Under the assumption of Voronoi tessellation cellular networks, our goal is to compare performance metrics such as average resource allocation and total cell coverage probability through the stochastic ordering tools. The spatial coverage of cellular networks is also compared based on the LF order of point processes for BSs modeling.

In order for the total cell coverage probability to be compared, the signal to interference plus noise ratio (SINR) of a user at $x \in \Phi_{\text{M}}$ is of interest to quantify. The effective channel power between a user x and its associated typical BS B_0 is $h_{\text{S}}^{(x)}$, which is a non-negative RV. The SINR with additive noise power σ^2 is given by

$$SINR(x) = \frac{h_{\text{S}}^{(x)} g(\|x\|)}{\sigma^2 + I(x)}, \tag{6.25}$$

where $g(\cdot) : \mathbb{R}^+ \to \mathbb{R}^+$ is the path-loss function which is a continuous, positive, non-increasing function of $\|x\|$ and assumed to depend only on the Euclidean distance $\|x\|$ from the user x to the typical BS B_0. The following is an example of a path-loss model [54, 5, 43, 4]:

$$g(\|x\|) = (a + b\|x\|^{\delta})^{-1} \tag{6.26}$$

for some $b > 0$, $\delta > d$ and $a \in \{0, 1\}$, where δ is called the path-loss exponent, a determines whether the path-loss model belongs to a singular path-loss model ($a = 0$) or a non-singular path-loss model ($a = 1$), and b is a compensation parameter to keep the total receive power normalized regardless the values of path-loss exponent. In (6.25), $I(x)$ is the accumulated interference power at a user x given by

$$I(x) = \sum_{y \in \Phi_{\text{B}} \setminus \{B_0\}} h_{\text{I}}^{(y)} g(\|y - x\|) \tag{6.27}$$

where Φ_{B} denotes the set of all BSs which is modeled as a point process on $\mathbb{R}^2$ and $h_{\text{I}}^{(y)}$ is a positive random variable capturing the (power) fading coefficient between a user x and the y^{th} interfering BS. Moreover, $h_{\text{I}}^{(y)}$ are i.i.d. random variables and independent of the point process.

6.5.1.2 Ordering of Performance Metrics in a Cellular Network

In the following discussion, we will introduce performance metrics involving the stochastic ordering of aggregate process.

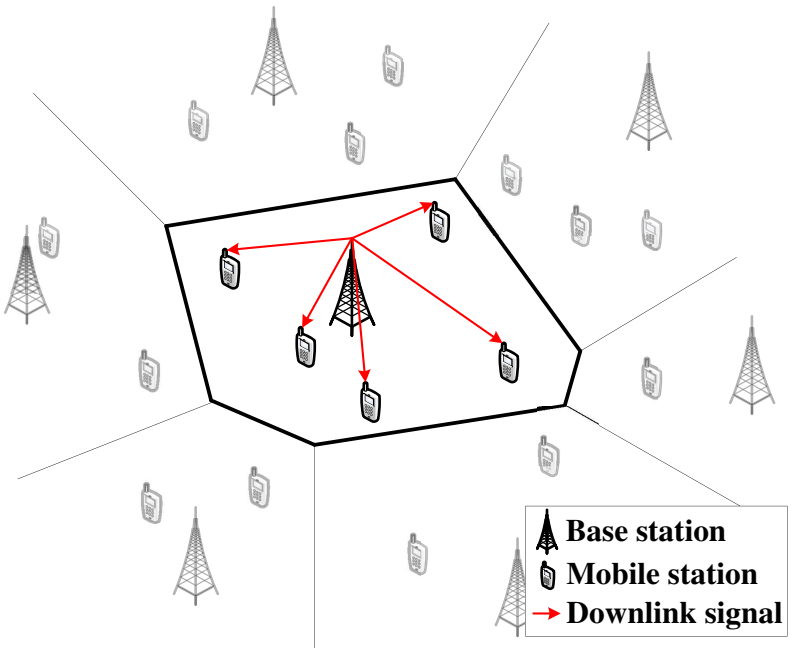

Figure 6.2: Typical cell

Number of Served Users: Firstly, we study the number of served users in a cell. Let Φ_{M_1} and Φ_{M_2} be the point processes for user distributions respectively and Φ_B be the point process for BSs distribution. From the relationship between the LF ordering of point processes and the LT ordering of random variables in (5.28) with $u(x) = \mathbf{1}\{x \in C_0\}$ which is the indicator function, $\mathbf{1}\{x \in C_0\} = 1$ if $x \in C_0$ and $\mathbf{1}\{x \in C_0\} = 0$ if $x \notin C_0$, we can define the number of served users $N = \sum_{x \in \Phi_M} \mathbf{1}\{x \in C_0\}$ in the typical Voronoi cell C_0 as shown in Fig. 6.2, and establish the stochastic ordering of number of served users as follows:

$$\Phi_{M_1} \leq_{\text{Lf}} \Phi_{M_2} \Longrightarrow N_1 \leq_{\text{Lt}} N_2. \tag{6.28}$$

In the system model, it is assumed that the association between a BS and a MS is carried out in a large time scale compared to the change of channel. Under this assumption, the optimal resource allocation of the BS's system bandwidth is equal

allocation [107], i.e,.

$$Y = \frac{1}{N}, \tag{6.29}$$

where Y is the equal fraction of the associated BS's system bandwidth for all users $j = 1, 2, ..., N$ and N is the number of served users by the BS. This is the Round-Robin type scheduling scheme with the most fairness. Since $1/z$ is a c.m. function with z, $N_1 \leq_{\mathrm{Lt}} N_2$ in (6.28) imply that the optimal resource allocations satisfy $\mathbb{E}[Y_1] \geq \mathbb{E}[Y_2]$. This means average of resource fraction in Φ_{M_1} is always greater than that in Φ_{M_2}. If the point processes for spatial distribution of MSs are stationary, the average numbers of served users are equal in both point processes, Φ_{M_1} and Φ_{M_2} from Campbell's theorem. However, it still remains $\mathbb{E}[Y_1] \geq \mathbb{E}[Y_2]$.

Total Cell Coverage Probability: Given the realization of the point processes for BSs and MSs, Φ_{B} and Φ_{M}, the coverage probability of a mobile user $x \in \Phi_{\mathrm{M}}$ can be defined as

$$P_{\mathrm{C}}(x) := P\left(SINR(x) \geq T\right), \tag{6.30}$$

and can be thought of equivalently as the probability that a mobile user x can achieve a SINR better than T. Since it is assumed that users' motions are relatively slow, the coverage probability is averaged across the fading effects, h_{S} and h_{I} as follows:

$$\begin{aligned} P_{\mathrm{C}}(x) &= \mathbb{E}_{h_{\mathrm{S}},h_{\mathrm{I}}}\left[P\left(\frac{h_{\mathrm{S}}^{(x)} g(\|x\|)}{\sigma^2 + I(x)} \geq T\right)\Big| h_{\mathrm{S}}, h_{\mathrm{I}}\right] && (6.31)\\ &= \mathbb{E}_{h_{\mathrm{S}},h_{\mathrm{I}}}\left[P\left(h_{\mathrm{S}} \geq \frac{T(\sigma^2 + I(x))}{g(\|x\|)}\right)\Big| h_{\mathrm{S}}, h_{\mathrm{I}}\right] && (6.32)\\ &= \mathbb{E}_{h_{\mathrm{I}}}\left[\bar{F}_{h_{\mathrm{S}}}\left(\frac{T(\sigma^2 + I(x))}{g(\|x\|)}\right)\Big| h_{\mathrm{I}}\right] && (6.33) \end{aligned}$$

In (6.32), we drop the index x since $h_{\mathrm{S}}^{(x)}$ is independent of x. In (6.33), $\bar{F}_{h_{\mathrm{S}}}(x) := 1 - F_{h_{\mathrm{S}}}(x)$ is a CCDF of h_{S}.

In multicast/broadcast scenario, multiple users receive the common signal from their associated BS. Therefore, the probability that SINRs of all served users are

greater than the minimum requirement T is an important measurement to ensure the signal reception quality of every user. We call the probability as *total cell coverage probability* and define as follows:

$$P_{\mathrm{C}} = P\left(SINR(x_1) \geq T, \ldots, SINR(x_N) \geq T\right), \ (x_1, \ldots, x_N \in C_0 \cap \Phi_{\mathrm{M}}), \quad (6.34)$$

$$= \prod_{x \in C_0 \cap \Phi_{\mathrm{M}}} P_{\mathrm{C}}(x). \quad (6.35)$$

Equation (6.35) is followed from the assumption that users' activities are independent each other. The number of served user N is random according to the realization of Φ_{B} and Φ_{M}. Therefore, the total cell coverage probability is averaged across the spatial distribution for Φ_{B} and Φ_{M}. When $h_{\mathrm{S}}^{(x)}$ is exponential distributed, i.e., Rayleigh fading, (6.35) can be expressed as

$$P_{\mathrm{C}} = \mathbb{E}_{\Phi_{\mathrm{M}}, \Phi_{\mathrm{B}}} \left[\prod_{x \in C_0 \cap \Phi_{\mathrm{M}}} P_{\mathrm{C}}(x) \middle| \Phi_{\mathrm{M}}, \Phi_{\mathrm{B}} \right] \quad (6.36)$$

$$= \mathbb{E}_{\Phi_{\mathrm{M}}, \Phi_{\mathrm{B}}} \left[\prod_{x \in C_0 \cap \Phi_{\mathrm{M}}} \mathbb{E}_{h_{\mathrm{I}}} \left[\bar{F}_{h_{\mathrm{S}}} \left(\frac{T(\sigma^2 + I(x))}{g(\|x\|)} \right) \middle| h_{\mathrm{I}} \right] \middle| \Phi_{\mathrm{M}}, \Phi_{\mathrm{B}} \right] \quad (6.37)$$

$$= \mathbb{E}_{\Phi_{\mathrm{M}}, \Phi_{\mathrm{B}}, h_{\mathrm{I}}} \left[\prod_{x \in C_0 \cap \Phi_{\mathrm{M}}} \exp\left(-\frac{T(\sigma^2 + I(x))}{g(\|x\|)} \right) \middle| \Phi_{\mathrm{M}}, \Phi_{\mathrm{B}}, h_{\mathrm{I}} \right] \quad (6.38)$$

$$= \mathbb{E}_{\Phi_{\mathrm{M}}, \Phi_{\mathrm{B}}, h_{\mathrm{I}}} \left[\exp\left(-\sum_{x \in \Phi_{\mathrm{M}}} \frac{T(\sigma^2 + I(x))}{g(\|x\|)} \mathbf{1}\{x \in C_0\} \right) \middle| \Phi_{\mathrm{M}}, \Phi_{\mathrm{B}}, h_{\mathrm{I}} \right], \quad (6.39)$$

Equation (6.37) follows from substituting (6.33) into (6.36). Equation (6.38) follows from the assumption that h_{I} is independent of the point processes Φ_{B} and Φ_{M}. Conditioned on Φ_{B} and h_{I}, $u(x) = (T(\sigma^2 + I(x))/g(\|x\|))\mathbf{1}\{x \in C_0\}$ is a non-negative function with x. Therefore, if $\Phi_{\mathrm{M}_1} \leq_{\mathrm{Lf}} \Phi_{\mathrm{M}_2}$, then $\mathbb{E}_{\Phi_{\mathrm{M}_1}}[\exp(-\sum_{x \in \Phi_{\mathrm{M}_1}} u(x)) | \Phi_{\mathrm{M}_1}, \Phi_{\mathrm{B}}, h_{\mathrm{I}}] \geq \mathbb{E}_{\Phi_{\mathrm{M}_2}}[\exp(-\sum_{x \in \Phi_{\mathrm{M}_2}} u(x)) | \Phi_{\mathrm{M}_2}, \Phi_{\mathrm{B}}, h_{\mathrm{I}}]$ by the property of LT ordering in (2.5) and the relationship between point processes and their aggregate processes in (5.28) since $\exp(-z)$ is a c.m. function with z. By averaging over identical distributions of Φ_{B}

and h_{I} in both cases, we have $P_{\mathrm{C}_1} \geq P_{\mathrm{C}_2}$. This implies the probability that the SINR of all served users are greater than the minimum threshold T with Φ_{M_1} is always greater than the probability with Φ_{M_2}.

Network Spatial Coverage: The network spatial coverage is an important performance metric to design BSs deployment in cellular networks. We assume that BSs are distributed by a point process Φ_{B} and each BS has a fixed radius of coverage R. Denote the random number of BSs covering any arbitrary location y in $\mathbb{R}^d$ by

$$S(y) = \sum_{x \in \Phi_{\mathrm{B}}} \mathbf{1}\{y \in B_x(R)\}, \tag{6.40}$$

where $B_x(R)$ is a d-dimensional ball of radius R centered at the point x. Denote the probability generating function of the random number of BSs covering location y by $G(t) = \mathbb{E}[t^{S(y)}]$. When $0 \leq t \leq 1$, t^z is a c.m. function with z. Note that $1 - G(0)$ represents the probability whether the location y is covered by at least one BS from the definition of the probability generation function. Thus, if $\Phi_{\mathrm{B}_1} \leq_{\mathrm{Lf}} \Phi_{\mathrm{B}_2}$, then $G_1(t) \geq G_2(t)$ and consequently $1 - G_1(0) \leq 1 - G_2(0)$. This means the probability that any arbitrary point y in $\mathbb{R}^d$ is covered by at least one BS with the cell deployment by Φ_{B_1} is always less than the probability with Φ_{B_2}. Due to random effects of real systems such as shadowing, different transmission power per each BS, and obstacles, the range of coverage R can be a non-negative random variable. Since the random range of coverage R can be considered as independent marking $m = R$ in Section 6.4.1, the ordering of spatial coverage probabilities still holds from Lemma 6.4.1

6.5.2 Cognitive Networks

In the following discussion, we will consider the applications of stochastic orders to cognitive network systems. In a cognitive network, there is an increasing interest

in developing efficient methods for spectrum management and sharing. This motivates to exploit spectrum opportunities in space, time, frequency while protecting users of the primary network from excessive interference due to spectrum access from secondary networks. Secondary users (SUs) can access the spectrum owned by the primary users (PUs) using spectrum underlay or spectrum overlay. In an underlay cognitive network where a PU and SUs can transmit simultaneously, as long as a certain interference constraint is satisfied. In an overlay cognitive network where SUs only can transmit when a PU does not transmit its signal, the SUs should detect the signal from the PU to make a decision if it can transmit. Spectrum underlay and overlay techniques are the basis for designing emerging cognitive radio networks.

The application of stochastic ordering to interference analysis from SUs has been discussed in Chapter 5. We now discuss another application of stochastic ordering ideas to a cognitive radio setup.

6.5.2.1 System Model

Let us consider a cognitive radio network which contains a PU and many SUs. The PU is located at the origin. The L SUs are uniformly randomly located in a certain area $B \subset \mathbb{R}^d$ [114, 115, 116]. The SUs can be modeled as a binomial point process Φ_{SU} which is introduced in Section 6.3.4. The geometry of the cognitive radio network is illustrated in Fig. 6.3. It is also assumed that there is a BS for SUs to manage the SUs' transmission even though it is not shown in Fig. 6.3. The BS selects only N random number of users among L total users called as *active secondary users* through user selection schemes and only active SUs are allowed to transmit their signals to the BS. The main idea of user selection schemes is to make the thinned point process $\Phi_{\text{SU,th}}$ for active SUs by applying independent random thinning operations to Φ_{SU}. The resulting thinned point process $\Phi_{\text{SU,th}}$ which has uniformly distributed random

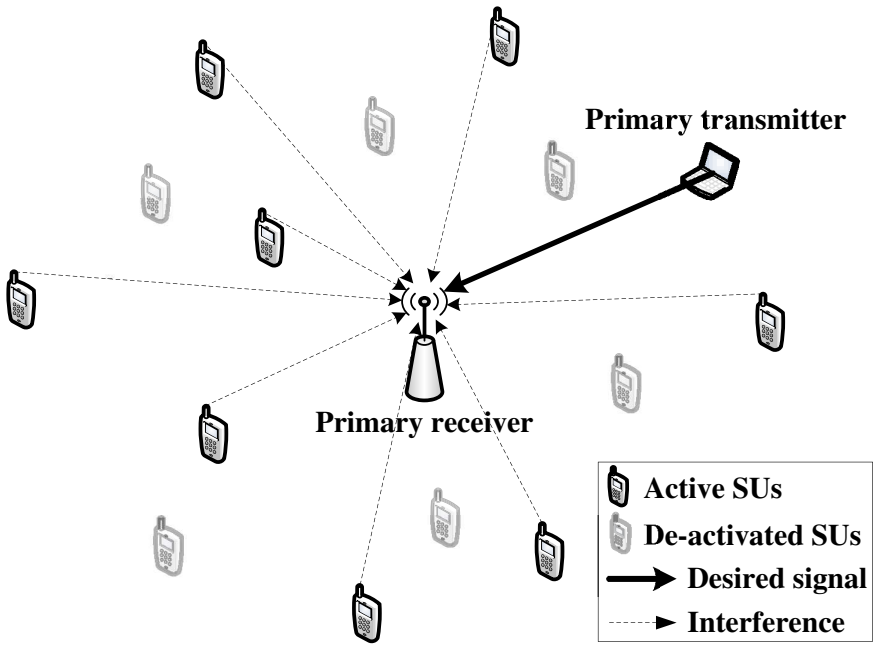

Figure 6.3: Illustration of a cognitive network.

number of points N can be considered as the mixed binomial point processes in Section 6.3.4. In the resulting point processes for the active SUs, the active SUs always cause the same average interference power to the PU and provide the same average sum rates of the active SUs. However, the instantaneous interferences from the active SUs are LT ordered and cause the ordered performance metrics such as a coverage probability and an achievable rate of the PU according to independent thinning operations for selecting active SUs. These will be discussed in detail later.

Average Interference Power Constraint: We assume an underlay cognitive network with a average interference power constraint Γ_{I}. Therefore, the average of aggregate interference should be less than the interference constraint $\mathbb{E}[I_{\mathrm{SU}}] \leq \Gamma_{\mathrm{I}}$. The instantaneous aggregate interference from the active SUs to the PU, I_{SU} is random and can be expressed as:

$$I_{\mathrm{SU}} = \sum_{x \in \Phi_{\mathrm{SU,th}}} h_{\mathrm{I}}^{(x)} g(\|x\|), \tag{6.41}$$

where $\Phi_{\mathrm{SU,th}}$ is a point process for active SUs and $h_{\mathrm{I}}^{(x)}$ is a positive random variable capturing the (power) fading coefficient between a active SU x and the PU. From Campbell's theorem, the average of aggregate interference from the active SUs, $\mathbb{E}[I_{\mathrm{SU}}]$ is the same as long as the average number of the active SUs is equal to $\mu = \mathbb{E}[N]$ regardless of random distribution for N. The proof is as follows:

Proof. From Campbell's theorem in (2.7) and the intensity measure of the mixed binomial point processes $\Lambda(B) = \lambda|B|$, the average of interference can be expresses as follows:

$$\mathbb{E}[I_{\mathrm{SU}}] = \mathbb{E}_{\Phi_{\mathrm{SU,th}},h_{\mathrm{I}}}\left[\sum_{x\in\Phi_{\mathrm{SU,th}}} h_{\mathrm{I}}^{(x)} g(\|x\|)\Big|\Phi_{\mathrm{SU,th}}, h_{\mathrm{I}}\right] \tag{6.42}$$

$$= \mathbb{E}_{h_{\mathrm{I}}}\left[\underbrace{\lambda\int_B h_{\mathrm{I}}^{(x)} g(\|x\|)\mathrm{d}x}_{A}\Big|h_{\mathrm{I}}\right]. \tag{6.43}$$

Conditioned on h_{I}, A is always equal. Therefore, the expectation of (6.43) with respect to h_{I} is still equal. The proof is completed. □

Therefore, we need to select μ in order to satisfy the average interference power constraint $\mathbb{E}[I_{\mathrm{SU}}] \leq \Gamma_{\mathrm{I}}$.

Average Sum Rate: On the other hand, if there is no interference between active SUs by adopting code-division multiple access (CDMA) like access scheme, then the sum of achievable rates of active SUs, C_{SU} is also random and can be expressed as

$$C_{\mathrm{SU}}(z) = \sum_{x\in\Phi_{\mathrm{SU,th}}} \log\left(1 + \frac{h_{\mathrm{S}}^{(x)} g(\|x-z\|)}{\sigma^2 + I_{\mathrm{P}}(x)}\right), \tag{6.44}$$

where $\Phi_{\mathrm{SU,th}}$ is a point process for active SUs, $h_{\mathrm{S}}^{(x)}$ is a effective fading channel between a active SU x and the BS for SUs located at z, $I_{\mathrm{P}}(x) = h_{\mathrm{I}}^{(x)} g(\|x\|)$ is a interference power from the PU to the SU x, and σ^2 is a additive noise power. From Campbell's

theorem, the average of sum of achievable rates of active SUs, $\mathbb{E}[C_{\text{SU}}(z)]$ is the same regardless of the point processes for the active SUs as long as the average number of the active SUs is equal to $\mu = \mathbb{E}[N]$. The proof is the same as the previous proof for equal average interference power with a different function.

6.5.2.2 User Selection Scheme for Secondary Users

Under previous observation on average interference constraint and average sum rate in the previous sections, we can apply stochastic ordering tool to design user selection schemes based on Theorem 6.3.4 in Section 6.3.4. Given $\mu = \mathbb{E}[N]$ which satisfies the interference constraint $\mathbb{E}[I_{\text{SU}}] \leq \Gamma_{\text{I}}$, the smaller LT ordered random number of active SUs N provides the smaller LF ordered point process $\Phi_{\text{SU,th}}$, that is $N_1 \leq_{\text{Lt}} N_2 \Rightarrow \Phi_{\text{SU,th}_1} \leq_{\text{Lf}} \Phi_{\text{SU,th}_2}$ from Theorem 6.3.4. Consequently, if $N_1 \leq_{\text{Lt}} N_2$, then the resulting point processes, $\Phi_{\text{SU,th}_1} \leq_{\text{Lf}} \Phi_{\text{SU,th}_2}$ cause LT ordered aggregate interferences to the PU, $I_{\text{SU}_1} \leq_{\text{Lt}} I_{\text{SU}_2}$. The LT ordered aggregate interferences from the active SUs to the PU yield ordered performance metrics for the PU such as a coverage probability and an achievable rate as mentioned in Chapter 5. On the other hand, the average sum of achievable rates of the active SUs and the average of interference power remain the same, $\mathbb{E}[C_{\text{SU}_1}] = \mathbb{E}[C_{\text{SU}_2}]$ and $\mathbb{E}[I_{\text{SU}_1}] = \mathbb{E}[I_{\text{SU}_2}]$ as we discussed above.

We give the examples of user selection scheme using stochastic ordering approach. If the active SUs are chosen among L total SUs with a probability p independently, the number of active SUs is a binomial random variable, N_{B}. The number of active SUs can follow discrete distributions other than binomial if different modes of operation are adopted. For another example, if the SUs before a predetermined number r with a probability p are selected, then the number of selected active SUs follows a negative binomial distribution with parameter r and p denoted as N_{NB}. Since $N_{\text{NB}} \leq_{\text{Lt}} N_{\text{B}}$

[117], $\Phi_{\text{NB}} \leq_{\text{Lf}} \Phi_{\text{B}}$ from Theorem 6.3.4. Therefore, the aggregate interferences from the active SUs are LT ordered $I_{\text{NB}} \leq_{\text{Lt}} I_{\text{B}}$, while $\mathbb{E}[C_{\text{NB}}] = \mathbb{E}[C_{\text{B}}]$ and $\mathbb{E}[I_{\text{NB}}] = \mathbb{E}[I_{\text{B}}] \leq \Gamma_{\text{I}}$. For these operations, the BS for SUs only needs to know the number of total SUs L and the average number of active SUs μ.

6.5.3 Discussion and Trade-offs

Coverage vs. Interference: As shown in the previous sections, the stochastic ordering of point processes can be applied to performance comparison and system design. Since the performance metrics depend on the stochastic ordering of point processes for spatial distribution of nodes, we can study spatial character of networks and investigate the spatial distributions of transmitting nodes in order to evaluate system performances using stochastic ordering approach. Then our investigations can be applied to the comparison of performance metrics such as number of served users and total cell coverage probability without having closed form expressions for the metrics. With the performance metrics such as network spatial coverage and network interference, our study can provide the design guideline for network deployment to increase spatial coverage of networks or provide less interference from networks. As an example, consider the effects of clustering. The clustering of nodes "reduces" a point process in the LF order. From an interference point of view, the clustering of interfering nodes causes less interference in the LT order between interference distributions. This translates into an increased coverage probability and improved capacity for the system as mentioned in Chapter 5. However, the clustering of nodes also causes less spatial coverage. Therefore, the proper point process for network deployment should be studied for balancing between interference and spatial coverage.

Burstiness vs. Fairness: The stochastic ordering approach can also be applied to design user selection schemes for SUs in cognitive networks which satisfy the con-

straints of the system. Under the certain system setup as described in 6.5.2, the smaller LT ordered active SUs N causes less interference to the PU, while the average interference $\mathbb{E}[I_{\text{SU}}]$ and average sum rate $\mathbb{E}[C_{\text{SU}}]$ are the same. From Theorem 5.A.21 in [7] and the discussion in Section 6.3.3, the smallest and biggest LT ordered N can be obtained as follows:

$$N_{\min} \leq_{\text{Lt}} N \leq_{\text{Lt}} N_{\min}, \tag{6.45}$$

where N is any non-negative integer random variable, $N_{\min}$ is $P\{N = 0\} = 1 - P\{N = 2\mu\} = 1/2$, and $N_{\max}$ is the fixed $N = \mu$. Even though the smallest LT ordered random number N causes the smallest LT ordered interference to the PU, it causes more bursty traffic from the active SUs and the more instantaneous interference when $N = 2\mu$. Otherwise, the biggest LT ordered N provides balanced traffic from the active SUs since the fixed number of random set of users μ is always selected. However, it causes the bigger LT ordered interference to the PU than any other distributions for active random SUs N. Therefore, the proper distribution for active random SUs should studied for balancing burstiness of interference and fairness of active SUs' traffic.

Random Effects: The system performances do not only depend on spatial deployment of a network, but also random effects of real systems such as random moving of mobile stations, coexisting of heterogeneous networks, shadowing, etc. From the preservation properties of LF ordering of point processes, it is noted that the random effects do not change the LF ordering of original point process when independent identical random effects are considered in two different spatial network deployment scenarios. As an example, consider two mobile networks where every node is independently identically randomly moving. If the initial point processes of two mobile networks are LF ordered, then interferences raised from the mobile networks are LT

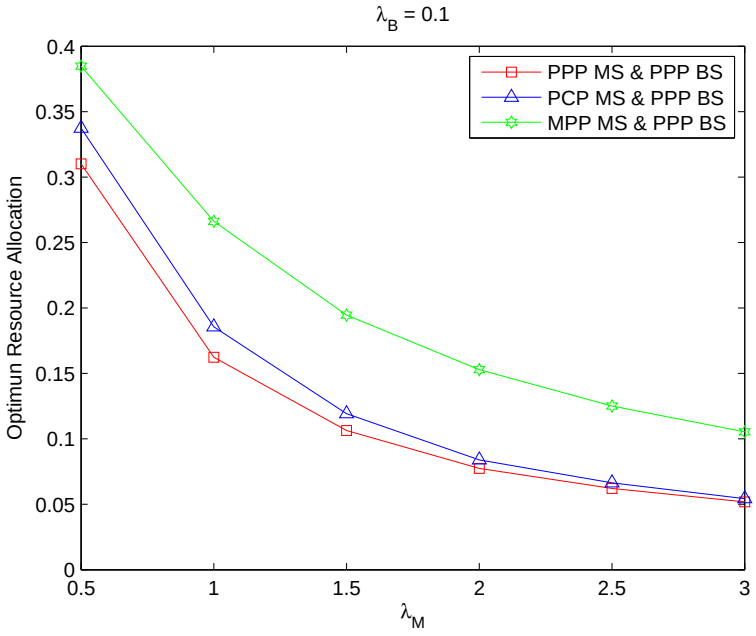

Figure 6.4: Average optimal resource allocation

ordered. Consequently the ordered interferences imply ordered performance metric results such as a coverage probability and an achievable rates. The ordered performance metric results are not changed regardless of the different mobility models such as constrained i.i.d. mobility, random walk, and Brownian motion as long as each node moves independently and identically. Since these random effects do not affect the performance comparison results and design guidelines using stochastic ordering approach, we need to focus the stochastic ordering of spatial deployments of nodes. It will be the most important factor for the design of wireless network systems.

6.6 Numerical Results

In this section, we verify our theoretical results through Monte Carlo simulations.

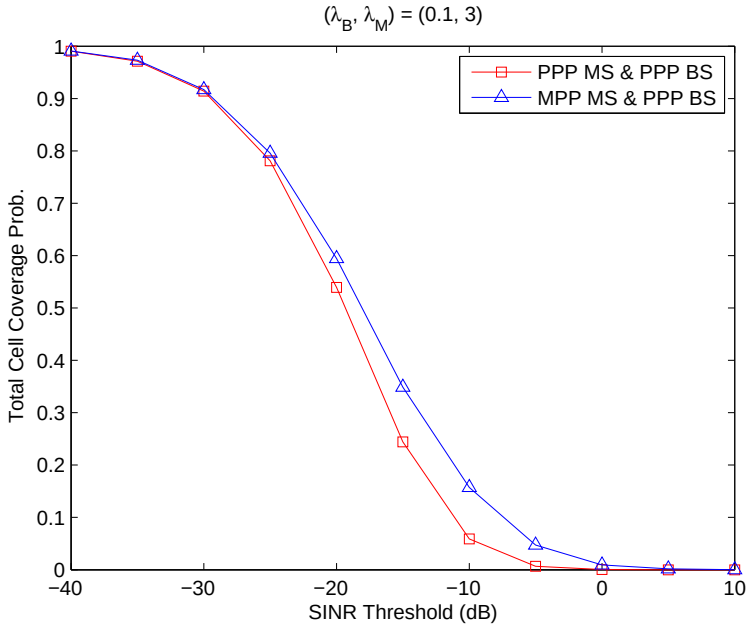

Figure 6.5: Total cell coverage probability

6.6.1 Cellular Networks

In Fig. 6.4 the average of resource fractions which are occupied by each user are shown. The stationary Poisson point process, Φ_{B} with λ_{B} is assumed for BSs and the stationary Poisson point process Φ_{PPP}, Poisson cluster process Φ_{PCP} and mixed Poisson process Φ_{MPP} with same intensity λ_{M} are assumed for spatial user distributions. Since it has been proved that $\Phi_{\mathrm{PCP}}, \Phi_{\mathrm{MPP}} \leq_{\mathrm{Lf}} \Phi_{\mathrm{PPP}}$ from Chapter 5, we can observe $\mathbb{E}[Y_{\mathrm{PCP}}], \mathbb{E}[Y_{\mathrm{MPP}}] \geq \mathbb{E}[Y_{\mathrm{PPP}}]$ as predicted from our theoretical result in Section 6.5.1. Even though the average number of served users are the same, the average of resource fractions of Φ_{PCP} and Φ_{MPP} are larger than that of Φ_{PPP}.

We show in Fig. 6.5 the total cell coverage probabilities. It is assumed that stationary Poisson point process Φ_{B} for BSs and Poisson point process Φ_{PPP} and mixed Poisson process Φ_{MPP} with same intensity λ_{M} for user distributions. From $\Phi_{\mathrm{MPP}} \leq_{\mathrm{Lf}} \Phi_{\mathrm{PPP}}$, it is obvious $P_{\mathrm{C}_{\mathrm{MPP}}} \geq P_{\mathrm{C}_{\mathrm{PPP}}}$.

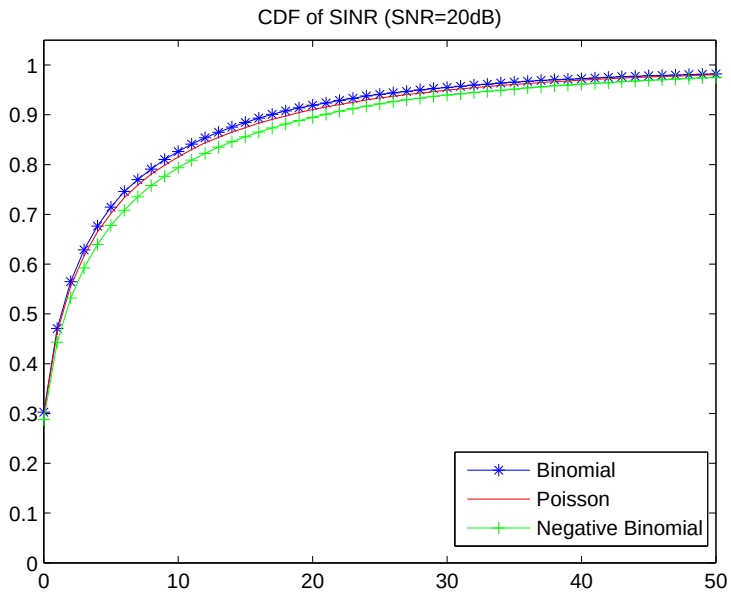

Figure 6.6: Coverage probabilities of primary user

6.6.2 Cognitive Networks

In Fig. 6.6, the CDFs of SINR of the primary user are shown according to LF ordered point processes for spatial distributions of SUs. The LT ordered number of SUs $N_{\mathrm{NB}} \leq_{\mathrm{Lt}} N_{\mathrm{P}} \leq_{\mathrm{Lt}} N_{\mathrm{B}}$ ensures $\Phi_{\mathrm{NB}} \leq_{\mathrm{Lf}} \Phi_{\mathrm{P}} \leq_{\mathrm{Lf}} \Phi_{\mathrm{B}}$ from Theorem 6.3.4. Since the aggregate interferences from LF ordered point processes for spatial distributions of active SUs are LT ordered [111, Theorem 6], we observe $SIR_{\mathrm{NB}} \geq_{\mathrm{st}} SIR_{\mathrm{P}} \geq_{\mathrm{st}} SIR_{\mathrm{B}}$ consequently. However, the average of the sum of achievable rates of active SUs in (6.44) are the same regardless of LF ordered point processes as shown in Fig. 6.7.

6.7 Comparison Between LF and DCX Ordering

In this dissertation, we advocate the LF ordering of point processes over the DCX ordering in [96, 118]. In order to define the DCX order of point processes, it is needed to define directionally convex functions and the DCX ordering of random vectors [7]:

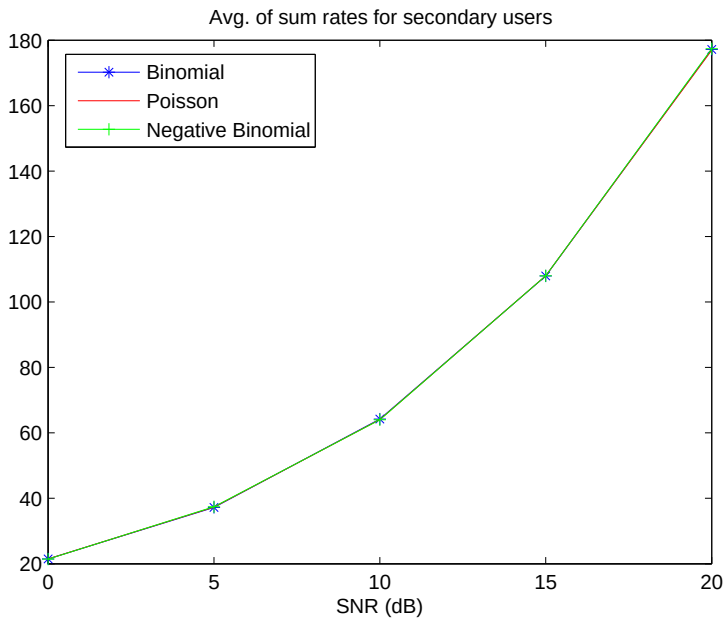

Figure 6.7: Average sum rates of secondary users

Let '$\leq$' in $\mathbb{R}^n$ denote the componentwise order, i.e. $(x_1, ..., x_n) \leq (y_1, ...y_n)$ if $x_i \leq y_i$ for every i. For $x, y, z \in \mathbb{R}^d$ we use the notation $[x, y] \leq z$ as a shorthand for $x \leq z$ and $y \leq z$. Also, the notation $z \leq [x, y]$ stands for $z \leq x$ and $z \leq y$. A function $l : \mathbb{R}^d \to \mathbb{R}$ is said to be *directionally convex* if for any $x_i \in \mathbb{R}^d, i = 1, 2, 3, 4$, such that $x_1 \leq [x_2, x_3] \leq x_4$ and $x_1 + x_4 = x_2 + x_3$, one has

$$l(x_2) + l(x_3) \leq l(x_1) + l(x_4).$$

With the directionally convex functions, we can define the DCX ordering of random vectors as follows: Let X and Y be two random vectors. Suppose that X and Y are such that

$$\mathbb{E}[l(X)] \leq \mathbb{E}[l(Y)],$$

for all functions $l : \mathbb{R}^d \to \mathbb{R}$ that are directionally convex, provided the expectations exist. Then X is said to be smaller than Y in the *directionally convex* (DCX) *order* (denoted by $X \leq_{\text{dcx}} Y$). From the definition of directionally convex functions and

the DCX order of random vectors, the definition of DCX ordering of point processes is as follows [96]:

Definition 6.7.1. *Let Φ_1 and Φ_2 be two random measures in $\mathbb{R}^d$ such that*

$$(\Phi_1(B_1), ..., \Phi_1(B_n)) \leq_{\text{dcx}} (\Phi_2(B_1), ..., \Phi_2(B_n))$$

for any bounded subsets $B_1, ..., B_n$ in $\mathbb{R}^d$. Then we say that $\Phi_1 \leq_{\text{dcx}} \Phi_2$.

The LF order has several advantages compared to the DCX order as follows: **(i)** The LF ordering of point processes is defined based on the well-known Laplace functional. Thus, it is easier to compare point processes since the expressions for Laplace functional of several point process are known. **(ii)** The condition for DCX order is stricter than that of LF order. Therefore, the LF order can be applied to broader class of point processes. For example, in case of the perturbed lattice processes which will be discussed later in Section 6.3.3, the LT ordered random number of points implies the LF ordered point processes with uniformly located points. On the other hand, the convex (CX) ordered random number of points implies the DCX ordered point processes with the same assumption. From Theorem 4.A.34 and Theorem 5.A.16 in [7], $X \leq_{\text{cx}} Y \Longrightarrow Y \leq_{\text{Lt}} X$. Therefore, the smaller set of random variables can be applied to the DCX order of point processes than the LF order. **(iii)** The performance metrics such as a coverage probability, an achievable rate, and a spatial coverage in [96, 118] can also be compared through LF ordering of point processes. **(iv)** In limited scenarios, the Laplace functional of point process can provide closed form expressions for some of performance metrics such as a coverage probability and an achievable rate. Otherwise, at least it provides simple expressions (not closed-form) for the metrics which can be quantified through simple numerical evaluation [8, 11, 13, 107]. **(v)** In the case that the Laplace functional of point process is required, but there is no

expression for that, the Laplace functional of point process can be estimated called as the *empirical Laplace functional* and the estimator is easy to formulate [42].

Unlike DCX order, however, in case of LF order high order properties of point process such as k-th ($k \geq 2$) order moment measures cannot be compared. These properties have been used to compare *Ripley's K* and *pair correlation* functions of point processes which are tools for measuring of clustering property of point processes [96, 6] and prove that a certain class of point processes (called as *sub-Poisson* point processes, $\Phi \leq_{\text{dcx}} \Phi_{\text{PPP}}$) has a finite critical radius $r_{\text{c}} := \inf\{r > 0 : P(C(\Phi, r) \text{ percolates}) > 0\}$ where $C(\Phi, r) = \cup_{x \in \Phi} B_x(r)$ is the Boolean model generated by Φ, $B_x(r)$ is a ball centered at $x \in \mathbb{R}^d$ of radius r, and '$C(\Phi, r)$ *percolates*' means there exists an unbounded, connected subset of $C(\Phi, r)$ [118]. Even though the 'clustering' property can be compared by the ordered Ripley's K and pair correlation functions which are inherent from the DCX ordered point processes, the property can be also captured by the LF ordering between a Poisson point process and a Poisson cluster process as mentioned in Chapter 5. For the percolation, the DCX ordering does not imply the comparison of percolation properties between two different point processes. It is a tool to prove the specific property (having a finite critical radius r_{c}) of the class of point processes.

Chapter 7

CONCLUSIONS

In Chapter 3 of this dissertation, we considered a symmetric α-stable noise model for MIMO fading channels, and discussed different receivers. In symmetric α-stable noise environments, the diversity order depends on the noise parameter, α, and noise correlation model. Under Model I, we derived the diversity order for the GAR and MDR. The maximum possible diversity order of GAR is shown to be a benchmark for any receiver, given by $\alpha N_{\mathrm{t}}/2$. The MDR, though simple, is vulnerable to impulsive noise: the diversity order is always $\alpha/2$ regardless the number of antennas. Under Model II we have seen that the diversity order for GAR will be larger than that of Model I. In contrast, for MDR the diversity order is $\alpha/2$ also for Model II. Since the GAR is impractical to implement, we are motivated to use the ML receiver. However, the ML receiver is computationally complex and requires knowledge of the noise parameters. Thus, we also develop an asymptotically optimal receiver, which performs near optimally at high SNRs and does not require the noise parameters. Since the conventional MDR has poor performance, the usage of the MDR should be avoided in symmetric α-stable noise environments.

In Chapter 4, we assumed two Poisson distributed networks coexist. In this environment, we showed the signal and interference converged to the class of α-stable distributions. From these results we defined the α-stable random signal detection problem in α-stable random noise. Since the ML detector is computationally complex, we have also developed the mixed-FLOM detector, which performs within 0.5 dB to the ML detector when the number of sample for detection is not small. We verified our results through Monte Carlo simulations.

In Chapter 5 of this dissertation, we used stochastic orders to compare performance in wireless networks. We showed that when interference is LT ordered, it is possible to order the SIR in the usual stochastic ordering sense when the effective channel has a c.m. CCDF. Similar results hold when the metric is the bandwidth-normalized capacity. This lead to the study of the conditions for LT ordering of interference. Three factors affecting interference are the fading channel from the interfering nodes to the receiver, the path-loss model and the distribution of the interfering node location. We derived conditions on these factors so that LT ordering between interferences holds. In addition, we defined Laplace functional ordering of point processes and derived its inherent stochastic ordering of interferences when the fading channel and the path-loss model are assumed to be same for both point processes. The power of this approach is that such comparisons can be made even in cases where a closed form expression for the interference is not analytically tractable. We verified our results through Monte Carlo simulations.

Finally, in Chapter 6, we studied stochastic order of point process. The stochastic ordering of broad classes of point processes are investigated. We showed that the preservation of stochastic ordering of point process with respect to the several operations, such as independent marking, thinning, superposition, clustering, random translation and so on. We introduced the applications of stochastic ordering of point processes to wireless networks such as cellular networks and cognitive networks. It provided the guideline for design of user selection schemes and transmission strategy for wireless networks. The power of this approach is that network performance comparisons can be made even in cases where a closed form expression for the performances is not analytically tractable. We verified our results through Monte Carlo simulations.

REFERENCES

[1] J. Silvester and L. Kleinrock, "On the capacity of multihop slotted ALOHA networks with regular structure," *IEEE Trans. Commun.*, vol. 31, no. 8, pp. 974–982, Aug. 1983.

[2] R. Mathar and J. Mattfeldt, "On the distribution of cumulated interference power in Rayleigh fading channels," *Wireless Netw.*, vol. 1, no. 1, pp. 31–36, Feb. 1995.

[3] D. Stoyan, W. S. Kendall, and J. Mecke, *Stochastic Geometry and its Applications*, 2nd ed. New York: Wiley, 1995.

[4] F. Baccelli and B. Błaszczyszyn, S*tochastic geometry and wireless networks, Volume 1-Theory.* New York: NOW: Foundations and Trends in Networking, 2009.

[5] M. Haenggi and R. Ganti, "Interference in large wireless networks," *Foundations and Trends in Networking*, vol. 3, no. 2, pp. 127–248, 2008.

[6] M. Haenggi, *Stochastic Geometry for Wireless Netwokrs*, 1st ed. Cambridge: Cambridge University Press, 2013.

[7] M. Shaked and J. Shanthikumar, *Stochastic orders.* Springer, 2007.

[8] K. Gulati, B. Evans, J. Andrews, and K. Tinsley, "Statistics of co-channel interference in a field of Poisson and Poisson-Poisson clustered interferers," *IEEE Trans. Signal Process.*, vol. 58, no. 12, pp. 6207–6222, Dec. 2010.

[9] F. Baccelli, M. Klein, M. Lebourges, and S. Zuyev, "Stochastic geometry and architecture of communication networks," *J. Telecommun. Syst.*, vol. 7, no. 1, pp. 209–227, 1997.

[10] T. X. Brown, "Cellular performance bounds via shotgun cellular systems," *IEEE J. Sel. Areas Commun.*, vol. 18, no. 11, pp. 2443–2455, Nov. 2000.

[11] J. Andrews, F. Baccelli, and R. Ganti, "A tractable approach to coverage and rate in cellular networks," *IEEE Trans. Commun.*, vol. 59, no. 11, pp. 3122–3134, Nov. 2011.

[12] H. Dhillon, R. Ganti, F. Baccelli, and J. Andrews, "Modeling and analysis of K-tier downlink heterogeneous cellular networks," *IEEE J. Sel. Areas Commun.*, vol. 30, no. 3, pp. 550–560, Apr. 2012.

[13] S. Mukherjee, "Distribution of downlink SINR in heterogeneous cellular networks," *IEEE J. Sel. Areas Commun.*, vol. 30, no. 3, pp. 575–585, Apr. 2012.

[14] H.-S. Jo, Y. J. Sang, P. Xia, and J. Andrews, "Heterogeneous cellular networks with flexible cell association: a comprehensive downlink SINR analysis," *IEEE Trans. Wireless Commun.*, vol. 11, no. 10, pp. 3484–3495, Oct. 2012.

[15] R. Heath, M. Kountouris, and T. Bai, "Modeling heterogeneous network interference using Poisson point processes," *IEEE Trans. Signal Process.*, vol. 61, no. 16, pp. 4114–4126, Aug. 2013.

[16] H. Wang, X. Zhou, and M. C. Reed, "Coverage and throughput analysis with a non-uniform femtocell deployment," Available Online: http://arxiv.org/abs/1305.3694, 2013.

[17] X. Lin, , J. Andrews, and A. Ghosh, "Modeling, analysis and design for carrier aggregation in heterogeneous cellular networks," *IEEE Trans. Commun.*, vol. 61, no. 9, pp. 4002–4015, Sept. 2013.

[18] H. Dhillon, R. Ganti, and J. Andrews, "Load-aware modeling and analysis of heterogeneous cellular networks," *IEEE Trans. Wireless Commun.*, vol. 12, no. 4, pp. 1666–1677, Apr. 2013.

[19] T. D. Novlan, H. S. Dhillon, and J. G. Andrews, "Analytical modeling of uplink cellular networks," *IEEE Trans. Wireless Commun.*, vol. 12, no. 6, pp. 2669–2679, Jun. 2013.

[20] T. Novlan, R. Ganti, A. Ghosh, and J. Andrews, "Analytical evaluation of fractional frequency reuse for OFDMA cellular networks," *IEEE Trans. Wireless Commun.*, vol. 10, no. 12, pp. 4294–4305, Dec. 2011.

[21] ——, "Analytical evaluation of fractional frequency reuse for heterogeneous cellular networks," *IEEE Trans. Commun.*, vol. 60, no. 7, pp. 2029–2039, Jul. 2012.

[22] S. Akoum and R. Heath, "Interference coordination: Random clustering and adaptive limited feedback," *IEEE Trans. Signal Process.*, vol. 61, no. 7, pp. 1822–1834, Apr. 2013.

[23] S. Y. Jung, H.-K. Lee, and S.-L. Kim, "Worst-case user analysis in Poisson Voronoi cells," *IEEE Commun. Lett.*, vol. 17, no. 8, pp. 1580–1583, Aug. 2013.

[24] A. Giovanidis and F. Baccelli, "A stochastic geometry framework for analyzing pairwise-cooperative cellular networks," Available Online: http://arxiv.org/abs/1305.6254, 2013.

[25] H. Dhillon, R. Ganti, and J. Andrews, "Modeling non-uniform ue distributions in downlink cellular networks," *IEEE Wireless Commun. Lett.* (Early Access Articles), 2013.

[26] Q. Ye, B. Rong, Y. Chen, M. Al-Shalash, C. Caramanis, and J. G. Andrews, "User association for load balancing in heterogeneous cellular networks," *IEEE Trans. Wireless Commun.* (Early Access Articles), 2013.

[27] X. Lin, R. Ganti, P. Fleming, and J. Andrews, "Towards understanding the fundamentals of mobility in cellular networks," *IEEE Trans. Wireless Commun.*, vol. 12, no. 4, pp. 1686–1698, Apr. 2013.

[28] S. Singh, H. S. Dhillon, and J. G. Andrews, "Offloading in heterogeneous networks: Modeling, analysis, and design insights," *IEEE Trans. Wireless Commun.*, vol. 12, no. 5, pp. 2484–2497, May 2013.

[29] S. Lee and K. Huang, "Coverage and economy of cellular networks with many base stations," *IEEE Commun. Lett.*, vol. 16, no. 7, pp. 1038–1040, Jul. 2012.

[30] L. Xiang, X. Ge, C.-X. Wang, F. Y. Li, and F. Reichert, "Energy efficiency evaluation of cellular networks based on spatial distributions of traffic load and power consumption," *IEEE Trans. Wireless Commun.*, vol. 12, no. 3, pp. 961–973, Mar. 2013.

[31] X. Lin, R. Ganti, P. Fleming, and J. Andrews, "Towards understanding the fundamentals of mobility in cellular networks," *IEEE Trans. Wireless Commun.*, vol. 12, no. 4, pp. 1686–1698, Apr. 2013.

[32] X. Lin, J. G. Andrews, and A. Ghosh, "Spectrum sharing for device-to-device communication in cellular networks," *IEEE Trans. Wireless Commun.* (submitted), Available Online: http://arxiv.org/abs/1305.4219, Nov. 2013.

[33] N. Lee, X. Lin, J. G. Andrews, and R. W. H. Jr., "Power control for D2D underlaid cellular networks: Modeling, algorithm and analysis," *IEEE J. Sel. Areas Commun.* (submitted), Available Online: http://arxiv.org/abs/1305.6161, May 2013.

[34] A. Guo and M. Haenggi, "Spatial stochastic models and metrics for the structure of base stations in cellular networks," *IEEE Trans. Wireless Commun.*, vol. 12, no. 11, pp. 5800–5812, Nov. 2013.

[35] H. Inaltekin, M. Chiang, H. Poor, and S. Wicker, "On unbounded path-loss models: effects of singularity on wireless network performance," *IEEE J. Sel. Areas Commun.*, vol. 27, no. 7, pp. 1078–1092, Sept. 2009.

[36] A. Rabbachin, T. Quek, H. Shin, and M. Win, "Cognitive network interference," *IEEE J. Sel. Areas Commun.*, vol. 29, no. 2, pp. 480–493, Feb. 2011.

[37] Y. Wen, S. Loyka, and A. Yongacoglu, "Asymptotic analysis of interference in cognitive radio networks," *IEEE J. Sel. Areas Commun.*, vol. 30, no. 10, pp. 2040–2052, Nov. 2012.

[38] C.-H. Lee and M. Haenggi, "Interference and outage in Poisson cognitive networks," *IEEE Trans. Wireless Commun.*, vol. 11, no. 4, pp. 1392–1401, Apr. 2012.

[39] R. Schilling, R. Song, and Z. Vondraček, *Bernstein Functions: Theory and Applications*. Walter de Gruyter, 2010.

[40] M. Shaked and J. Shanthikumar, *Stochastic orders and their applications*, 1st ed. Springer, 1994.

[41] C. Tepedelenlioğlu, A. Rajan, and Y. Zhang, "Applications of stochastic ordering to wireless communications," *IEEE Trans. Wireless Commun.*, vol. 10, no. 12, pp. 4249–4257, Dec. 2011.

[42] A. F. Karr, *Point Processes and Their Statistical Inference*, 2nd ed. New York: Marcel Dekker, Inc., 1991.

[43] M. Win, P. Pinto, and L. Shepp, "A mathematical theory of network interference and its applications," *Proc. IEEE*, vol. 97, no. 2, pp. 205–230, Feb. 2009.

[44] R. Ganti and M. Haenggi, "Interference and outage in clustered wireless Ad Hoc networks," *IEEE Trans. Inf. Theory*, vol. 55, no. 9, pp. 4067–4086, Sept. 2009.

[45] R. Tresch and M. Guillaud, "Performance of interference alignment in clustered wireless ad hoc networks," in *Proc. IEEE ISIT'10*, Jun. 2010, pp. 1703–1707.

[46] S. Haas and J. Shapiro, "Capacity of wireless optical communications," *IEEE J. Sel. Areas Commun.*, vol. 21, no. 8, pp. 1346–1357, Oct. 2003.

[47] M. Garetto, A. Nordio, C. Chiasserini, and E. Leonardi, "Information-theoretic capacity of clustered random networks," *IEEE Trans. Inf. Theory*, vol. 57, no. 11, pp. 7578–7596, Nov. 2011.

[48] C. Nikias and M. Shao, *Signal Processing with alpha-Stable Distributions and Applications*. New York: Wiley, 1995.

[49] H. Fofack and J. Nolan, "Tail behavior, models and other characteristics of stable distributions," *Available Online: http://academic2.american.edu/∼jpnolan/stable/tails.pdf*, Jan. 1998.

[50] G. Samorodnitsky and M. Taqqu, *Stable non-Gaussian Random Processes*. New York: Chapman and Hall, 1994.

[51] D. Middleton, "Statistical-physical models of electromagnetic interference," *IEEE Trans. Electromagn. Compat.*, vol. EMC-19, no. 3, pp. 106–127, Aug. 1977.

[52] H. Kanemoto, S. Miyamoto, and N. Morinaga, "Statistical model of microwave oven interference and optimum reception," in *Proc. IEEE ICC'98*, Oct. 1998, pp. 1660–1664.

[53] E. Sousa, "Performance of a spread spectrum packet radio network link in a Poisson field of interferers," *IEEE Trans. Inf. Theory*, vol. 38, no. 6, pp. 1743–1754, Nov. 1992.

[54] J. Ilow and D. Hatzinakos, "Analytic alpha-stable noise modeling in a Poisson field of interferers or scatterers," *IEEE Trans. Signal Process.*, vol. 46, no. 6, pp. 1601–1611, Jun. 1998.

[55] X. Yang and A. Petropulu, "Co-channel interference modeling and analysis in a Poisson field of interferers in wireless communications," *IEEE Trans. Signal Process.*, vol. 51, no. 1, pp. 64–76, Jan. 2003.

[56] B. Hughes, "Alpha-stable models of multiuser interference," in *Proc. IEEE ISIT'00*, Jun. 2000, p. 383.

[57] M. Haenggi, J. Andrews, F. Baccelli, O. Dousse, and M. Franceschetti, "Stochastic geometry and random graphs for the analysis and design of wireless networks," *IEEE J. Sel. Areas Commun.*, vol. 27, no. 7, pp. 1029–1046, Sep. 2009.

[58] A. Spaulding and D. Middleton, "Optimum reception in an impulsive interference environment - Part I: Coherent detection," *IEEE Trans. Commun.*, vol. 25, no. 9, pp. 910–923, Sep. 1977.

[59] D. Middleton, "Non-Gaussian noise models in signal processing for telecommunications: new methods an results for class a and class b noise models," *IEEE Trans. Inf. Theory*, vol. 45, no. 4, pp. 1129–1149, May 1999.

[60] H. Tarokh, H. Jafarkhani, and A. Caldcrbank, "Space-time block coding for wireless communications: performance results," *IEEE J. Sel. Areas Commun.*, vol. 17, no. 3, pp. 451–460, Mar. 1999.

[61] M. Gharavi-Alkhansari, A. Gershman, and M. Haardt, "Exact error probability analysis of orthogonal space-time block codes over correlated Rician fading channels," in *Proc. IEEE WSA'04*, Mar. 2004, pp. 274–278.

[62] H. Zhang and T. Gulliver, "Capacity and error probability analysis for orthogonal space-time block codes over fading channels," *IEEE Trans. Wireless Commun.*, vol. 4, no. 2, pp. 808–819, Mar. 2005.

[63] C. Giovaneli, J. Yazdani, P. Farrell, and B. Honary, "Application of space-time diversity/coding for power line channels," in *Proc. IEEE ISPLC'02*, Apr. 2002, pp. 101–105.

[64] P. Gao and C. Tepedelenlioglu, "Space-time coding over fading channels with impulsive noise," *IEEE Trans. Veh. Technol.*, vol. 6, no. 1, pp. 220–229, Jan. 2007.

[65] X. Wang, Y. Gong, and B. Lin, "SER performance of orthogonal space-time block coding over fading channels with impulsive noise," in *Proc. IEEE WiCom'07*, Sep. 2007, pp. 45–48.

[66] A. Li, Y. Wang, W. Xu, and Z. Zhou, "Performance evaluation of MIMO systems in a mixture of Gaussian noise and impulsive noise," in *Proc. IEEE APCC/MDMC'04*, Aug. 2004, pp. 292–296.

[67] A. Rajan and C. Tepedelenlioglu, "Diversity combining over Rayleigh fading channels with symmetric alpha stable noise," *IEEE Trans. Wireless Commun.*, vol. 9, no. 9, pp. 2968–2976, Sep. 2010.

[68] S. Niranjayan and N. Beaulieu, "The BER optimal linear rake receiver for signal detection in symmetric alpha-stable noise," *IEEE Trans. Commun.*, vol. 57, no. 12, pp. 3585–3588, Dec. 2009.

[69] ——, "BER optimal linear combiner for signal detection in symmetric alpha-stable noise: small values of alpha," *IEEE Trans. Commun.*, vol. 9, no. 3, pp. 886–890, Mar. 2010.

[70] V. Tarokh, H. Jafarkhani, and A. R. Calderbank, "Space-time block codes from orthogonal designs," *IEEE Trans. Inf. Theory*, vol. 45, no. 5, pp. 1456–1467, Jul. 1999.

[71] M. Abramowitz and I. A. Stegun, *Handbook of Mathematical Functions with Formulas, Graphs, and Mathematical Tables*, 9th ed. New York: Dover, 1972.

[72] F. Qi and C.-P. Chen, "A complete monotonicity property of the gamma function," *J. Math. Anal. and Applicat.*, pp. 603–607, Jul. 2004.

[73] J. Nolan, "Multivariate elliptically contoured stable distributions: theory and estimation," *Available Online: http://academic2.american.edu/∼jpnolan/stable/EllipticalStable.pdf*, Oct. 2006.

[74] M. Nassar, K. Gulati, A. Sujeeth, N. Aghasadeghi, B. Evans, and K. Tinsley, "Mitigating near-field interference in laptop embedded wireless transceivers," in *Proc. IEEE ICASSP'08*, Apr. 2008, pp. 1405–1408.

[75] Y. Sung, L. Tong, and A. Swami, "Asymptotic locally optimal detector for large-scale sensor networks under the poisson regime," *IEEE Trans. Signal Process.*, vol. 53, no. 6, pp. 2005–2017, Jun. 2005.

[76] A. Anandkumar, L. Tong, and A. Swami, "Optimal node density for detection in energy-constrained random networks," *IEEE Trans. Signal Process.*, vol. 56, no. 10, pp. 5232–5245, Oct. 2008.

[77] D. Avidor, S. Mukherjee, and F. Onat, "Transmit power distribution of wireless ad-hoc networks with topology control," *IEEE Trans. Wireless Commun.*, vol. 7, no. 4, pp. 1111–1116, Apr. 2008.

[78] I. Howitt, "WLAN and WPAN coexistence in UL band," *IEEE Trans. Veh. Technol.*, vol. 50, no. 4, pp. 1114–1124, Jul. 2001.

[79] I. Howitt and J. Gutierrez, "IEEE 802.15.4 low rate - wireless personal area network coexistence issues," in *Proc. IEEE WCNC'03*, Mar. 2003, pp. 16–20.

[80] D. Cavalcanti, S. Das, J. Wang, and K. Challapali, "Cognitive radio based wireless sensor networks," in *Proc. IEEE ICCCN'08*, Aug. 2008, pp. 1–6.

[81] S. Nethi, J. Nieminen, and R. Jantti, "Exploitation of multi-channel communications in industrial wireless sensor applications: Avoiding interference and enabling coexistence," in *Proc. IEEE WCNC'11*, Mar. 2011, pp. 345–350.

[82] S. Zozor, J.-M. Brossier, and P.-O. Amblard, "A parametric approach to suboptimal signal detection in α-stable noise," *IEEE Trans. Signal Process.*, vol. 54, no. 12, pp. 4497–4509, Dec. 2006.

[83] T. Fu, S. Zhou, and X. Zhang, "Detection for signal in ELF atmospheric noise interference," in *Proc. IEEE ICIME'10*, Apr. 2010, pp. 409–412.

[84] S. Ma, C. Zhao, and Y. Wang, "Fractional low order cyclostationary spectrum sensing based on eigenvalue matrix in alpha-stable distribution noise," in *Proc. IEEE PCSPA'10*, Sept. 2010, pp. 500–503.

[85] J. Park, G. Shevlyakov, and K. Kim, "Maximin distributed detection in the presence of impulsive alpha-stable noise," *IEEE Trans. Wireless Commun.*, vol. 10, no. 6, pp. 1687–1691, Jun. 2011.

[86] J. Kingman, *Poisson Processes.* Oxford, U.K.: Oxford Univ. Press, 1993.

[87] I. S. Gradshteyn and I. M. Ryzhik, *Tables of Integrals, Series, and Products*, 7th ed. San Diego, CA: Academic, 2007.

[88] W. Feller, *An Introduction to Probability Theory and Its Applications, Volume 2.* New York: Wiley, 1966.

[89] R. Niu and P. K. Varshney, "Performance analysis of distributed detection in a random sensor field," *IEEE Trans. Signal Process.*, vol. 56, no. 1, pp. 339–349, Jan. 2008.

[90] J. Behboodian, "Symmetric sum and symmetric product of two independent random variables," *J. Theor. Prob.*, vol. 2, no. 2, pp. 267–270, Apr. 1989.

[91] E. Kuruoglu, "Density parameter estimation of skewed α-stable distributions," *IEEE Trans. Signal Process.*, vol. 49, no. 10, pp. 2192–2201, Oct. 2001.

[92] G. Tsihrintzis and C. Nikias, "Evaluation of fractional, lower-order statistics-based detection algorithms on real radar sea-clutter data," *IEE Proc. - Radar, Sonar and Navig.*, vol. 144, no. 1, pp. 29–38, Feb. 1997.

[93] J.-P. Linnartz, "Exact analysis of the outage probability in multiple-user mobile radio," *IEEE Trans. Inf. Theory*, vol. 40, no. 1, pp. 20–23, Jan. 1992.

[94] F. Baccelli and P. Blaszczyszyn, B.and Muhlethaler, "An Aloha protocol for multihop mobile wireless networks," *IEEE Trans. Inf. Theory*, vol. 52, no. 2, pp. 421–436, Feb. 2006.

[95] S. Ross, "Average delay in queues with non-stationary Poisson arrivals," *J. Appl. Prob.*, vol. 15, no. 3, pp. 602–609, Sept. 1978.

[96] B. Blaszczyszyn and D. Yogeshwaran, "Directionally convex ordering of random measures, shot noise fields, and some applications to wireless communications," *Adv. Appl. Prob.*, vol. 41, no. 3, pp. 623–646, 2009.

[97] X. Shang, G. Kramer, and B. Chen, "A new outer bound and the noisy-interference sum-rate capacity for Gaussian interference channels," *IEEE Trans. Inf. Theory*, vol. 55, no. 2, pp. 689–699, Feb. 2009.

[98] E. Salbaroli and A. Zanella, "Interference analysis in a Poisson field of nodes of finite area," *IEEE Trans. Veh. Technol.*, vol. 58, no. 4, pp. 1776–1783, May 2009.

[99] A. Hasan and J. G. Andrews, "The guard zone in wireless ad hoc networks," *IEEE Trans. Wireless Commun.*, vol. 4, no. 3, pp. 897–906, Mar. 2007.

[100] F. Baccelli and B. Błaszczyszyn, S*tochastic geometry and wireless networks, Volume 2-Applications*. New York: NOW: Foundations and Trends in Networking, 2009.

[101] M. Simon and M. Alouini, *Digital Communication over Fading Channels*. Wiley-IEEE Press, 2000.

[102] R. Griffiths and R. Milne, "A class of bivariate Poisson processes," *J. Mult. Anal.*, vol. 8, no. 3, pp. 380–395, Sept. 1978.

[103] S. Srinivasa and M. Haenggi, "Modeling interference in finite uniformly random networks," in *Proc. WITS'07*, Jun. 2007.

[104] R. Heath and M. Kountouris, "Modeling heterogeneous network interference," in *Proc. IEEE ITA'12*, Feb. 2012, pp. 17–22.

[105] D. J. Daley and D. Vere-Jones, *An Introduction to the Theory of Point Processes, Volume II: General Theory and Structure*, 2nd ed. New York: Springer, 2008.

[106] L. B. Le and E. Hossain, "Resource allocation for spectrum underlay in cognitive radio networks," *IEEE Trans. Wireless Commun.*, vol. 7, no. 12, pp. 5306–5315, Dec. 2008.

[107] Q. Ye, B. Rong, Y. Chen, M. Al-Shalash, C. Caramanis, and J. G. Andrews, "User association for load balancing in heterogeneous cellular networks," *IEEE Trans. Wireless Commun.*, vol. 12, no. 6, pp. 2706–2716, Jun. 2013.

[108] Z. Gong and M. Haenggi, "Interference and outage in mobile random networks: Expectation, distribution, and correlation," *IEEE Trans. Mobile Comput.*, vol. 13, no. 2, pp. 337–349, Feb. 2014.

[109] P. Madhusudhanan, J. Restrepo, Y. Liu, T. Brown, and K. Baker, "Stochastic ordering based carrier-to-interference ratio analysis for the shotgun cellular systems," *IEEE Wireless Commun. Lett.*, vol. 1, no. 6, pp. 565–568, Dec. 2012.

[110] H. S. Dhillon, M. Kountouris, and J. G. Andrews, "Downlink MIMO HetNets: Modeling, ordering results and performance analysis," *IEEE Trans. Wireless Commun.*, vol. 12, no. 10, pp. 5208–5222, Oct. 2013.

[111] J. Lee and C. Tepedelenlioğlu, "Stochastic ordering of interferences in large-scale wireless networks," *IEEE Trans. Signal Process.*, vol. 62, no. 3, pp. 729–740, Feb. 2014.

[112] M. Haenggi, "Interference in lattice networks," *IEEE Trans. Commun. (submitted),* Available Online: http://arxiv.org/abs/1205.2833, Mar. 2010.

[113] D. J. Daley and D. Vere-Jones, *An Introduction to the Theory of Point Processes, Volume I: Elementary Theory and Methods*, 2nd ed. New York: Springer, 2003.

[114] S. Pai, T. Datta, and C. Murthy, "On the design of location-invariant sensing performance for secondary users," in *Proc. IEEE UKIWCWS'09*, Dec. 2009, pp. 1–5.

[115] K. W. Sung, M. Tercero, and J. Zander, "Aggregate interference in secondary access with interference protection," *IEEE Commun. Lett.*, vol. 15, no. 6, pp. 629–631, Jun. 2011.

[116] D. Grace and H. Zhang, *Cognitive Communications: Distributed Artificial Intelligence (DAI), Regulatory Policy and Economics, Implementation*, 1st ed. New York: Wiley, 2012.

[117] R. Zeng and C. Tepedelenlioglu, "Cognitive radio with random number of secondary number of users," *IEEE Trans. Wireless Commun. (submitted),* Available Online: http://arxiv.org/abs/1310.1105, Oct. 2013.

[118] B. Blaszczyszyn and D. Yogeshwaran, "Connectivity in sub-Poisson networks," in *Proc. IEEE Allerton'10*, Sept. 2010, pp. 1466–1473.